An Investigation of the Cellular Mechanisms Underlying Ultrasound Neuromodulation

A DISSERTATION
SUBMITTED TO THE FACULTY OF THE
UNIVERSITY OF MINNESOTA

BY

Morgan Newhoff

IN PARTIAL FULFILLMENT OF THE REQUIREMENTS
FOR THE DEGREE OF
DOCTOR OF PHILOSOPHY

Dr. Karen A. Mesce (advisor)

August 2020

© Morgan Newhoff, 2020

COPYRIGHT PERMISSIONS

Chapter 2 has been previously published as:

Newhoff M, Mesce KA. Small steps and larger strides in understanding the neural bases of crawling in the medicinal leech. In: Whelan PJ and Sharples SA (Eds). *The Neural Control of Movement: Model Systems and Tools to Study Locomotor Function.* San Diego: Elsevier Inc./Academic Press, 2020: 31-55.

ACKNOWLEDGEMENTS

First and foremost, I would like to thank my advisor, **Dr. Karen Mesce**, for her tireless support over the past six years. She granted me the freedom to pursue a project of my choosing, the culmination of which has been this dissertation. This work would not have been possible without her keen insights, patience, support, and wisdom.

I would also like to thank the past and present members of my thesis committee. The cross-disciplinary nature of this project has required expertise and resources beyond those of a single lab. Each of these individuals has lent both time and equipment to the pursuit of this project, and for that I will be forever grateful. I'd like to thank **Dr. Wynn Legon**, who introduced me to ultrasound, and whose knowledge of the literature has shaped each of the chapters that comprise this thesis. I'd also like to thank my committee chair, **Dr. Tay Netoff**, who was a fabulous rotation advisor, and who has lent me critical equipment. I'd like to thank **Dr. Emad Ebbini**, whose ultrasound expertise far outweighs my own, and who was kind enough to allow me to perform experiments with his unique dual-mode ultrasound array. Finally, I'd like to thank **Dr. Hubert Lim**, whose students assisted me with hydrophone recordings, and with whom I look forward to working in the future.

I would also like to thank the many post-docs and graduate students who helped with this project. First, I would like to thank **Dr. Jerel Mueller**, formerly of the Legon lab, for teaching me to build and characterize ultrasound transducers. I

would also like to thank **Gerardo Rodriguez** and **John Basile** of the Lim lab for their assistance in obtaining hydrophone recordings. Finally, I would like to give special thanks to **Collin Smith** and **Parker O'Brien**, with whom I spent many hours in the Ebbini lab in pursuit of neuromodulation data generated with unprecedented precision.

I must also thank the past and present members of the Mesce lab who contributed to this project, either directly via assistance with dissections or electrophysiological recordings, or (perhaps more importantly) through their friendship. These include **Dr. Cindy Harley**, **Dr. JOsh Puhl**, **Mara Chin-Purcell Rue**, **Tony Bigelow**, **Dr. Mike Baltzly**, and **Lisa Ledwidge**. I would especially like to thank **Dr. Anthony Auletta**, my fellow PhD student and one of my dearest friends, whose unyielding support, commiseration, and random acts of mischief brightened even my most frustrating days.

I would also like to thank the many support staff who have assisted me in myriad ways, and without whom this project would not have been possible. These include **Felicia Christy** and **Tammi Pekkala-Matthews** from the Department of Entomology, and **Elaine McCauley**, **Rebecca Hervonen**, and **John Paton** from the Department of Neuroscience. These also include the past and present Directors of Graduate Study during my time in the Graduate Program in Neuroscience, **Dr. A. David Redish**, **Dr. Bob Meisel**, and most especially **Dr. Linda McLoon**, whose support and guidance have been invaluable.

I am also very thankful for the funding sources that made my project possible. Funding for my research was provided by a **NIH predoctoral training grant 5T32GM008471-23**, a **MnDRIVE Neuromodulation Fellowship**, **NSF Grants #1454904** and **#1451007** (to K.A.M.), and a **Grant-in-Aid** (UMN). Additionally, I was able to present my findings at the International Congress for Neuroethology thanks to a **Heiligenberg Travel Award** (International Society for Neuroethology), and was able to attend a computational neuroscience short course at the Okinawa Institute of Science and Technology thanks to a **Stark Award** (Graduate Program in Neuroscience).

Last, but never least, I would like to thank my family for their love and support, including my mother **Bonnie**, my father **Alan**, my brother **David**, and my mother-in-law **Selden**. Finally, I would like to thank my husband **Mahlon**, who has held my hand literally and figuratively throughout this process, and for whom I am very grateful.

DEDICATION

To my parents, Bonnie and Alan Newhoff. Mom, for your limitless faith in my ability to achieve whatever my heart desires, and for your unwavering support of my academic adventures, even when they take me very far from home. Dad, for introducing me to science and continually fostering your own curiosity of how the world works in me, your eternally grateful daughter.

ABSTRACT

Focused ultrasound is an emerging neuromodulation technology with the unique potential to noninvasively modulate neuronal activity in deep brain structures with high spatial specificity, offering a potential alternative to invasive neural stimulators. Decades of research have confirmed that ultrasound induces profound effects on neuronal firing rates in a wide range of animal systems, yet the direction (increase or decrease) and primary effector of these effects remain a subject of debate. Here, we describe experiments designed to assess these core questions in a tractable invertebrate model, the medicinal leech (*Hirudo verbana*). We examined the effects of ultrasound (960 kHz) on an identified motoneuron, a class of cells believed to lack canonical mechanosensitive ion channels, and whose response to ultrasound we predict to be reflective of effects on most neuronal cell types. We observed both neuronal excitation and inhibition, with a bias towards inhibitory effects. These effects were direct, and persisted in the presence of synaptic blockers. Importantly, these effects were only observed when applying ultrasound of sufficient duration to generate heating in excess of 2 °C. Similar durations of ultrasound in a low-heat paradigm were insufficient to induce changes in neuronal firing rate. We thus concluded that heat is the primary effector of ultrasound neuromodulation in this system, which was reinforced by our ability to elicit comparable effects through the targeted application of heat alone. Additional experiments using non-thermal short pulses of ultrasound on sensory neurons failed to produce neuronal activation at and

above intensities at which others have reported excitation, with the exception of effects we deemed artifactual due to electrode resonance, and which could be reliably mimicked with micromovements of the recording electrode. We conclude that the mechanical effects of ultrasound, which are frequently described in the literature, are less reliably achieved than thermal effects, and observations ascribed to mechanical effects may be confounded by activation of synaptically-coupled sensory structures or artifact associated with electrode resonance. Nonetheless, ultrasound can generate significant modulation at temperatures < 5 °C, which are believed to be safe for moderate durations. Ultrasound should therefore be investigated as a thermal neuromodulation technology for clinical use.

TABLE OF CONTENTS

LIST OF TABLES

LIST OF FIGURES

CHAPTER 1

Introduction: Ultrasound as an emerging neuromodulation modality

1.1 | Overview

Focused ultrasound (FUS) neuromodulation uses high frequency sound (>20 kHz, the upper limit of sound frequencies audible to humans) to modulate neuronal activity. It is an emerging technology with tremendous clinical potential for the treatment of neurological disorders. Interest in FUS neuromodulation has soared in recent years, buoyed by the success of implantable neuromodulation technologies including deep brain stimulation, which has proven therapeutic in treating disorders ranging from epilepsy to Parkinson's disease (Miocinovic et al., 2013). Unlike other noninvasive technologies including transcranial magnetic stimulation (Deng et al., 2013) and transcranial direct current stimulation (Neuling et al., 2012), FUS is able to deliver energy noninvasively to deep brain areas with spatial specificity on the order of millimeters (Hynynen and Clement, 2007; Ai et al., 2016), sparing future patients the risks and financial burdens associated with surgical placement of implanted devices. Though the use of FUS in combination with non-endogenous ion channels is currently under investigation ("sonogenetics"(Ibsen et al., 2015; Ye et al., 2018)), FUS neuromodulation does not require the heterologous expression of proteins a la optogenetics (Fenno et al., 2011), and thus avoids subjecting patients to genetic manipulation. In sum, FUS's precise yet noninvasive nature yields strong advantages over current neuromodulatory technologies, and the technique merits intensive investigation

on a basic level (the subject of this thesis), as well as synergistic development on a clinical level.

1.2 | History

Ultrasound is a natural phenomenon; sounds at frequencies up to ca. 200 kHz are utilized by a diverse array of animal species to communicate with their young (Portfors and Perkel, 2014), detect prey (Jones and Holderied, 2007), evade predators (Kawahara and Barber, 2015), and navigate (Au, 2004). The origins of man-made ultrasound date to the Curie brothers' 19th century discovery of piezoelectricity, a concept wherein the application of pressure to some materials including quartz generates an electrical potential (and it's reverse: application of a potential generates pressure) (Newman and Rozycki, 1998). The development of ultrasound technology was subsequently accelerated during the first world war, fueled by demand for SONAR-based submarine detection (Manbachi and Cobbold, 2011).

The effects of ultrasound on living organisms were first documented in 1927, wherein its application for several minutes was found to be lethal to "lower forms of life" including fish and frogs (R. W. Wood and A. L. Loomis, 1927). The following year, the first examination of ultrasound's effects on nervous tissue was undertaken, and it was reported that ultrasound was unable to stimulate frog sciatic nerves (Harvey and Loomis, 1928). Intensive study of FUS's effects on the nervous system began in the 1950s by W. J. Fry, F. J. Fry, and others.

Reports from this era included descriptions of FUS-induced suppression of neural firing in the crayfish ventral nerve cord and frog spinal cord (Fry et al., 1950; Wulff et al., 1951), and reduction of amplitude of visual evoked potentials following sonication of the lateral geniculate nucleus in cats (Fry et al., 1958).

Early reports of FUS's excitatory actions date to the 1970s. This work, spearheaded by L. R. Gavrilov and others, demonstrated the technology's ability to activate mechanosensory structures when targeting human skin (Gavrilov et al., 1977a) and isolated Pacinian corpuscles from cats (Gavrilov et al., 1977b). FUS was also found to evoke auditory potentials in frogs (Gavrilov et al., 1977b), cats (Wiederhold, 1978), and humans (Tsirulnikov et al., 1988).

Non-sensory FUS-induced excitation was described in the 1980s, when a report was published describing stimulation of non-sensory mammalian cortex in cats and rabbits (Velling and Shklyaruk, 1988). In the last 15 years, this idea has gained tremendous traction as interest in FUS neuromodulation has surged, though the ability of FUS to activate non-sensory structures remains, in some circles, a matter of debate.

1.3 | Effect direction

The current Renaissance of FUS neuromodulation has yielded dozens of publications describing effects on an ever-increasing array of animal species (invertebrate, reptile, mammal) in diverse paradigms (transcranial, peripheral nerve, cell culture, slice, etc.). Despite this enormous collective undertaking,

researchers have thus far failed to reach a consensus regarding the technology's most critical element; that is, whether FUS induces neuronal excitation or inhibition. The following section provides an overview of the FUS neuromodulation literature to date. Studies employing high-intensity focused ultrasound (HIFU) have been omitted. Although some researchers have found success in blocking action potential conduction with HIFU (Foley et al., 2008; Lee et al., 2015a, 2015b), it is more commonly used for destructive applications (e.g., ablating tissue) (Elhelf et al., 2018). Most neuromodulation researchers have opted to use less destructive low-intensity FUS that falls within the FDA-permissible range for non-ophthalmic diagnostic applications (spatial peak pulse average intensity (I_{SPPA}) of $\leq$ 190 W/cm^2) (FDA, 2019); this work is discussed below.

1.3.1 | Transcranial brain studies

Transcranial FUS (tFUS) applications have been the subject of enthusiastic research, as there exists tremendous demand for noninvasive neuromodulatory therapies to normalize pathological aberrant firing in cortical (e.g., epilepsy (Chevassus-Au-Louis et al., 1999)) and subcortical (e.g., Parkinson's disease (Galvan and Wichmann, 2008)) brain areas. Output metrics vary, but are commonly tFUS-induced changes in the amplitude of sensory-evoked potentials (SEPs) (Kim et al., 2014; Legon et al., 2014; Chu et al., 2015; Kim et al., 2015; Legon et al., 2018a; Darrow et al., 2019), or motor responses

(Tufail et al., 2010; Kim et al., 2012; King et al., 2013; Younan et al., 2013; Mehić et al., 2014; Kamimura et al., 2015; Lee et al., 2016). The majority of studies examining effects on the SEPs report reductions in amplitude; these include reduction of somatosensory-evoked potentials in rats (Chu et al., 2015; Darrow et al., 2019) and humans (Legon et al., 2014, 2018a), and visual-evoked potentials in rats. By contrast, studies examining motor responses typically report excitation, including the elicitation of limb movements in mice (Younan et al., 2013; Mehić et al., 2014; Kamimura et al., 2016) and sheep (Lee et al., 2016).

A few groups have explored the use of fMRI blood-oxygen-level dependent (BOLD) signal as a signifier of tFUS-induced neuromodulation. One group reported an increase in BOLD signal in the thumb-mapped portion of primary motor cortex in humans when tFUS was applied during a thumb-tapping task (Ai et al., 2018). Another human study found a tFUS-induced reduction in BOLD signal in the somatosensory cortex, which aligned with EEG-measured reductions in somatosensory-evoked potential amplitudes (Chu et al., 2015). Intriguingly, a third group reported a tFUS-driven increase in BOLD signal in the motor cortex of rabbits and a decrease in BOLD signal in the visual cortex (Yoo et al., 2011a), with response direction biased by pulse parameters. This "bimodal" effect, in which dual responses may be obtained in the same system with the same or different parameters, has been reported in other transcranial studies (Velling and Shklyaruk, 1988; Wattiez et al., 2017).

Several groups have also examined the effects of tFUS on behavior, a more nuanced metric that evades binary classification as excitatory or inhibitory. In humans, it was shown that tFUS targeting the primary sensory cortex increased performance on a two-point discrimination task, suggesting an improvement in tactile sensitivity (though somewhat counterintuitively, the authors also reported a tFUS-driven reduction in the amplitude of somatosensory-evoked potentials) (Legon et al., 2014). In another study, it was reported the tFUS applied to the thalamus of rats quickened the time to emergence of voluntary movement following sedation (Yoo et al., 2011b). In monkeys, tFUS applied to the prefrontal cortex is reported to disrupt saccade processing in the frontal eye fields, as measured by changes in anti-saccade latency (Wattiez et al., 2017). While these latter studies are interesting, it remains difficult to fully interpret the effects of tFUS on behaviors mediated by recruitment of multiple brain areas.

1.3.2 | Peripheral mammalian studies

In addition to the aforementioned transcranial studies, there is enthusiasm regarding FUS's potential as a peripheral neuromodulatory therapy. Invasive peripheral nerve stimulation is currently utilized in the treatment of chronic pain (Chakravarthy et al., 2016); FUS could potentially provide a noninvasive alternative to implantable devices. Several mammalian peripheral studies have explored effects on the sciatic nerve, though reported outcomes have varied.

One group reported that FUS applied to the sciatic nerve evoked muscle activity in mice (Downs et al., 2018), while another, also in mice, found that FUS was unable to evoke potentials, though it did increase the conduction velocity of single units (Ilham et al., 2018).

Cranial nerves have also been targets of attempted FUS modulation. One group transcranially targeted the abducens nerve in rats, and were successful in eliciting abductive eye movements (Kim et al., 2012). Another group working in rats targeted the vagus nerve, and reported a predominately inhibitory effect (Juan et al., 2014). Efforts to modulate the vagus nerve via FUS may prove especially fruitful, as implantable vagus nerve stimulators have demonstrated the therapeutic potential for the treatment of several neurological and inflammatory disorders, and are currently FDA-approved for the treatment of epilepsy and depression (Johnson and Wilson, 2018).

1.3.3 | In vitro studies

Determining effect direction in intact systems, particularly with respect to transcranial studies, can be confounded by factors including skull reflection and incidental activation of mechanosensitive sensory structures, including auditory hair cells in the cochlea. The former can cause unintended delivery of FUS to off-target areas, particularly in small animals (Younan et al., 2013). The latter has been demonstrated to generate broad cortical activation independent of focus location in guinea pigs (Guo et al., 2018). A similar result was reported in mice

(Sato et al., 2018), which were also found to exhibit auditory-based startle reflexes in response to FUS application, a finding with implications for studies that report FUS-induced elicitation of movement (Younan et al., 2013; Mehić et al., 2014; Kamimura et al., 2016; Lee et al., 2016).

Researchers seeking to clarify the effect direction of FUS and its mechanisms of action have attempted to circumvent these confounding constraints through the use of *in vitro* mammalian preparations or invertebrate models. With respect to *in vitro* preparations, groups have described effects in cultured primary neurons and slice preparations, though the directions of these reported effects are inconsistent.

Several studies have examined effects in rodent hippocampal slice preparations. One group reported that FUS elicited Na^+ and Ca^{2+} transients and evoked action potentials in CA1 neurons in mice (Tyler et al., 2008). Another group reported FUS-induced reduction in evoked fiber volley and dendritic potentials of CA1 neurons from rats (Rinaldi et al., 1991). A third group, recording from the dentate gyrus of rats, found response direction varied with respect to hippocampal sublayer; fiber volleys and cell bodies were inhibited, but dendritic potentials were enhanced (Bachtold et al., 1998).

The few reports of neuromodulation outcomes in cultured neurons have largely described FUS-driven excitation. Cultured primary neurons from embryonic rats were reported to display increased firing when targeted with FUS (Khraiche et al., 2017). Others found that FUS induced increases in neuronal

activity in mouse primary neurons as measured by an increase in c-Fos (Qiu et al., 2019). A third group found FUS elicited action potentials in cultured hippocampal neurons that heterologously expressed a mechanosensitive bacterial ion channel; however, this effect was absent in the wild-type control cells (Ye et al., 2018).

1.3.4 l Reptile studies

The earliest nervous tissue exposed to FUS in a laboratory environment was from the frog (Harvey, 1929). In recent years, several groups have examined effects of FUS on the frog sciatic nerve. One group reported FUS-induced inhibition attributed to conduction block (Colucci et al., 2009), while two others reported both neuronal enhancement and suppression, with outcomes biased by parameters (Mihran et al., 1990; Tsui et al., 2005).

In salamanders, two papers have described the effects of FUS on the *ex vivo* retina. FUS was found to indirectly stimulate retinal ganglion cells via activation of photoreceptors and post-photoreceptor interneurons (Menz et al., 2013, 2019).

1.3.5 l Invertebrate studies

Explorations of FUS's effects on invertebrate nervous systems date back to at least the 1960s (Lele, 1963), but the last five years have produced a flurry of FUS publications utilizing "simpler" systems, which offer greater accessibility and

fewer regulatory constraints. These systems typically contain far fewer neurons than mammalian models, and their neurons – many of which can be identified across specimens – are often highly stereotyped with respect to their membrane and synaptic properties. These characteristics aid investigators in reducing experimental variability associated with, for example, incidental targeting of different sub-populations of cells across preparations, which could account for some of the differences in reported outcomes among researchers studying mammalian systems. Unfortunately, despite these advantages, the inconsistencies in effect direction present in the mammalian FUS neuromodulation literature is similarly present in the invertebrate literature.

A few studies have examined the effects of FUS on the nematode *C. elegans*. One group reported that wild-type *C. elegans* were insensitive to low-intensity FUS, though heterologous expression of a mechanotransductive ion channel sensitized neurons to FUS, causing the mutant strain to exhibit behavioral responses following its application (Ibsen et al., 2015). A second group failed to replicate this finding, but reported that wild-type nematodes did respond to FUS perturbation, and this behavioral response was dependent on the expression of a mechanosensitive ion channel involved in touch sensation (Kubanek et al., 2018). A third group similarly found that FUS was able to initiate a behavioral response by activating a mechanosensitive cell (Zhou et al., 2017).

Another popular invertebrate model is the giant axon of the earthworm. One group found that FUS application to the lateral giant fibers of the axon was

effective in eliciting trains of action potentials (Vion-Bailly et al., 2017). A different group reported an FUS-induced reduction in action potential amplitude and conduction velocity following sonication. A third group, targeting the medial and lateral giant fibers, replicated this reduction in action potential amplitude, though they did not observe a decrease in conduction velocity (Yoo et al., 2017).

Others have published a series of papers documenting the effects of FUS on the crab leg nerve. Each describe the ability of FUS to stimulate *ex vivo* nerves, including by the generation of *de novo* action potentials (Wright et al., 2015, 2017; Wright, 2016; Saffari et al., 2017). Excitation was also reported in a crayfish paradigm, in which FUS was found to depolarize an isolated motor axon (Lin et al., 2019a), In the leech, it was found that FUS could elicit action potentials in a sensory cell (Dedola et al., 2020).

1.3.6 | The role of parameters in biasing effect direction

The aforementioned studies demonstrate the variability in reported response direction that pervades the FUS neuromodulation literature, regardless of system (e.g., mammalian or invertebrate) or paradigm (e.g., transcranial or peripheral). Among the few studies that have reported both excitatory and inhibitory outcomes, several authors have cited parameter selection as a contributing factor to the resultant effect direction (Velling and Shklyaruk, 1988; Tsui et al., 2005; Juan et al., 2014; Kim et al., 2015).

The parameter space for FUS is immense, and an exhaustive discussion of the myriad parameter combinations that have been employed in neuromodulation studies is beyond the scope of this thesis (for reference, these combinations were recently reviewed by Pasquinelli et al (Pasquinelli et al., 2019)). The following paragraphs provide a brief introduction to ultrasound parameters and their relation to the bioeffects of FUS on tissue, as well as how they factor into safety regulations governing clinical applications.

FUS waveforms are characterized by two key variables: frequency (cycles per second, measured in Hz) and pressure amplitude (measured in Pa). Pressure oscillates from positive (compresses tissue) to negative (expands tissue) with each cycle of FUS. Negative pressure applied to a fluidic medium (e.g. most body tissues) can generate cavitation bubbles from dissolved gasses within this medium. These microbubbles, typically several microns in diameter, oscillate in size and can collapse (inertial cavitation), resulting in destructive mechanical stress and localized heating (Azhari, 2010). Cavitation increases with increasing peak negative pressure and decreases with frequency. This relationship is described by the Mechanical Index (MI), a measure of cavitation risk. For non-ophthalmic diagnostic applications, FDA guidelines require MI to be less than or equal to 1.9 (FDA, 2019).

1.3.7 | Mechanical index

$$MI = \frac{Max(P_n)}{\sqrt{f}} \quad where \quad P_n = \text{negative pressure}, \; f = \text{frequency}$$

FUS is frequently pulsed in neuromodulatory contexts to reduce the risk of rapid heating, which can occur with continuous applications of ultrasound. The number of pulses per second is the pulse repetition frequency (PRF, measured in Hz), and the pulse duration (PD) is the duration in seconds of each pulse. The duty cycle, or percentage of time ultrasound is actively delivered during the application period, is the PRF x PD.

Ultrasound intensity is a measure of the amount of energy delivered to tissue. One common metric reported by FUS neuromodulation researchers is the spatial peak pulse average intensity (I_{SPPA}), a measure of the average intensity of a single ultrasound pulse at the location of peak pressure within the ultrasound focus. The I_{SPPA} varies by tissue type, dependent on the speed of sound in the targeted tissue and the tissue density. For reference, the speed of sound in human nervous tissue is approximately 1500 m/s; the density of nervous tissue is approximately 1.06g/cm^3 (Azhari, 2010). FDA-permissible I_{SPPA} for non-ophthalmic diagnostic applications is $\leq$ 190 mW/cm^2.

1.3.8 I I_{SPPA}

$$I_{SPPA} = \frac{P_n^2}{2\rho c} \quad where \quad \begin{array}{rcl} P_n & = & \text{peak negative pressure} \\ \rho & = & \text{tissue density} \\ c & = & \text{speed of sound in tissue} \end{array}$$

Another commonly reported intensity metric is the spatial peak time averaged intensity (I_{SPTA}), the average intensity of the pulse repetition period. The I_{SPTA} is equal to I_{SPPA} x duty cycle. Higher I_{SPTA} yields greater tissue heating. FDA-approved upper limits for I_{SPTA} vary by tissue type, from 720 mW/cm^2 for peripheral vessel applications, to 94 mW/cm^2 for cephalic (adult and fetal) applications (FDA, 2019).

Parameter selection can bias the type of bioeffects induced by FUS in targeted tissue. Higher frequencies are associated with greater tissue heating (though this effect is nonlinear, and dependent on tissue type), as are higher intensities and longer periods of acoustic radiation (Azhari, 2010). Cavitation increases with pressure and decreases with frequency (see MI equation). Importantly, heat and mechanical stress can each induce a wide range effects on nervous tissue, many of which could result in an increase or decrease in neuronal firing.

1.4 | Proposed Mechanisms of Action

Debate persists among researchers studying FUS neuromodulation with respect to the precise FUS-induced bioeffects that underlie effects, a question that has plagued investigators since the field's infancy (Fry, 1953). The most popular theories of the neuromodulatory mechanisms underlying FUS attribute effects to mechanical stress (direct or via cavitation) or heat. Most 21st century FUS investigations have cited mechanical effects as the probable primary driver

modulating neural activity (e.g., (Tufail et al., 2010; Wahab et al., 2012; Kim et al., 2015; Wright et al., 2017; Kubanek et al., 2018; Dedola et al., 2020)). These mechanical effects are most often predicted to influence neuronal firing via the mechanical gating of ion channels or by alternating membrane capacitance.

1.4.1 | Mechanical Gating of Ion Channels

Many ion channels have mechanosensitive properties. While this property is particularly well-established for classes of channels involved in the transduction of sensory stimuli (e.g., TRP (Christensen and Corey, 2007), Piezo (Coste et al., 2010), ASIC (Lee and Chen, 2018)), evidence is accumulating that other types of ion channels, including voltage-gated ion channels, also have some degree of mechanosensitivity. FUS activation of voltage-gated sodium channels, of particular interest to neuromodulation researchers given their role in generating the rising phase of the action potential, has been cited as a potential driver of FUS-induced neuronal excitation (Tyler et al., 2008; Tufail et al., 2010; Wright et al., 2015; Kubanek et al., 2018). These channels have known mechanosensitive properties (Morris and Juranka, 2007), and prior work has shown that FUS increases channel conductance when heterologously expressed in *Xenopus* oocytes (Kubanek et al., 2016). At present, however, evidence remains weak that FUS activation of voltage-gated sodium channels is an effective actuator of excitation in neurons. In crayfish axons, FUS-induced depolarization persisted following application of the channel blocker TTX (Lin et

al., 2019a). Additionally, in cultured mammalian neurons, high frequency FUS (43 MHz) was not sufficient to activate sodium channels in a patch clamp preparation (Prieto et al., 2018). Assessing the precise contribution of these channels to FUS-induced increases in firing rate remains difficult, as channel blockers concurrently block neuronal firing.

Another family of channels that has been implicated in FUS neuromodulation is the two-pore potassium channel (K2P), a family of potassium-permeable leak channels. Subtypes TRAAK, TREK-1 and TREK-2 are highly mechanosensitive, widely expressed in the CNS, and display increased conductance in response to changes in membrane tension induced by sub atmospheric pressure and laminar stress (Enyedi and Czirják, 2010). FUS has been shown to increase conductance of these channel subtypes when expressed in *Xenopus* oocytes (Kubanek et al., 2016). Increases in K2P conductance hyperpolarizes neurons; effects on these channels could contribute to FUS-induced inhibition.

Perhaps unsurprisingly, FUS has also been shown to activate canonical mechanosensitive ion channels. In cultured mammalian neurons, FUS increased conductance of Piezo1, a channel believed to be a primary actuator of somatosensory mechanotransduction (Prieto et al., 2018). The broader contribution of Piezo channels to FUS-induced neuronal excitation, however, remains unclear. Although these channels are highly expressed in sensory

neurons, including those in dorsal root ganglia, expression in the CNS is at least 10-fold lower (Coste et al., 2010).

In *C. elegans*, a behavioral response to FUS has been shown to be dependent on expression of MEC-4, a pore-forming component of a mechanosensitive channel expressed by sensory neurons and belonging to the DEG/ENaC/ASIC family (Kubanek et al., 2018). Most mammalian members of this voltage-independent, sodium-selective channel family are expressed primarily in sensory neurons and are believed to contribute to somatosensation (Eastwood and Goodman, 2012). Acid-sensing ion channels (ASICs), however, are broadly expressed in the CNS (Boscardin et al., 2016). DEG/ENaC/ASIC channels have largely conserved sequences and highly similar structures (Eastwood and Goodman, 2012); it is entirely probable that FUS is able to activate mammalian channels in a manner comparable to its activation of an invertebrate homolog. Although activation of members of this channel family, particularly ASICs, may contribute to FUS-induced neuronal excitation, whether it is desirable to target these channels (e.g., via specialized parameters) is another matter. ASIC hyperactivity is implicated in the pathology of inflammatory neurological disorders including pain and neurodegenerative disease, and channel inhibitors are currently under exploration as therapeutics (Boscardin et al., 2016).

With respect to FUS activation of other sensory ion channels, a brief mention of the transmembrane channel-like family (TMC) is warranted. To the

best of our knowledge, no studies have directly examined the effects of FUS on these channel-like proteins via two-electrode voltage clamp in *Xenopus* oocytes or elsewhere. Two isoforms of this family, TMC1 and TMC2, are believed to transduce sound stimuli following deflection of the tip links on auditory hair cells in the cochlea (Delmas and Coste, 2013). This is highly relevant to *in vivo* mammalian FUS studies, as FUS has been shown to activate auditory hair cells, in turn causing widespread cortical activation (Guo et al., 2018; Sato et al., 2018). Activation of TMC proteins, the likely actuators of sound transduction, may be responsible for cortical excitation reported in *in vivo* studies.

1.4.2 | Intra- and Extracellular Cavitation

Another popular theory of FUS's excitatory mode of action is cavitation. Intramembrane cavitation, the effects of which have been described by a "bilayer sonophore" model, is proposed to induce excitation via FUS-induced cyclic expansions and contractions of sonophores in the intramembrane space, which in turn modulate membrane capacitance (Krasovitski et al., 2011). Changes in membrane capacitance are predicted to alter ionic currents, resulting in depolarization of the resting membrane potential and a corresponding increase in firing (Plaksin et al., 2014). To the best of our knowledge, FUS-induced intramembrane cavitation-driven neuronal excitation has yet to be empirically demonstrated in neurons.

Cavitation has also been proposed to enact modulation extracellularly by inducing membrane stretch (via microstreaming drag, direct jetting or radiation force), which is thought to increase the conductance of ion channels (Wright et al., 2017). Several invertebrate studies have reported results consistent with an extracellular cavitation mechanism. In crab axons, for example, neurostimulation was found to require high pressures, occur as an “all or nothing” phenomenon (consistent with sporadic formation of microbubbles), and occasionally induce tissue damage, as is known to accompany inertial cavitation (Wright et al., 2017). The same group also reported that stimulation in this system occurs in concert with stable or inertial cavitation as measured with a Passive Cavitation Detector, and does not occur in its absence. (Wright, 2016) In earthworms, researchers hypothesized a cavitation-based mechanism, and found that stimulation of the medial and lateral giant fibers was most successful at cavitation-promoting parameters (e.g. higher pressures) (Vion-Bailly et al., 2017). Importantly, these systems applied FUS to isolated axons, utilizing pressures in excess of those used in the majority of mammalian studies reporting FUS-induced excitation. Future work is needed to determine whether cavitation is similarly achievable with nondestructive parameters in intact preparations and thus might be FUS’s primary excitatory mode of efficacy.

1.4.3 | Thermal Effects

Tissue absorbs ultrasound as heat, itself a potent neuromodulator (Janssen, 1992). The contribution of tissue heating to the neuromodulatory effects of FUS has been a matter of contention since the field's infancy, with several early groups assuming a thermal mode of action (Lele, 1963; Ueda et al., 1977), and others proposing a nonthermal mechanism (Fry et al., 1950, 1958; Barnard et al., 1955; Takagi et al., 1960). Some early justifications for a nonthermal mechanism stem from assumptions since proven false. One group dismissed the possibility of thermal suppression of firing of the crayfish ventral nerve cord at temperatures in the 1-2 °C range; this "slight" temperature increase was believed to be capable only of increasing neural activity (Wulff et al., 1951). It has since been shown that temperature increases close to this range provided via FUS application (Darrow et al., 2019) or other heating modalities (e.g., infrared (Cayce et al., 2011; Lothet et al., 2017)) can, indeed, inhibit neuronal activity. Other groups argued against a thermal effect by demonstrating that bath heating to equivalent temperatures to those induced by FUS failed to elicit a comparable response (Fry et al., 1950; Takagi et al., 1960). More recent work has shown that thermal effects are, in part, dependent on the spatial dimensions of tissue heating (Wells et al., 2007a), a factor lost by manipulating broad bath temperature. My results in Chapter III further demonstrate the relevance of the spatial distribution of a thermal stimulus.

Heat has been reported to have a wide range of effects on the nervous system, many of which could contribute to excitatory or inhibitory FUS

neuromodulation (or both). On a basic level, heat potentiates enzymatic reactions. Many neuronal functions are governed by these reactions, and are thus susceptible to thermal modulation. One example is the N^+/K^+-ATPase enzyme that maintains sodium and potassium ion concentration gradients, whose activity is known to increase in hyperthermic conditions (Gorman and Marmor, 1970). This pump exchanges three intracellular sodium ions for two extracellular potassium ions with each cycle (Kaplan, 2002); increasing pump activity thus has a net hyperpolarizing effect, which could inhibit neuronal firing.

Heat is also known to increase the gating kinetics of ion channels (Janssen, 1992), the gross effects of which would depend on the channels most affected. As previously mentioned, voltage-gated sodium channels are commonly cited as potential actuators of FUS neuromodulation (Tyler et al., 2008; Tufail et al., 2010; Wright et al., 2015; Kubanek et al., 2018). The gating of these channels has long been known to be influenced by temperature—as temperature rises, sodium conductance increases, though inactivation kinetics are also increased (Collins and Rojas, 1982). The implications of FUS-induced heat on sodium channels would depend on which effect was dominant – increased sodium conductance would excite neurons, while accelerating channel inactivation would result in inhibition via conduction block.

Another channel family implicated in an FUS response, K2P, has members known to be highly thermosensitive. The three channel subtypes shown to be responsive to FUS stimulation (TREK-1, TREK-2, and TRAAK)

(Kubanek et al., 2016) are particularly sensitive to changes in temperature. Specifically, heat is known to potentiate the activity of these potassium-permeable leak channels, which inhibits neural activity by hyperpolarizing the resting membrane potential (Schneider et al., 2014).

Finally, heat has also been shown to influence synaptic activity. Heat is believed to act presynaptically by facilitating synaptic vesicle exocytosis, and to exert further influence on neuronal signaling by modulating the diffusion of neurotransmitters in the synaptic cleft (Wang et al., 2014). This is noteworthy, as it remains an open question whether many observed effects of FUS are direct, or result from input from synaptically coupled sensory cells (Guo et al., 2018; Sato et al., 2018). Though heat may not be the primary actuator in the latter instances, it could nonetheless potentiate these synaptic effects.

The preceding paragraphs describe a small number of heat's myriad effects on neuronal function. While elucidating the contribution of heat to FUS neuromodulation may appear overwhelming, from a basic science perspective, its many potential actions ensure that FUS-generated heat holds tremendous possibility as a clinical neuromodulatory therapy. Despite this promise, there remains a reluctance on the part of FUS researchers to embrace heat as a viable neuromodulatory mechanism. One cited factor for this reluctance is the potential for heat to damage tissue (Tyler et al., 2018). This concern, however, is unfounded and based on several early studies where heat-attributed damage was found following FUS application. For example, in one report, FUS applied to

cat brain induced localized temperature increases of up to 20°C, causing demyelination of white matter, hemorrhage, and necrosis (Barnard et al., 1955). While this damage was striking, it should be noted that this type of FUS-induced temperature increase was far beyond that which has been shown to effect neuromodulation (ca. 2°C (Darrow et al., 2019), which is presumed safe for exposures of < 1 hour (Haar, 2011)).

While my colleagues and I are of the opinion that a thermal mode of action does not preclude clinical usage of FUS neuromodulation, additional research is needed to determine the extent to which heat contributes to FUS's effects. Two ways to address this question are by examining changes in observed effects following heat minimization, and by attempting to faithfully replicate FUS-induced heating (e.g., while maintaining a similar spatial profile). Thus both efforts are described in Chapter II.

1.5 | The Single-Cell Approach

The previous section illustrates the major mechanisms hypothesized to underlie FUS neuromodulation. Despite tremendous efforts by researchers, it remains unclear which mechanism(s) are primarily responsible for observed effects, and whether these effects, in the absence of confounding factors including the activation of sensory structures, are excitatory or inhibitory in nature. Determining this technology's root effect is prohibitively difficult in intact mammalian systems, in which results may be biased by unintentionally targeting

different subpopulations of neurons across preparations, incidentally activating mechanosensitive sensory receptors, or causing other off-target effects due to factors including skull reflection.

In recognition of the limitations posed by intact neural systems, FUS neuromodulation researchers investigating mechanisms of action have applied their efforts to pared down systems, typically cultured mammalian neurons (Rinaldi et al., 1991; Mihran et al., 1996; Prieto et al., 2018; Qiu et al., 2019), mammalian slice preparations (Rinaldi et al., 1991; Bachtold et al., 1998; Tyler et al., 2008; Muratore et al., 2009), or tractable invertebrate models (Wahab et al., 2012; Wright et al., 2015; Vion-Bailly et al., 2017; Zhou et al., 2017; Kubanek et al., 2018; Lin et al., 2019a; Dedola et al., 2020). Isolation in culture is known to alter the intrinsic electrical properties of neurons (Turrigiano et al., 1994); FUS effects on cultured cells may thus differ from outcomes in intact systems. Slice preparations, which maintain some neural circuitry, benefit from "natural" neuronal activity, yet lack experimental flexibility, particularly when compared to highly tractable invertebrate models. I have adopted this latter strategy by exploring the effects of FUS on identified neurons in the medicinal leech, *Hirudo verbana*. This approach requires sacrificing the use of perfect proxies of intact mammalian neurons (invertebrate neurons, for example, lack myelin), but benefits from a tremendous gain in experimental accessibility. Moreover, the basic properties of most invertebrate neurons closely resemble those in mammalian neurons; invertebrates have been the subject of many seminal

investigations that defined major principles of neuroscience, most notably the determination of the ionic currents underlying the action potential in the squid giant axon (Hodgkin and Huxley, 1952), and the discovery of the molecular basis of learning and memory in the sea slug (Walters et al., 1979; Glanzman, 1995).

1.6 | The Medicinal Leech, *Hirudo verbana*

The experiments described in this thesis utilized the medicinal leech, *Hirudo verbana,* as the experimental model of choice. The medicinal leech has a uniquely rich and storied history as a tractable and experimentally accessible animal preparation to study the structure and function of the nervous system. Its extensive use in medicine until the turn of the 20th century ensured its presence in the earliest neuroscience laboratories, where it attracted the interest of anatomists including Ramon y Cajal and Gustav Retzius (Muller et al., 1982).

The leech CNS consists of a cephalic compound ganglion (“head brain”), a caudal compound ganglion (“tail brain”), and a ventral nerve cord interspersed with 21 segmental ganglia. These ganglia contain approximately 400 neurons separated into “packets” by giant glial cells, and are highly stereotyped with the exception of ganglia 5 and 6, which innervate the sex organs (Muller et al., 1982). Leech neurons are 10-80 μm in diameter, monopolar, and form synaptic connections within the neuropil, the glia-lined layer sandwiched between somata on the dorsal and ventral surfaces of the ganglia (Muller et al., 1982). Like other invertebrates, leeches lack myelinating glia. Their giant glial cells are electrically

coupled and regulate the potassium concentration of the extracellular milieu in a manner comparable to astrocytes in vertebrates (Muller et al., 1982).

1.6.1 | Identified Neurons

Roughly 50% of the ~400 neurons in the segmentally-arranged (non-sex) ganglia of the leech have been described, and can be identified across preparations by their location and physiological properties (Kristan et al., 2005). Most neurons are paired with a contralateral homolog; thus, the number of unique neuronal types per ganglion is close to 200. Among these neuronal types are sensory neurons, including the T ("touch"); P ("pressure"); and N ("nociceptive") cells, which respond to heat and tactile stimuli of increasing magnitude, interneurons, and motoneurons, including the Dorsal Excitor cell 3 (DE-3), which is essential for the generation of rhythmic motor behaviors including swimming and crawling (Muller et al., 1982). Other cells, including the large Retzius neurons, have more complex neuromodulatory roles.

1.6.2 | Major Conductances

Leech action potentials are governed by the same classes of ion channels that generate mammalian action potentials. Voltage clamp studies performed in the 1980s on leech neurons demonstrated the existence of voltage-gated sodium, potassium, and calcium currents (Stewart et al., 1989). Recently, the leech transcriptome was published in collaboration with the Mesce lab, which

confirmed the expression of the major classes of voltage-gated ion channels, as well other types of ion channels implicated in FUS responses in mammalian systems, including TRP and K2P (Northcutt et al., 2018).

As in vertebrates, spike waveforms vary considerably across neuronal subtypes (e.g., sensory cells generate much larger amplitude spikes than motoneurons), which has been attributed to relative differences in the density of voltage-gated sodium channels, as well as differences in the types of potassium channels expressed (e.g., motoneuron potassium channels have faster activation and inactivation dynamics, yielding a shorter duration spike) (Stewart et al., 1989). These differences are apparent when examining spike waveforms from the neurons utilized in the experiments in this thesis; DE-3 neurons (Chapter II) have a truncated waveform with minimal undershoot, while Retzius cells (Chapter III) have a larger amplitude and more closely resemble a typical mammalian spike. These cells are discussed in greater detail in the following paragraphs.

1.6.3 | The DE-3 Motoneuron

The experiments described in Chapter III describes the empirical effects of FUS when applied to the Dorsal Excitor cell 3 (DE-3) motoneuron. DE-3 excites the dorsal longitudinal muscles of the leech, firing phasically during swimming and crawling behaviors (Granzow et al., 1985). Its soma is located on the dorsal surface of each ganglion (bilaterally paired), and its axon exits the ganglion

through the contralateral dorsal posterior (DP) nerve. Its spike is the largest spontaneously active unit in an extracellular DP recording. DE-3 is electrically coupled to its contralateral homolog, as well as to ~20 other motoneurons and interneurons (Fan et al., 2005).

We intentionally chose first to assess the effects of FUS on a motoneuron, a class of neurons not "built" to respond to mechanical stimuli. Effects on motoneurons, which are unlikely to express canonical mechanotransductive ion channels, are more representative of the effects of FUS on a broad range of neuronal cell types other than sensory neurons, which possess unique cellular machinery to sense and transduce mechanical stimuli.

1.6.4 | The Retzius Neuron

The experiments described in Chapter IV were performed on the bilaterally paired Retzius neurons, which were first described by Gustav Retzius in 1891 (Carretta, 1988). These experiments required rapid exit and re-entry of the same cell; the large (50-80 μm) Retzius cell somata, located centrally on the ventral surface of each ganglion, are much more rapidly identifiable than the smaller, dorsal DE-3 somata. The function of Retzius neurons is more complex than that of DE-3. These cells are believed to play a modulatory role over the animal's behavior. This is achieved in part by releasing serotonin, which is known to induce swimming in the leech in response to synaptic input from sensory afferents (Kristan et al., 2005). Retzius neurons have been shown to respond to

several neurotransmitters common to mammalian systems, including acetylcholine, which increases cell firing via activation of both nicotinic and muscarinic receptors, and serotonin and dopamine, which hyperpolarize Retzius cells through the activation of chloride channels (Carretta, 1988).

Bilaterally paired Retzius neurons are electrically coupled, and are nearly isopotential (Carretta, 1988). This proved advantageous in one set of experiments described in Chapter III. In these experiments, we recorded the membrane potential and spike properties from one Retzius cell prior to the application of FUS. Following FUS, we returned to the same cell or the contralateral cell to assess possible outcomes on membrane properties. The contralateral cell served as an internal control, enabling us to determine if FUS-associated actions could be linked to whether the cell had been impaled prior to FUS application. This exercise would test whether the electrode impalement might have caused a leak current, thus confounding the effects of FUS.

1.6.5 | Advantages over other systems

The leech is an advantageous animal preparation in which to explore the cellular effects of FUS. As the preceding paragraphs attest, the leech is exceedingly well characterized with respect to identified neurons and their conductances. Additional key advantages are its size, and the ease with which single units from identified neurons can be recorded intra- and extracellularly. While other commonly utilized invertebrate models share some of these

attributes, they also present one or more limitations that restrict their utility for usage in the types of experiments performed in this thesis.

Several prior studies have examined the effects of FUS in *C. elegans* (Ibsen et al., 2015; Zhou et al., 2017; Kubanek et al., 2018), a popular invertebrate model system due to its limited cell number (ca. 302 neurons), relatively simple neural circuitry, and the ease by which it can be manipulated genetically. Despite the completeness of its genome and connectome, its atypical form of neural signaling somewhat limits its relevance. Unlike all vertebrates and most invertebrates (including leech), *C. elegans* neurons do not express voltage-gated sodium channels, nor do they fire sodium-mediated action potentials; neurotransmission occurs via graded calcium waves (Bargmann, 1998). Thus, the lack of voltage-gated sodium channels may lessen the relevance of FUS-related effects reported in this system, as these channels have been hypothesized to be actuators of FUS's neuromodulatory effects (Tyler et al., 2008; Tufail et al., 2010; Wright et al., 2015; Kubanek et al., 2018). Another limitation in utilizing *C. elegans* in FUS paradigms is its small size (~ 1 mm in length). Targeting subpopulations of neurons, much less single cells, is more difficult in this system than in the much larger leech (for reference, the ultrasound transducer used in the experiments performed for this thesis has a peak focus of approximately 1 mm in diameter). Consequently, two of the three FUS investigations utilizing this model of which we are aware measured gross behavioral responses to FUS stimuli versus individual neuronal responses (Ibsen

et al., 2015; Kubanek et al., 2018). Similar size concerns would apply to another popular invertebrate model system, the fruit fly *Drosophila melanogaster*.

The earthworm, *Lumbricus terrestris*, has also been explored as a model system in FUS experiments. The medial and lateral giant axonal fibers of the worm are large and easily accessible, and the animal's size prevents experimental limitations associated with smaller invertebrates. In contrast to our leech experiments, however, paradigms examining FUS actions have required electrically evoking spikes in these fibers (Wahab et al., 2012; Vion-Bailly et al., 2017; Yoo et al., 2017). Despite widespread use of artificial neuronal electrical stimulation in neuroscience studies, evoked activity is believed to differ intrinsically from natural activity (Albensi et al., 2007); FUS effects on evoked potentials may not necessarily fully reflect effects in intact systems. In addition, the somata of the giant axonal fibers are relatively inaccessible to intracellular recording electrodes, precluding the potential for the types of intracellular experiments described in Chapters II and III, which were made possible by the accessible positioning of leech neuronal somata.

Other groups have reported the effects of FUS on neurons extracted from crabs (Wright et al., 2015, 2017; Saffari et al., 2017) (*Cancer pagurus*). These experiments have investigated the ability of FUS to evoke and modulate compound action potentials (Wright et al., 2015, 2017; Saffari et al., 2017). These compound action potentials measure multiunit activity; interpreting results of the technology's effects on a population level can be challenging, as it is

difficult to determine whether effects stem from a direct inhibition or excitation of all targeted neurons, or from the selective modulation of a subpopulation of cells, which synaptically influence the activity of the remaining population. Ultimately, this approach lacks the precision of measurement of single units, which can easily be achieved in the leech.

In conclusion, the leech has been an exemplary model in which to perform the experiments described in this thesis. The large, robust and identifiable neurons enabled extensive electrophysiological investigations into FUS's neuromodulatory mechanisms. The spontaneous firing properties of neurons including DE-3 and the Retzius neuron permitted analysis of FUS's effects on natural – versus evoked – firing activity. The size and flexibility of the preparation enabled paradigms that are challenging in other systems, including simultaneous intracellular somatic and extracellular axonal recording from the same cell (Chapter II), and intracellular recording during FUS application (Chapter III). The extensive literature describing leech neuronal ionic conductances facilitated prediction of the technology's likely actions, and instructed our efforts in determining contributions of factors including indirect synaptic effects.

It is my hope that the work described here has helped to clarify the neuromodulatory effects of FUS at the single neuron level. In this dissertation I aim to demonstrate that these effects are *predominantly* inhibitory, and that the technology's *principal* actuator is the generation of localized heating. I believe that the thermal properties of FUS have great clinical promise, and merit further

investigation and development towards usage in a clinical neuromodulatory setting.

1.7 | Thesis summary

1.7.1 | Chapter II

Chapter II is adapted from a chapter by Mesce and Newhoff in the book, “The Neural Control of Movement.” This chapter outlines the current understanding of the neural bases of behavior in the leech, with a particular emphasis on crawling, a behavior characterized by prior Mesce lab members in a series of impactful papers. This behavior is dependent on rhythmic activity of DE-3, a motoneuron whose rhythmic firing during crawling is responsible for the contraction phases of the leech crawl cycle. DE-3 was the subject of the majority of experiments performed throughout the course of this thesis; this work is described in Chapter III.

This chapter finishes by describing the utility of the leech as a model in which to test new neural technologies, with an overview of how it has been used in this fashion in the development of new electrophysiological recording modalities, imaging systems, and neuromodulation techniques.

1.7.2 | Chapter III

Chapter III is adapted from a publication by Collins, Legon and Mesce entitled, “Unraveling the actions of focused ultrasound on an identified, single motoneuron.” This paper explores the effects of FUS on the DE-3 motoneuron, a spontaneously firing cell whose large unit can be readily identified in an extracellular recording paradigm. DE-3 activity was predominantly inhibited by FUS. Effects persisted in the absence of synaptic activity, suggesting mechanical activation of synaptically-coupled sensory cells did not contribute to our observed modulation, as had been reported as a confound in other paradigms. All observed effects could be replicated by the targeted application of heat via laser or electrical current. We conclude that FUS inhibition is direct, predominantly thermally mediated, and potentially therapeutically viable as a treatment for neurological disorders characterized by excessive neuronal firing, including chronic pain.

1.7.3 | Chapter IV

Chapter IV is adapted from a publication by Collins and Mesce entitled, “Focused ultrasound neuromodulation and the perils of intracellular electrophysiological investigation.” We describe the potential pitfalls of combining FUS with classical electrophysiological recording techniques. These techniques had previously been combined by other groups to demonstrate that FUS application induces depolarization of the resting membrane potential of single neurons, an effect that could account for FUS-driven neuronal excitation. We first

replicate this FUS-induced depolarization of the resting membrane potential in leech Retzius neurons, finding a dose-dependent effect in which higher intensities and pressures yielded greater depolarizations. This depolarization was accompanied by increases in spike frequency and decreases in spike amplitude comparable to previously reported findings in leech and mammalian neurons. We show, however, that these results can be convincingly replicated through subtle mechanical manipulation of the recording electrode. Electrode resonance is a well-established complication of paradigms combining single-cell recording and FUS application; we conclude that this resonance is likely responsible for observations of FUS-induced membrane potential depolarization recorded in this fashion.

1.7.4 | Conclusion

This dissertation concludes with a retrospective analysis of the likely mechanistic drivers of both excitatory and inhibitory FUS neuromodulation as informed by the experiments described in the previous chapters, as well as extensive probing of the existing literature. I describe how a thermal mechanism, supported by the experimental results reported in previous chapters, could account for seemingly disparate neuromodulatory outcomes, and explore potential avenues for implementing ultrasound as a noninvasive therapy for the treatment of neurological disorders.

CHAPTER 2

Small Steps and Larger Strides in Understanding the Neural Bases of Crawling in the Medicinal Leech

Publication Citation:
Newhoff M, Mesce KA. Small steps and larger strides in understanding the neural bases of crawling in the medicinal leech. In: Whelan PJ and Sharples SA (Eds). *The Neural Control of Movement: Model Systems and Tools to Study Locomotor Function.* San Diego: Elsevier Inc./Academic Press, 2020: 31-55.

2.1 l Summary

The nervous system of the medicinal leech (*Hirudo* species) has often provided elegant solutions to long-standing questions in the field of locomotor control. Such outcomes stem from its easily accessible and relatively large neurons, metameric organization, identified aminergic neuromodulation, and known role of action-selection neurons descending from the brain. Neural circuits underlying leech swimming were first revealed in the 1970s, but it has only been in the past two decades that crawling, the focus of this chapter, has shared the spotlight. In this review, we will discuss the functional architecture of crawling, its differences compared to swimming, and the inherent plasticity that enables the leech to recover its locomotion after injury. We will also underscore the full utility of the leech model while looking towards the future, focusing on the technological advances and expanded tool kits that will ensure that the leech persists as a valuable preparation for generations to come.

2.2 l Overview

The nervous system of the medicinal leech (*Hirudo verbana*)* can be quite captivating. As one peers through a stereomicroscope equipped with dark-field illumination, one can easily view the shimmering outlines of the relatively large neuronal somata (up to 80 μm) that decorate each segmental ganglion (ca. 200 cell pairs per ganglion). For students learning to conduct intracellular recordings, a single leech will provide 21 of these ganglia for target practice. Furthermore, the entire central nervous system (CNS), including the compound ganglion in the head (i.e., brain) and tail ganglion (capping the 21 ganglia), sits within a ventral blood sinus, thus the CNS has a negligible 'blood-brain' barrier, facilitating cellular, developmental, pharmacological and neuroanatomical studies (Muller et al., 1982). Because of these and many other attributes affording experimental accessibility, the leech preparation has become a favorable system to study diverse physiological processes and the neural substrates of behavior (Kristan et al., 2005). [*Note: for over 40 years, commercial suppliers have provided *H. verbana* labeled as *H. medicinalis*. These species do have some distinguishing features but can interbreed. Their CNSs are not notably different and the current view is that many references to *H. medicinalis* are that of *H. verbana*.]

The internal beauty of the leech CNS is equally matched by the leech's exquisite and fluid locomotor behaviors: swimming and crawling. In 1938, the basic kinematics of swimming and crawling were first reported by Gray et al. (Gray et al., 1938) In their report, the primary muscle groups for locomotion were identified (circular, longitudinal, and dorso-ventral muscles), and the issue of

whether the swim and crawl locomotor rhythms were based on a chain of reflexes or were intrinsic to the CNS was examined. In addition, the role of the brain (i.e., supra- and sub-esophageal ganglion) in supporting sustained locomotion and shaping its form was tested via decapitation. Although Gray et al. (1938) failed to conclude correctly that crawl and swim rhythms can originate centrally, their acquired data and questions posed remain surprisingly relevant today, as will be discussed throughout subsequent sections.

As compared to crawling behavior, leech swimming has historically received significantly more attention, and thus more is known about its neuronal control. In the 1960s and early 1970s, leech sensory neurons, motoneurons, and their connections were beginning to be identified in detail (Coggeshall and Fawcett, 1964; Nicholls and Baylor, 1968; Nicholls and Purves, 1970; Stuart, 1970), although it is worth noting that Gustav Retzius had examined the morphology of leech neurons as early as 1891 (Retzius, 1892). Over an intensive period of investigation, the mechanisms underlying swimming movements were swiftly becoming elucidated (Kristan et al., 1974). By 1978, a compelling review of the neuronal generation of leech swimming, published in the journal *Science* (Stent et al., 1978), detailed how “an oscillatory network of neurons driving a locomotory rhythm had been identified”. Some of its young authors included scientists who would remain devoted to the leech preparation throughout their illustrious scientific careers (for example, Kristan, Friesen, and Calabrese). More recent reviews of swimming and its neuronal control have highlighted its

descending command-like cells, feedback loops, neuromodulation, inter-circuit interactions, computational modeling, and shared control strategies across taxa (Brodfuehrer and Burns, 1995; Brodfuehrer and Thorogood, 2001; Kristan et al., 2005; Friesen and Kristan, 2007; Mullins et al., 2011; Wagenaar, 2015).

Because crawling behavior in the leech has received much less of the spotlight, in this chapter we have opted to focus on crawling behavior, highlighting the ways in which its underlying organizational features compare to swimming, and are often shared across taxa. We will also discuss the functional architecture and inherent plasticity that enables the leech to recover its locomotion after injury, providing new insights into how a locomotor system can adaptively reconfigure itself over time. Lastly, we will underscore the full utility of the leech model as it is presently and looking into the future, focusing on the technological advances and expanded tool kits that will ensure that the leech persists as a valuable preparation for generations to come.

2.3 | Kinematics of crawling

After the initial report of Gray et al. (1938), a more extensive kinematic analysis of leech crawling was not published until almost 50 years later by Stern-Tomlinson et al. (Stern-Tomlinson et al., 1986). While moving over a terrestrial substrate, the amphibious medicinal leech can locomote by using either a vermiform- or inchworm-type of crawling (Sawyer, 1981; Stern-Tomlinson et al., 1986). Vermiform crawling is typically observed and is characterized as the

alternating elongation and contraction (i.e., shortening) of the body with coordinated sucker attachments, which essentially drag the leech's body forward across the substrate (Stern-Tomlinson et al., 1986; Baader, 1997; Cacciatore et al., 2000). Importantly, the movements of the body propagate caudally in a metachronal wave during each elongation and contraction phase (Fig. 1). During inch-worm crawling, which occurs over especially uneven terrain, the head and tail suckers are closely positioned at the end of a cycle and the body loops upwards, extending off the substrate. As compared to swimming, crawling is a much more flexible locomotor behavior (Cacciatore et al., 2000; Kristan et al., 2000). For example, a leech can stop crawling during the middle of an elongation cycle and begin a series of whole-body bending and searching movements; it can eventually resume its elongation, thus completing its paused crawl cycle. In contrast, during swimming, the leech needs to maximize its propulsive forces while moving through a fluid environment, thus its segmental swim circuits require more precise intersegmental phase relationships and cycle periods (Cang and Friesen, 2002).

2.4 | The centrally-generated crawl motor pattern

In 1938, Gray failed to observe fictive crawling in the isolated nerve cord (Gray et al., 1938), but in 2000, Eisenhart et al. demonstrated for the first time that the nerve cord of the leech isolated from the body was capable of producing a crawl rhythm similar to that observed in semi-intact preparations (Eisenhart et

al., 2000). This later group showed that the circular muscle motoneurons (CV cells), which generate elongation movements, fired out of phase with some of the motoneurons (e.g., VE-4) innervating the longitudinal muscles that are active during the contraction phase of crawling; furthermore, this activity progressed along the nerve cord in a caudally-directed wave. Note: one crawl cycle (period) consists of the two-step elongation and contraction phase; cycles are repeated during continued crawling (Fig. 1).

Important questions, however, about the anatomical location of the crawl central pattern generator(s) (CPG) would not be answered until the study of Puhl and Mesce (Puhl and Mesce, 2008). Might the crawl CPG be distributed across limited but multiple ganglia, as in the locust flight system (Robertson and Pearson, 1983, 1985) or might its location reflect the organization of the crayfish swimmeret system, whereby a complete CPG for the movement of one swimmeret is housed within a single abdominal ganglion (Murchison et al., 1993; Mulloney and Smarandache-Wellmann, 2012)? Puhl and Mesce (2008) found that each of the 21 segmental ganglia possessed the ability to produce a reliable, robust and sustained crawl motor pattern. To ensure that the fictive motor pattern obtained was, indeed, that of crawling and not some other type of motor pattern, an extensive number of crawl-related motoneurons and their phase relationships was recorded, including both the dorsal and ventral longitudinal (muscle) excitor motoneurons (DE-3 and VE-4) and the annulus erector (AE) motoneurons, together with the dorsal and ventral longitudinal inhibitory motoneurons (DI-1 and

VI-2) and ventrolateral circular (muscle) excitor motoneurons (CVs) (which fire out of phase with DE-3, VE-4 and AE). Importantly, in the single ganglion, the burst duration of the DE-3 motoneuron (i.e., duration of the contraction phase) was found to have a linear relationship to the crawl-cycle period, a relationship that was equal to that during overt crawling in the intact animal; the crawl-cycle period during overt crawling, however, was shorter. These results have demonstrated that the crawl CPG in a single ganglion has all the timing elements needed to produce the two-step coordinated pattern of crawling and set the crawl-cycle period independent of sensory and inter-circuit influence. This crawl CPG is essentially a rare biological example of what Grillner (Grillner, 2006, 2011) has referred to as “the unit burst generator” for locomotion.

What is an especially relevant lesson for those in search of unit burst generators in mammals, including humans (Minassian et al., 2017), is that even in the simpler system of leech, the unitary crawl CPG is elusive—if cephalic inputs are absent and if a single ganglion has an additional ganglion (or chain) attached, its rhythmicity is lost (Puhl and Mesce, 2008). Furthermore, the right chemical neuromodulator must be applied to awaken the pattern-generating capacity of the crawl CPG, as will be discussed below.

2.5 l Role of dopamine (DA) and serotonin (5-HT) in locomotor selection

Our success in activating fictive crawling, either in the isolated whole nerve cord (with the brain) or in a single ganglion, was largely dependent on the

application of DA to the CNS. This approach was based on our previous studies that had shown that some of the leech's dopaminergic neurons (Crisp et al., 2002) were dye-coupled (i.e., electrically coupled) to a cephalic descending command-like neuron, Tr-2, (Crisp and Mesce, 2004), which was shown previously to suppress swimming (O'Gara and Friesen, 1995). We quickly discovered that, indeed, DA was a potent blocker of swimming even under conditions where swim-inducing electrical stimulation was co-applied (Crisp and Mesce, 2004). Because DA turns swimming off, we tested the idea that it might influence or activate another behavior such as crawling, which it did reliably (Puhl and Mesce, 2008). Our current position is that D1-like DA receptors, together with other DA receptor sub-types, are needed to help shape the membrane properties and phase-relationships of cell-specific members of the crawling networks (Crisp et al., 2012) as in vertebrates (Lapointe et al., 2009). It is important to note, however, that the ability of DA to elicit crawling is state-dependent; for example, any given segmental ganglion connected to another ganglion or chain of ganglia will not exhibit appropriate crawl bursting patterns. Essentially, it is 'an all or one' phenomenon, such that a single ganglion (without interference from neighboring inputs) or the entire CNS is required for DA to induce crawl-specific rhythmic (fictive) locomotor activity (Puhl and Mesce, 2008).

DA and 5-HT appear to act as neuromodulatory toggles to bias the mode of locomotion in the direction of either crawling or swimming (Mesce and Pierce-Shimomura, 2010). The classic study of Willard (Willard, 1981) first established

that the application of 5-HT to an isolated nerve cord could induce fictive swimming in the absence of other stimuli, including the electrical stimulation of nerve roots. He also reported that the intracellular stimulation of 5-HT-containing neurons activated fictive swimming and that it was correlated with elevated 5-HT levels in the blood. By depleting amines via treatment of whole leeches with reserpine, O'Gara et al. (1995) provided further, albeit indirect, evidence of swim activation by 5-HT, as reserpine-treated leeches had reduced or eliminated locomotor behaviors; bath treatment of 5HT restored swimming behaviors. Swim-activating sensory neurons have also been found to excite 5-HT-containing neurons (Gilchrist and Mesce, 1997). Finally, the effects of 5-HT are nuanced and do not always promote swimming; for example, 5-HT applied selectively to the brain can inhibit swimming, likely playing a role in the decision not to swim while the leech is actively feeding (Crisp and Mesce, 2003, 2006; Gaudry and Kristan, 2009). Because a large number of multifunctional neurons appear to participate in the generation of both leech crawling and swimming (Briggman and Kristan, 2006, 2008), one speculative idea is that DA and 5-HT help to sculpt and delineate the two forms of locomotion that otherwise would not be so readily distinguished from each other.

2.6 l Crawling and the brain

Having established that each of the 21 segmental ganglia of the leech nerve cord contains its own CPG for crawling (Puhl and Mesce, 2008), the next

problem to solve was how these independent CPGs (or oscillators) were coordinated. One hypothesis was that some type of oscillator-to-oscillator coordination strategy was in play, similar to that demonstrated for leech swimming (e.g., Friesen et al., 1978; Otto Friesen and Pearce, 1993), wherein isolated chains of segmental ganglia (separated from the brain) can be induced to express fictive swimming and show appropriate swim-specific intersegmental phase lags. We soon determined, however, that chains of segmental ganglia, separated from the brain, were incapable of producing coordinated crawl-specific intersegmental phase delays even in the presence of DA application (Puhl and Mesce, 2010). Through a number of reversible sucrose-blocks, whereby descending input from the brain was temporarily removed from the isolated ventral nerve cord or nearly-intact leech, we established that crawl-specific intersegmental coordination required the brain, supporting the much earlier conclusion of Gray (1938) that crawling, but not swimming, is reliant upon the brain. Although we discovered that local oscillator-to-oscillator interactions do exist and can help provide a caudally-directed 'drive' to facilitate the metachronal wave of crawl movements, such local interactions alone were never sufficient to generate appropriate crawl-specific intersegmental coordination (Puhl and Mesce, 2010).

2.7 l Intersegmental coordination, the cephalic cell R3b-1 and the CV motoneuron

In 2012, Puhl et al. identified a key neuron responsible for the crawl-specific coordination among the 21 independent crawl oscillators— that cell was R3b-1, its name stemming from the fact it is located in the 3rd neuromere (b sub-packet) of the fused suboesophageal ganglion (functionally considered the brain) (Puhl et al., 2012). While on a sabbatical working with William B. Kristan and his post doc Teresa Esch (at the University of California, San Diego), one of us (Mesce) had the wonderful opportunity to study this phenomenal neuron in a nearly-intact preparation developed by Esch. We discovered that intracellular excitation of a single R3b-1 cell (they are bilaterally paired) was able to command the overt expression of either swimming or crawling; importantly, each form of locomotion was dependent on whether the body of the leech was in an aquatic environment (i.e., surrounded by fluid) or in a terrestrial one (low level of bath fluid) (Esch et al., 2002). Thus, the decision to locomote is made first followed by a decision of the type of locomotion to display; essentially, the leech uses a sequential decision-making process.

R3b-1 is a long-distance projecting neuron that has the cytoarchitecture to communicate with both left and right halves of each segmental ganglion within the CNS, thus interacting directly with all 21 crawl oscillators (Puhl et al., 2012). R3b-1 is a truly remarkable cell as it serves numerous functions, including that of a bona fide crawl command cell (Puhl et al., 2012), fulfilling the strictest conditions of necessity and sufficiency (Kupfermann and Weiss, 1978, 2001). Aside from its command-related properties, R3b-1 was also found to modulate

crawl frequency. Under the influence of DA, crawling emerges as the exclusive locomotor pattern produced by R3b-1 (Fig. 2), and its bursting matches the crawl cycle period even when ascending inputs from the posterior crawl oscillators are removed (Puhl et al., 2012). Although the above attributes render R3b-1 an exceptional cell, it is its ability to coordinate the segmentally-distributed crawl oscillators that makes this singular neuron so notable. To our knowledge, R3b-1 provides the first example of a command neuron that is also responsible for the intersegmental coordination of a locomotor behavior.

One of the ways that R3b-1 promotes intersegmental coordination is by regulating the cycle periods of the 21 oscillators so that they all match. After removing descending input from one of the bilaterally-paired R3b-1 cells, we found that hyperpolarizing the remaining R3b-1 with negative current removed crawl-specific intersegmental coordination— crawl bursting in the segmental oscillators remained, but the periods were no longer the same (Puhl et al., 2012). Although no evidence has indicated that local oscillator-to-oscillator coupling alone is sufficient for intersegmental coordination (in contrast to swimming) it is important to note that inter-oscillator coupling is still important and works in tandem with R3b-1 to promote crawl-specific intersegmental coordination. For example, when synaptic connections between a subset of segmental ganglia were blocked to prevent inter-oscillator coupling, but ganglia still received R3b-1 input from the brain, coordinated crawl bursting in oscillators distal to the block was lost (Puhl et al., 2012). The current conceptual model for crawling is that a

given crawl CPG receives a combination of R3b-1 input and crawl 'drive' from its anterior (local) oscillator; these inputs are then fed into a logical AND gate to ensure the activation of successively more posterior ganglia, thus promoting the metachronal wave caudally along the nerve cord (Fig. 3). Only when dual inputs are received can the metachronal wave of crawl activation proceed (Puhl et al., 2012). This working model for crawl intersegmental coordination fits well with the inherent flexibility observed for overt crawling, whereby a leech can pause mid-cycle and then resume its crawling. If R3b-1 were to stop firing in response to sensory input, subtraction of this input would then halt propagation of the metachronal wave.

What are the targets of R3b-1? To date, we know relatively little about the pattern-generating elements that contribute to the crawl motor pattern in each ganglion, and thus which neurons are synaptically coupled to R3b-1. What we do know is that R3b-1 directly targets the CV motoneuron, which is active during the crawl elongation phase. This connection was demonstrated by recording from the R3b-1 and CV motoneurons simultaneously with intracellular electrodes, and a monosynaptic connection between the two cells was proposed (Puhl et al., 2012). This connection can also be seen using voltage-sensitive dye fluorescence (Fig. 4, unpublished data). In this experiment, R3b-1 was injected with 3 nA positive current pulses at 1 Hz and potential targets of R3b-1 were identified by their coherency (i.e., being phase locked). Colored somata (in M-10) had optical activity that was significantly coherent (Panel A), and the colored

vertical map indicates their phase relationships. The paired CV motoneurons can clearly be seen as being coherent. Future experiments of this type hold great potential in revealing not only the targets of R3b-1, but also of the cells comprising the crawl oscillators.

It is notable that crawling is always initiated with a body elongation, thus making the R3b-1 to CV connection relevant. Furthermore, new evidence indicates that within a single ganglion, the CV motoneuron can feed back onto the putative pattern generator that regulates the elongation phase of crawling (Rotstein et al., 2017). This is an interesting finding as it provides yet another example of how motoneurons can participate in pattern generation, which has been known to occur in the leech (e.g., Poon et al., 1978), but is less well established in vertebrate systems (Song et al., 2016; Falgairolle et al., 2017).

2.8 l The chronic loss of cephalic inputs and the ability to recover coordinated crawling

As one might predict based on the above discussion, decapitating a leech (thus removing R3b-1) should prevent coordinated crawling behavior, which is exactly what Gray reported in 1938 (Gray et al., 1938). As shown by Puhl and Mesce (2010), when descending information is reversibly blocked in a nearly-intact preparation (immediately below the brain), no amount of stimulation to the body can activate crawling. If one makes a surgical transection (i.e., full cut) of the intersegmental connectives (below the brain) and waits several days, leeches

appear a bit more responsive to sensory stimuli and a weak semblance of crawl-like activity emerges. Amazingly, by around 10-14 days post-surgical transection, a leech can recover its ability to crawl, displaying fully coordinated crawling and doing so without provocation (Harley et al., 2015). In addition, this recovery is not dependent on the growth or regeneration of descending inputs from the brain, as was tested, in part, by excising it completely (Harley et al., 2015). Finally, it was determined that the ganglion (i.e., crawl CPG) immediately below the site of injury was vital for the initiation and progression of the crawl motor pattern; this ganglion was ascribed the name 'lead ganglion'. If this singular lead ganglion were subsequently removed, then another full round of recovery, lasting several weeks or more, was required before the leech could once again express crawl-specific coordinated crawling. The burning question now is to understand what neural components compensate for the massive loss of essential information once provided by R3b-1.

2.9 l Homeostatic plasticity and a new dependence on peripheral information

As mentioned previously, R3b-1 plays a significant role in crawl activation, maintenance, cycle period and intersegmental coordination (Puhl et al., 2012). However, it was also discussed that the kernel for the two-step crawl motor rhythm is completely housed in each segmental ganglion. Although local inter-oscillator coupling does exist, it is simply not sufficient to support crawl-specific

intersegmental coordination. Might the crawl oscillators, in recovered leeches, somehow alter their coupling architecture so that a wave of crawl activity can be propagated caudally? In the Mesce lab, we tested this idea, in part, by examining whether complete nerve cords, isolated from fully crawl-recovered leeches, were capable of displaying coordinated crawling. Although we could induce crawl activity in the crawl oscillators with DA, these oscillators were never coordinated with each other (Puhl et al., 2018). Because these nerve cords were dissected from leeches that displayed fully coordinated overt crawling indistinguishable from uninjured control animals, information from the body appears to be a requirement for intersegmental crawl coordination. To explore this idea further, we took transected leeches destined for crawl recovery and removed afferent input specifically to the lead ganglion (i.e., anterior-most ganglion below the site of transection). In these dually-treated leeches, coordinated crawling was either severely delayed or prevented. When we filled the nerve roots distal to the site of nerve-root lesion, we found an exact match between the regrowth of peripheral fibers and the ability to exhibit coordinated crawling. Thus, during recovery after the removal of descending inputs, the leech becomes dependent on afferent information, especially to the lead ganglion (Puhl et al., 2018). Our future goals will attempt to identify the afferent information that is needed for crawl recovery and how it interacts with the crawl oscillators to promote intersegmental coordination. By substituting afferent information in the place of R3b-1, our conceptual model for crawl coordination can accommodate a potential switch to a

dependence on sensory information. Guided by the compelling work out of Friesen's lab, in which the stretch receptors have been shown to play important roles in the intersegmental coordination of the swim oscillators (Yu et al., 1999; Cang et al., 2001; Yu and Friesen, 2004; Fan and Friesen, 2006), we have begun looking at the role of the stretch receptors (Blackshaw and Thompson, 1988; Blackshaw, 1993) in contributing to crawl coordination in crawl-recovered leeches after transection. Interestingly, some of these stretch receptors (e.g., the ventral stretch receptors) also receive synaptic input from swim oscillatory interneurons in the CNS, which may control the gain of sensory feedback or information flow (Cang et al., 2001).

2.10 | Remodeling of the stretch receptors during crawl recovery

Preliminary studies of the segmentally-iterated stretch receptors in crawl-recovered leeches have focused on whether these sensory cells show any discernable differences in the morphology of their terminal projections, thus testing the hypothesis that they might sprout new terminal processes in their attempt to form new connections and/or strengthen previously established ones. To our delight, what we have discovered thus far is quite striking. By conducting intracellular tracer (Neurobiotin) fills of the stretch receptors, via their large axons located in the nerve roots (10-30 μm), we have been able to ascertain that a population of these proprioceptors becomes markedly remodeled (Mesce et al., 2018). In normal medicinal leeches, it has been firmly established that the

terminals of the morphologically distinct stretch receptors (8 pairs/per segment) are restricted to the single segmental ganglion they innervate (Retzius, 1892; Blackshaw and Thompson, 1988; Fan and Friesen, 2006). Some of the somata of these proprioceptive neurons have been shown to be associated with the segmental longitudinal muscles (Blackshaw, 1993; Huang et al., 1998; Fan and Friesen, 2006). Thus far, the most dramatic neuronal change we have observed in fully crawl-recovered leeches is that the stretch receptors (entering through the posterior nerve) deviate from the norm and extend their terminals both anteriorly and posteriorly through the intersegmental connectives. In the lead ganglion, we have observed that the terminal of stretch receptor P-4 (Fan and Friesen, 2006), for example, can project to the adjacent posterior ganglion, and likely further. These proprioceptors have now become intersegmental, thus having the capability to directly link multiple oscillators (Fig. 5). Because we have previously established that leeches with a lead ganglion rendered devoid of afferent input do not recover their ability to crawl (Puhl et al., 2018), we believe that the significant remodeling of the stretch receptors is very likely to play a key role in helping restore crawling. A fascinating problem for future study will be to unravel how different timing-related elements (i.e., input from stretch receptors) can substitute for those of interneuron R3b-1.

2.11 | Principles of flexible locomotor organization and action selection

Its metameric organization, sensory-feedback systems, descending cephalic control, aminergic neuromodulation, and experimental accessibility render the leech an especially instructive model system in which to study the neural substrates of locomotion. Numerous principles of locomotor organization and control have been shown to be shared across distantly related taxa, for example, swimming in the leech and the lamprey, a basal vertebrate (Mullins et al., 2011). In their comprehensive review, the authors highlight the many ways that locomotor initiation, maintenance, segmental oscillatory activity, intersegmental coordination, and sensory feedback are analogous across the two species. Because crawling is such a flexible locomotor behavior and dependent on descending cephalic inputs, it can provide new insights into potential mechanisms underlying flexible locomotor activity in other species, including mammals. For example, in rodents (Gordon and Whelan, 2008) and cats (Shimamura and Kogure, 1983; Drew et al., 2004), interlimb coordination can be influenced by midbrain and brainstem stimulation. Furthermore, flexible locomotor behaviors, such as walking (Juvin et al., 2005; Borgmann et al., 2009), may preclude a neural configuration wherein the unit oscillators are tightly coupled and governed primarily by the intrinsic elements within them.

The issue of how multiple descending neurons can function collectively to select a distinct motor action is not fully understood in any animal system (Heinrich, 2002; Zelenin et al., 2007). In the leech brain, Mesce et al. (2008) discovered two additional long-distance projecting neurons that reside in a small

cluster located aside cell R3b-1 (named R3b-2 and R3b-3). Taking a neuroethological approach and examining these cells in a nearly-intact preparation, they were found to be recruited during spontaneous crawling, receive sensory input, and generate motor sub-routines, likely enabling the leech to turn its body laterally and make outward-extended searching movements during the elongation phase of overt crawling. The functions of these neurons showed remarkable similarities with the reticulospinal neurons for locomotion in vertebrates (Whelan, 1996; Grillner and Wallén, 2002; Kiehn, 2006; Humphries et al., 2007; Orlovsky et al., 2012). Because of the limited number of these descending cells, they offer a tractable system for future studies to understand how ensembles of action-selection cells work together and shape naturalistic swim and crawl behaviors.

2.12 l The reconfiguration of locomotor networks and lessons for spinal cord injury

A pressing problem in the field of motor control is to understand how to restore locomotor function after a spinal cord injury has removed important descending and central pathways. The recovery of leech crawling is salient in this regard because, as mentioned previously, crawl recovery is not mediated by reconnections between higher-centers and the locomotor pattern generators. Under some circumstances, the restoration of motor functions in vertebrates can proceed without the successful reconnection of damaged central pathways

(Edgerton et al., 2004; Sakurai and Katz, 2009; Rossignol and Frigon, 2011). After injury, compensatory or homeostatic plasticity (Turrigiano, 1999, 2012; Marder, 2011) ensues, but this plasticity can also be detrimental to overall functional recovery (e.g., Beauparlant et al., 2013); however, it often leads to the reestablishment of the operation of a given cell or circuit. Although homeostatic plasticity underlying functional recovery after injury has been studied in a number of organisms across taxa (Muller et al., 1987; Edgerton et al., 2004; Ivanenko et al., 2013; Parker, 2017), fewer studies exist that describe the cellular underpinnings of how motor neural networks might achieve their new operational states (e.g., McClellan et al., 2008; Pozo and Goda, 2010; Husch et al., 2012).

As discussed previously, afferent information is essential for coordinated crawling in recovered animals, in sharp contrast to uninjured leeches that can show a complete independence of sensory information (Puhl and Mesce, 2010; Puhl et al., 2018). Similar to these results, in mammals, some locomotor functions can be restored after spinal cord injury when sensory inputs are provided and are active (Rossignol et al., 1996). Similarly, in chicks, phasic sensory feedback to spinal circuits appears to facilitate locomotor recovery (Muir and Steeves, 1995). After weeks to months of treadmill training, adult cats can exhibit limited locomotor abilities, including weight-bearing hind-limb stepping (Barbeau and Rossignol, 1987). When peripheral afferent fibers from the ankle of the hindlimb are denervated and the spinal cord is transected, subsequent locomotor recovery is blocked even with treadmill training (Carrier et al., 1997).

Such results are strikingly similar to the blockade of locomotor recovery we observed when nerve roots were severed (Puhl et al., 2018). In rats, after an incomplete spinal cord injury, treadmill and swim training have led to the partial recovery of weight-bearing stepping (Smith et al., 2006). In rats with a complete transection of the spinal cord, greater degrees of locomotor recovery were seen when treadmill training was supplemented with robotic devices, which increased proprioceptive feedback to the spinal CPGs as compared to treadmill training alone or no training (Cha et al., 2007). Finally, in humans, phasic afferent stimulation via robotic devices (Wirz et al., 2005; Cheung et al., 2017) or electrical and pharmacological stimulation (Minassian et al., 2017; Xavier et al., 2018) has facilitated the recovery of stepping ability.

Even when regeneration is possible, as in the lamprey, neuronal connections must be reintegrated within spinal locomotor networks correctly (Parker, 2017), and plastic changes within locomotor networks need to accommodate proprioceptive inputs to mediate successful recovery. Finally, it is likely that all locomotor recovery processes require some form of homeostatic plasticity in the synaptic connections, neuronal membrane properties, and chemical neuromodulation of recovering networks (Sharples et al., 2014). Determining how the central and peripheral nervous systems become retuned and work in concert to establish functional crawl patterns will clearly be facilitated by the experimental tractability of the leech nervous system.

2.13 | The next chapter of the leech model: a new, bigger and better tool kit

The centuries-old medicinal use of the leech, continued even today, has ensured its availability to neuroscientists around the world (Whitaker et al., 2004; Spear, 2016). The extensive characterization and ability to identify neurons as unique individuals have been invaluable for studying neural circuits; these same attributes will also be especially beneficial in emerging studies of device-related neuromodulation in medicine, where novel neuromodulation techniques are often prone to varying outcomes. Identifying cells as individuals enables researchers to reduce experimental variability by ensuring targeted neurons have stereotypical functional and structural properties across animals tested. The physiological robustness of the leech's body and its nervous system for promoting realistic fictive and overt locomotion have led to its use in the development of new neural recording and neuromodulation techniques (Wagenaar, 2015), as will be discussed below.

Lastly, next-generation gene technologies are bringing the medicinal leech (*H. verbana*) into the era of genomics, as evidenced by the recent publication of the animal's first *de novo* transcriptome assembly from the entire CNS (Northcutt et al., 2018). In the context of 'connectomics', development of serial block-face electron microscopy (a way to generate high resolution, 3D images) has revolutionized one's ability to interrogate established and novel synaptic connections in the medicinal leech (Pipkin et al., 2016, 2018). Thus new genetic and electron-microscopy tools promise to enrich the tool kit needed to study the

myriad, unresolved problems remaining in one's quest to understand how locomotion is controlled.

2.14 | Inspiring new neural recording techniques

Neuroscientists continually seek to improve their understanding of the nervous system through the targeted measurement of neural activity. While this has long been possible with classical electrophysiological methods (e.g., intra- and extracellular electrode recording), new and less invasive forms of measurement are needed, particularly in systems in which traditional electrophysiology is difficult, excessively time-consuming, or is difficult to maintain in behaving animals.

Optical recording techniques utilizing voltage- and ion-sensitive dyes are rapidly becoming a staple of neuroscience laboratories. The leech was among the first systems in which these dyes were implemented (Ross et al., 1987), and has since served to showcase the circuit-mapping abilities of subsequent generations of imaging tools, including FRET dyes (Cacciatore et al., 1999; Briggman et al., 2005, 2015). In recent years, a team of researchers used the leech to validate a new form of voltage imaging, photo-induced electron transfer (Miller et al., 2012). Researchers have also used the leech to design novel applications of existing voltage sensitive dyes. Recently, the leech has been employed in the development of a double-sided microscope imaging system, enabling simultaneous voltage-sensitive dye recording from both the ventral and

dorsal surfaces of an individual ganglion (Tomina and Wagenaar, 2017, 2018). This technology enabled voltages of both ventral sensory neurons and dorsal motoneurons to be measured during fictive local bending (Tomina and Wagenaar, 2017). Having the ability to record the dynamics of virtually all neurons in a single ganglion, this technology will certainly facilitate understanding the roles of individual neurons in a variety of motor behaviors, including locomotion.

Recent work in the leech also has led to the development of a transparent multi-electrode array that is compatible with optical recording techniques, including the use of voltage-sensitive dyes (Nagarah et al., 2015). In a leech ganglion, this novel recording array has been shown to capture widespread oscillatory activity during simultaneous voltage dye imaging. This dual functionality will enable researchers to switch between recording methods, thereby extending the period of voltage-sensitive dye recording that is often limited by the dyes' phototoxic effects (Nagarah et al., 2015).

A different group utilized the leech in a similar effort to optimize multi-electrode arrays, but with a focus on reducing electrical crosstalk while recording from ensembles of neurons (Naughton et al., 2016). Such crosstalk yields a noisy recording trace in which spikes from individual neurons may be difficult to differentiate, even with the best available spike-sorting algorithms. Their solution was to create a coaxial nanoelectrode array, which had a high density of insulated electrodes, allowing for simultaneous recording of many neurons with

minimal electrical crosstalk. Recordings from leech ganglia were included to demonstrate the feasibility of this new array in recording neural signals (Naughton et al., 2016); future uses of this technology will enable researchers to probe the activity of neural circuits with higher precision.

Researchers have also utilized the leech in the development of non-optical recording technologies, including nanowires. Nanowires, ultrafine electrodes created by the precise deposition of metals on the tips of microelectrodes, may be used in place of sharp electrodes for intracellular recording (Ferguson et al., 2012). Due to the fine tip of these electrodes (<100 nm), they exhibit fewer problems than traditional intracellular sharps, including damage to neuronal cell membranes and incompatibility with long-term recordings due to ionic leakage. During the development of this technology, researchers recorded simultaneously from intracellular sharp and microwire electrodes inserted in leech T and Retzius cells, which enabled them to demonstrate the fidelity of microwire electrodes in comparison to traditional intracellular sharp electrodes (Ferguson et al., 2012).

Lastly, Fromherz et al. (1991) described success in coupling a leech Retzius neuron to a field-effect transistor. Further work utilizing this technology, in the leech, has shed light into the ion currents that underlie differences in the waveforms of extracellular action potentials (Schätzthauer, 1998). Similar devices incorporating neuron-silicon junctions have since transitioned into use in mammals, and continue to evolve in exciting ways, including through the use of

nanoscale transistors (Duan et al., 2012), bidirectional stimulation and recording capabilities (Benfenati et al., 2013), and monoamine detection (Xu et al., 2016).

2.15 l The leech and new device-related neuromodulation technologies

The neuroscientific community is experiencing a boom in emerging device-related neuromodulation technologies, fueled in part by the clinical success of deep brain stimulation in treating a myriad of neurological disorders (Miocinovic et al., 2013). Researchers are working tirelessly to develop efficacious, less invasive therapies to spare patients the significant financial burden and health risks associated with implantable devices. The leech preparation is currently being used in the development of two neuromodulation technologies bearing special mention: millimeter wave irradiation, and focused ultrasound.

Humans are increasingly exposed to millimeter waves, for example, during airport security screening and local-area wireless networks. The health risks of exposure to millimeter waves are incompletely understood. Recent work has utilized the leech to assess whether millimeter waves impact neuronal activity (Pikov and Siegel, 2011; Romanenko et al., 2014a). Romanenko et al., (2014) have demonstrated that the activity of the large serotonergic Retzius neurons is inhibited by millimeter waves in a dose-dependent manner. Although this research may raise questions about the safety profile of this increasingly used

technology in our lives, researchers are also excited by the prospect of harnessing millimeter wave irradiation as a new neuromodulatory technology.

In the Mesce lab, focused ultrasound (fUS) is another emerging noninvasive neuromodulation technology currently being tested in the leech. Ultrasound has been shown in humans to influence neuronal activity noninvasively (Legon et al., 2014). Work on single identified neurons, in the leech, is underway to help elucidate this technology's enigmatic neuromodulatory mode of action, and to expand its repertoire of applications. One exciting finding is that fUS can be used repeatedly and reversibly to inhibit the activity of identified motoneurons noninvasively (Newhoff et al., 2018) (Fig. 6). Through the induction of reversible inhibition, one can begin to pattern neuronal activity, an effect previously achievable only through the intracellular injection of alternating bouts of positive and negative current. This ability to inhibit and pattern motoneuron activity will be an asset in future endeavors seeking to probe or facilitate motoneuron bursting patterns known to underlie behaviors governed by rhythmic neuronal firing, including locomotion and respiration. Ultimately, this pioneering work will yield insights into how this promising technology can be utilized in the treatment of human neurological disorders.

2.16 | The leech as an inspiration for the design of biomimetic robots

The innate locomotor behaviors of the leech have inspired researchers to build biomimetic robots. For example, researchers wanting to build a robot optimized

for traversing pipelines have built a leech-inspired “micro-peristaltic robot” that moves via crawl-mimicking elongation and contraction cycles (Liu et al., 2002). More recently, another team has built a soft robot able to navigate complex environments based on the kinematics of leech locomotion (Kanada et al., 2019). Called the Longitudinally Extensible Continuum-robot (LEeCH), this robot utilizes suction cups similar to leech suckers, and is able to achieve wall-to-wall transitions (Kanada et al., 2019). The leech sucker has also inspired Feng et al. (2014) to design a micro-medical robot with silicone rubber suckers capable of supporting up to 200 g of weight, which is able to adhere to the interior of the gastrointestinal tract while monitoring for signs of Functional Gastrointestinal Disorders. While it remains unclear if leech-inspired robots will make their way into mainstream medicine or industry, there is no question that the animal’s beautifully architected and elegant locomotor behaviors will continue to inspire scientists across disciplinary boundaries, and for generations to come.

2.17 l Figures

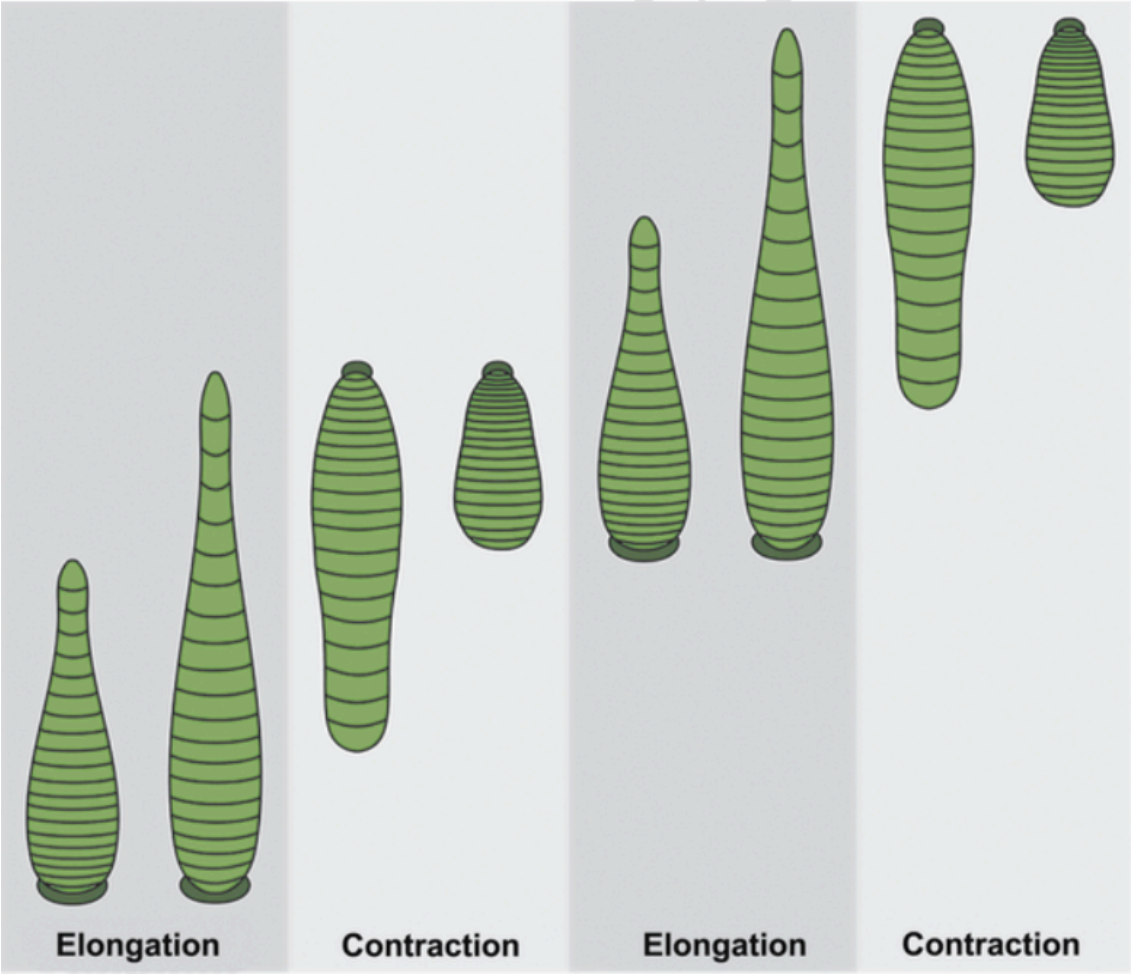

Figure 2.1. Cartoon of the medicinal leech (dorsal view) depicting the two phases (or steps) of vermi- form crawling: body elongation and contraction. Crawling is always initiated by elongation of the body and detachment of the front sucker. The metachronal wave of segmental elongation moves in the caudal direction. During the contraction phase, the rear sucker is detached and the segmental wave of segmental shortening also moves in the caudal direction. *(Drawing courtesy of Anthony Auletta.)*

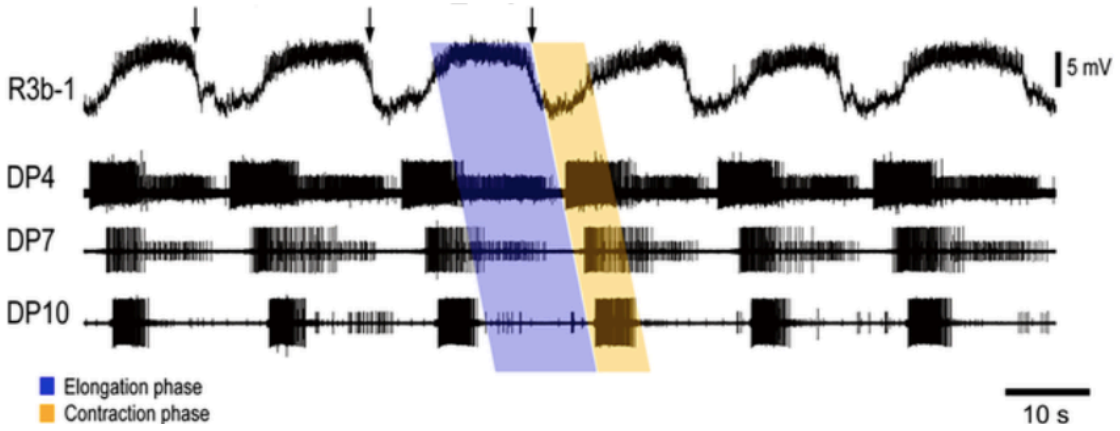

Figure 2.2. Fictive intersegmentally coordinated crawling obtained from the entire leech CNS re- moved from the body. DA-induced bursting in the cephalic neuron R3b-1, which was phase-locked to the elongation *(blue parallelogram)* and contraction *(amber parallelogram)* phases of crawling. The *arrows* indicate the initiation of the contraction phase. The largest spikes in bursts, from the segmental ganglia (M-4, M-7, M-10), were those of motoneuron DE-3. Cell DE-3 has one of the largest axons carried in the dorsal posterior (DP) nerve and innervates the dorsal longitudinal muscles that contract during the contraction (shortening) phase of crawling. Mean periods were all similar at just under 18 s with mean intersegmental phases (relative to R3b-1) at 0.046. *(Modified from Puhl JG, Masino MA, Mesce KA. Necessary, sufficient and permissive: a single locomotor command neuron important for intersegmental coordination. J Neurosci 2012;32(49):17646–57.*

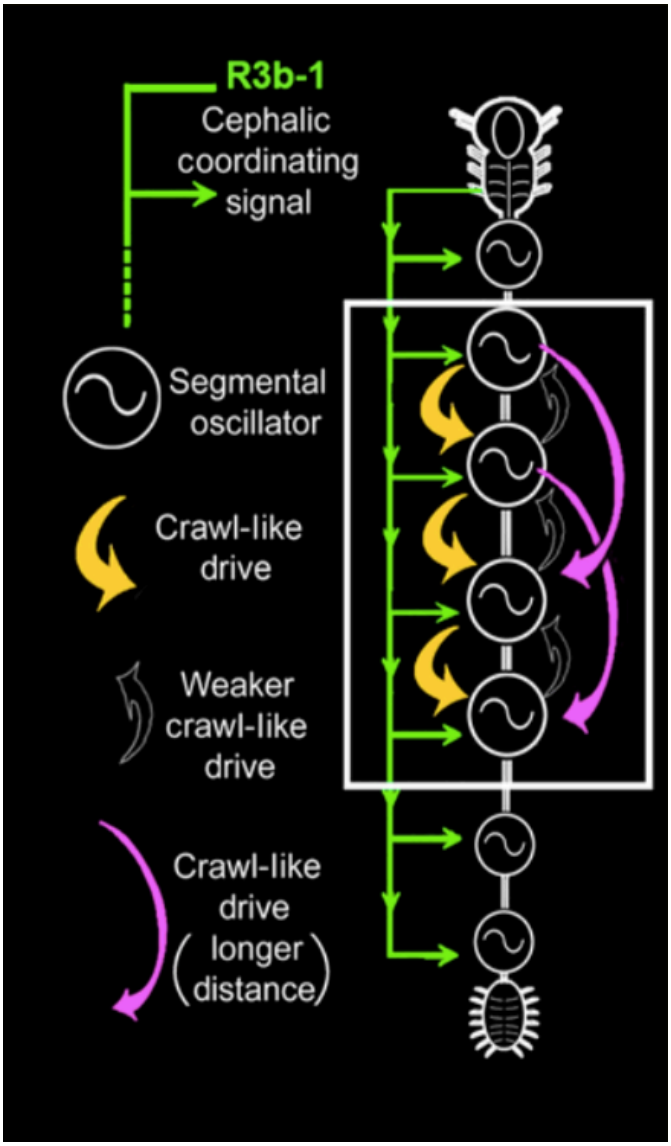

Figure 2.3. Schematic diagram of the leech CNS and neural elements contributing to leech crawling. Each of the segmental ganglia contains a crawl unit-burst generator (i.e., CPG), indicated by a white circle with a sigmoid symbol. Note that not all of the 21 segmental ganglia are depicted for illustrative purposes. The continuous *green line*, descending from the dorsally located brain, represents information from the long-distance projecting interneuron R3b-1, shown to be necessary and sufficient for crawl-specific intersegmental coordination [48]. The *curved arrows* represent different types of "drive" (i.e., the ability for one oscillator to activate another) across the CPGs [47]. In this model, dual inputs from R3b-1 and the posteriorly directed crawl drive are summed to provide for the metachronal wave of crawl activity, which is propagated caudally along the chain of ganglia comprising the ventral nerve cord. *(Modified from Puhl JG, Mesce KA. Keeping it together: mechanisms of intersegmental coordination for a flexible locomotor behavior. J Neurosci 2010;30(6):2373–83.)*

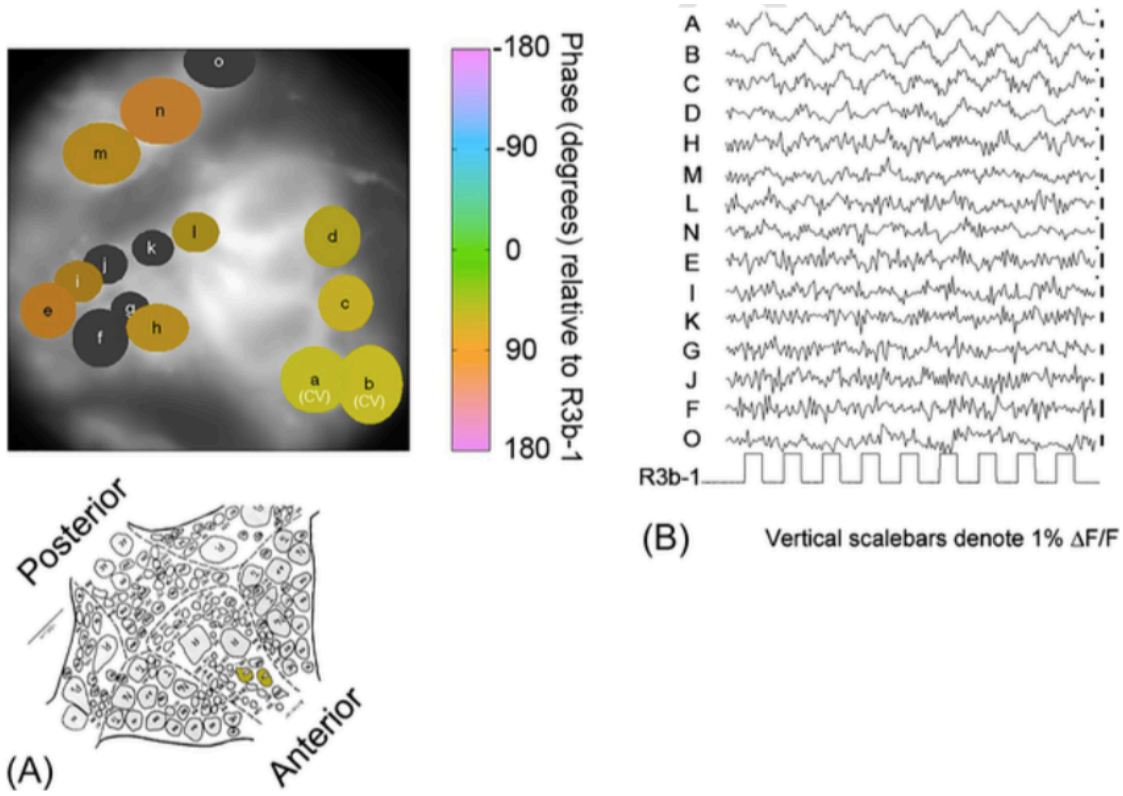

Figure 2.4. Motoneuron CV is a synaptic target of R3b-1 as indicated by FRET-based indicator dyes. **(a)** Image of voltage-sensitive dye (VSD) fluorescence from the ventral aspect of the ganglion, M10 (see schematic below for orientation of ganglion). The colored ovals (labeled a–o) identify individual neuronal somata that were in the plane of focus. Colored somata had optical activity that was significantly coherent (i.e., phase locked) with 1 Hz, 3 nA current pulses injected into R3b-1 [bottom trace in **(b)**]. The color map (right) denotes the phase of the optical activity relative to the membrane potential of R3b-1. Somata of the CV motoneurons are denoted in the VSD image as well as in the schematic (filled somata). **(b)** Δ*F*/*F* traces of the somata depicted in **(a)**. An *asterisk* next to the trace indicates optical activity that was significantly coherent with the membrane potential of R3b-1 (bottom trace). Vertical scale bars are 1% Δ*F*/*F*. *(Unpublished data courtesy of Joshua G. Puhl.)*

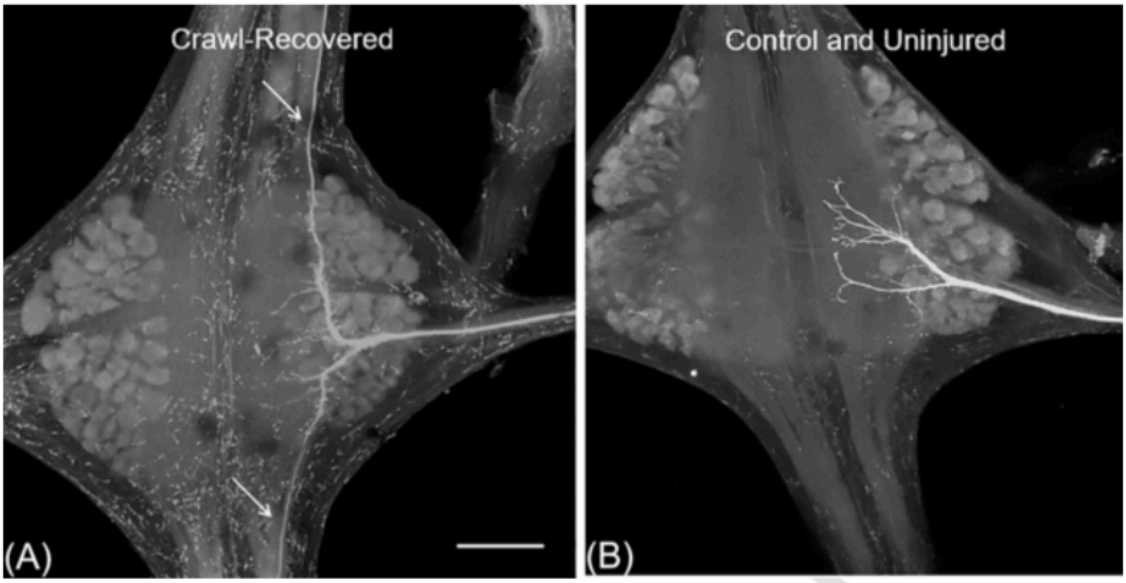

Figure 2.5. Body-wall stretch receptors become remodeled after transected leeches have recovered their ability to show coordinated crawling. **(a)** A remodeled posterior root (PR) stretch receptor [61] in a lead ganglion after transection (between M2 and M3). The leech was sacrificed 2 weeks after complete crawl recovery was observed. Note that the anterior and posterior projection fibers extend into the connectives. **(b)** A PR stretch receptor in ganglion M3 obtained from a control individual. Note that the receptor's terminal projection is completely restricted to its ganglion and segment of origin. Both cells were filled via the iontophoretic injection of Neurobiotin into the axon (in the posterior root) near the point of entry into the ganglion. Scale bar = 100 μm. *(Unpublished data courtesy of Anthony W. Bigelow, Joshua G. Puhl and Karen A. Mesce.)*

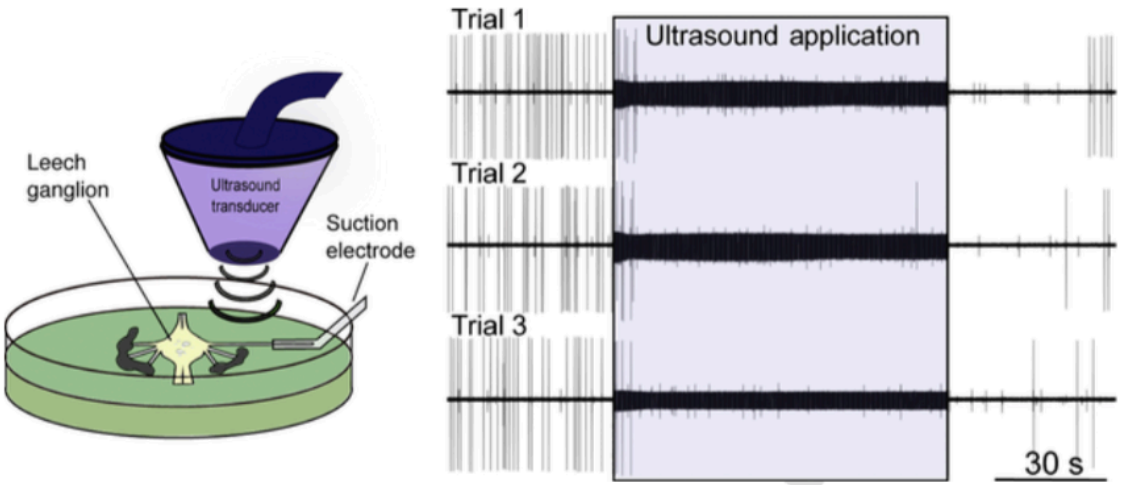

Figure 2.6. Focused ultrasound neuromodulation of motoneuron DE-3. ***Left*****:** Schematic of experimental design showing an isolated single leech ganglion and its dorsal posterior (DP) nerve pinned out in a petri dish. The ultrasound transducer is depicted, which generates and focuses the ultra- sound on the DP nerve. The firing rate of the DE-3 motoneuron, which sends its axon through the DP nerve, is recorded via a suction electrode. ***Right***: Ultrasound (960 kHz) induces repeatable, reversible inhibition of DE-3 spiking across multiple trials of ultrasound application. *(Unpublished data courtesy of Morgan Newhoff.)*

CHAPTER 3

Unraveling the actions of focused ultrasound on an identified, single motoneuron

3.1 | Summary

Focused ultrasound affects neural activity in a wide array of animal systems; however, its mode of action remains unclear. Here, we have examined the effects of ultrasound on a single, identified motoneuron within a tractable invertebrate preparation. Our approach aimed to limit the variability in ultrasound's responsiveness, which is often observed when ultrasound is applied across a diverse population of cells. We found that ultrasound largely inhibits tonic spiking activity through a predominately thermal mechanism. Effects persisted after blocking synaptic input, indicating that actions were direct on the targeted cell. Experiments also revealed that comparable heating blocks the axonal conduction of action potentials. We were unable to find evidence that the mechanical actions of ultrasound had significant effects on the neurons tested, a finding counter to previous studies. We conclude that a non-sensory cell can be directly inhibited via a thermal mechanism, a finding that holds promise for clinical neuromodulatory applications.

3.2 | Introduction

Focused ultrasound (fUS) is an emerging noninvasive technology that has the potential to modulate neuronal activity with great precision. Although

ultrasound's effects on neural tissues have been investigated for nearly a century (Harvey, 1929), renewed interest in fUS has recently emerged due to the recognized therapeutic value of various electrical neuromodulation technologies, including deep brain stimulation (Miocinovic et al., 2013), spinal cord stimulation (Grider et al., 2016), and peripheral nerve modulation (Chakravarthy et al., 2016). FUS can target deep neural structures with accuracy on the order of millimeters (Anderson et al., 1951; Hynynen and Clement, 2007; Legon et al., 2018a); it could thus pose a viable alternative to implantable neuromodulatory devices, sparing patients the risk and financial burdens of surgery.

Despite the advantages of fUS, variability in its outcomes across studies, have tempered widespread clinical adoption. Reported effects in mammalian systems range from neuronal excitation (Tyler et al., 2008; Tufail et al., 2010; Yoo et al., 2011a; Kim et al., 2012, 2014; Downs et al., 2018; Kubanek et al., 2018) to inhibition (Anderson et al., 1951; Fry et al., 1958; Takagi et al., 1960; Shealy and Henneman, 1962; Rinaldi et al., 1991; Min et al., 2011; Legon et al., 2014; Kim et al., 2015; Wright et al., 2015; Ilham et al., 2018). The invertebrate literature is similar, with reports of both neuronal excitation (Vion-Bailly et al., 2017; Kubanek et al., 2018; Lin et al., 2019b) and inhibition (Yoo et al., 2017; Zhou et al., 2017) encountered in preparations such as *C. elegans*, earthworms and crayfish.

Recent work on brain stimulation has demonstrated that the actions of fUS in intact mammalian preparations may be confounded by fUS directly activating

mechanosensitive auditory hair cells within the cochlea, thus causing indirect cortical activation (Guo et al., 2018; Sato et al., 2018). However, other studies utilizing *in situ* mammalian preparations, deaf mice, and invertebrates report that fUS modulation persists in the absence of auditory/mechanosensory input (Tyler et al., 2008; Wright et al., 2015; Mohammadjavadi et al., 2019), suggesting that fUS may have direct actions on neurons beyond those that are mechanosensory. Similarly, there are recent noninvasive stimulation studies reporting the ability of fUS to excite nerves or axons (Kim et al., 2012; Downs et al., 2018), though these results are inconsistent with several *in vitro* studies that directly stimulated nerves with ultrasound and did not observe any neural activation (Colucci et al., 2009; Ilham et al., 2018). In addition to these inconsistencies across studies, the precise mechanisms by which fUS exerts its neuronal actions are still unclear.

Several hypotheses have been put forth regarding ultrasound's direct mode of action, including cavitational forces (Krasovitski et al., 2011; Plaksin et al., 2014) and the mechanical gating of ion channels (Mihran et al., 1990, 1996; Kubanek et al., 2016, 2018). Another hypothesis involves the impact of ultrasound-associated tissue heating. Tissue absorbs ultrasound as heat, itself a potent neuromodulator (Hodgkin and Katz, 1949a; Janssen, 1992; Sharma and Hoopes, 2003). Early neuromodulatory work reported the occurrence of fUS-induced tissue heating in excess of 10°C, yielding results accompanied by significant tissue damage (Lehmann, 1953; Barnard et al., 1955). Subsequent studies indicated that some actions of fUS could be mimicked with heat alone

(Lele, 1963; Ueda et al., 1977), although the ultrasound intensities used were beyond those permissible for diagnostic use – a common benchmark to delineate safe versus unsafe intensities. In recent years, the use of lower intensities that generate less heating has shifted many researchers' focus to mechanical and cavitational forces. Others continue to explore the thermal hypothesis, as it was recently reported that ultrasound-induced suppression of somatosensory evoked potentials in the rat could be replicated with the targeted application of low heat (Darrow et al., 2019). Presently, the extent to which low heating (many studies estimate heating to be <1°C (Constans et al., 2018)) contributes to fUS-induced neuromodulation is unknown.

Typically, fUS experiments measure changes at the cell-population level, involving measures of multiunit activity that include: compound action potentials (Tsui et al., 2005; Wright et al., 2015; Yoo et al., 2017), event-related potentials[5,20,21] or BOLD signals (Yoo et al., 2011a; Ai et al., 2016, 2018). Experiments targeting nerves, , are often performed in intact preparations in which the targeted axons are immersed in surrounding tissue (Kim et al., 2012; Downs et al., 2018), enabling activation of receptors in the skin or muscle that confound nerve responses. In light of the difficulties in assessing ultrasound's direct effects on neurons in intact systems, some groups studying fUS have focused their efforts on cultured neurons (Mihran et al., 1996; Tyler et al., 2008; Muratore et al., 2009) or more tractable invertebrate systems (Vion-Bailly et al.,

2017; Yoo et al., 2017; Zhou et al., 2017; Kubanek et al., 2018; Lin et al., 2019b), as we have done here.

To reduce cell-to-cell variability and to minimize confounding indirect activation effects that could contribute to the reported differences in ultrasound's actions, we examined the isolated effects of fUS and its comparable heat output on an identified neuron, the dorsal longitudinal excitor-3 (DE-3) motoneuron. This neuron's morphology and its physiological activity can be uniquely identified across multiple preparations of the medicinal leech, *Hirudo verbana*, which has an extensively characterized and tractable nervous system (Kristan et al., 2005). We specifically targeted a motoneuron because such cells are not tuned or sensitive to detecting mechanical disturbance, such as auditory hair cells (Guo et al., 2018; Sato et al., 2018) and even retinal ganglion cells (Jiang et al., 2018; Menz et al., 2019). Thus one of our aims was to obtain results that could be more generalizable across cell types not specialized for sensory transduction. Furthermore, our paradigm did not require the removal of nervous tissue from the animal, allowing us to examine the effects of fUS on a single neuron within a functional neural network, as well as avoiding alterations to intrinsic neuronal properties that can occur in culture (Turrigiano et al., 1994). This single cell approach enabled us to detect, with precision, whether fUS was an effective actuator of neuronal change, and understand the extent to which its thermal actions contribute to its direct neuromodulatory effects.

3.3 l Results

3.3.1 l The single-cell approach

DE-3 is a motoneuron positioned bilaterally on the dorsal surface of each of the 21 segmental ganglia of the medicinal leech, *Hirudo verbana*. Its axon exits each ganglion via the dorsal posterior (DP) nerve, and its spike is the largest spontaneously active unit in the extracellular DP recording. Importantly, its spontaneous firing property allowed us to examine ultrasound's effects on spontaneous versus evoked activity. A diagram of the leech nervous system is shown in Fig. 1a alongside a Neurobiotin fill of DE-3 (Fig. 1b), and representative intra- and extracellular traces (Fig. 1c). The amplitude of the intracellular somatic spike is smaller than a typical mammalian action potential due to attenuation (via electrotonic spread) from the distal spike-initiating zone; the somata of invertebrate neurons typically have a low density of ion channels (Stuart, 1970; Melinek and Muller, 1996).

3.3.2 l Ultrasound modulates the activity of motoneuron DE-3

To determine the effects of fUS on DE-3, we measured the activity of DP nerves (N = 48) from 18 leeches. Twenty-six nerves were exposed to 30 seconds of 960 kHz fUS; a schematic of an experimental trial is shown in Fig. 2**.** The remaining nerves (N = 22) served as untreated controls. Six nerves (4 treated with fUS, 2 controls) were excluded from analysis due to low spontaneous firing rates (N = 3 from fUS group, N = 1 from control group) or high firing variability (N

= 1 each from fUS and control) (see Methods for exclusion criteria). Thus N = 22 nerves exposed to fUS were subsequently analyzed. Maximal changes in DE-3 firing occurred during the last 10 seconds of application and continued for an additional 10 seconds (see “Analysis” box in third trace of Fig. 2b). Firing rates during this 20 second peak period were normalized to the mean baseline firing rate. Representative traces of fUS-induced inhibitory and excitatory effects are shown in Fig. 3a alongside a representative control trial. Normalized means of fUS-treated and control nerve firing rates during the analysis period are displayed in Fig. 3b**.** Mean deviation from baseline of firing of all fUS-treated nerves was 47.3% ± 37% (statistics refer to mean ± SD unless otherwise specified). Mean deviation from baseline of control nerves was 4.56% ± 22.8%. In control nerves, firing during the analysis window was largely consistent with baseline, with only 2/20 (10.0%) having mean firing rates that differed by more than 20%. For the FUS condition, 18/22 (81.8%) of treated nerves showed substantial modulation of activity (Fisher’s Exact Test, p = 0.0043). In the fUS group, we observed mainly inhibitory responses (13 out of 18; mean = 43.3% ± 27.5% decrease in firing rate from baseline). There were a few excitatory cases (4 out of 18; mean = 60.7% ± 30.1% increase in firing). Some of these excitatory cases in the treated nerves may have been due to some inherent variability across preparations, since a similar extent of excitation was also observed across the control nerves. As will be addressed in the following sections, greater excitatory effects may be elicited through ultrasound stimulation of presynaptic or synaptic mechanisms rather

than direct activation of the somata or axon of a motoneuron; thus, we cannot rule out the possibility that fUS stimulation was not completely isolated to the DP nerve for the excitatory cases shown in Fig. 3b.

As multiple nerves were harvested from the same animal, we performed a Kruskal-Wallis test to determine whether normalized mean firing rate during the analysis period was affected by animal. Animal variability did not significantly affect normalized mean firing rate during the response period ($X^2(9) = 11.0629$, $p = 0.2714$), nor did it affect the mean absolute deviation of DE-3 firing from baseline during this period ($X^2(9) = 8.11$, $p = 0.5227$).

We also assessed whether the direction of modulation, or the magnitude of modulation, was affected by baseline firing rate. Normalized mean firing rate during the analysis period did not significantly correlate with baseline firing rate (Pearson's correlation, $r = 0.327$, $p = 0.137$). However, when we tested for correlation between absolute deviation from baseline during the analysis period and baseline firing rate, we found a significant correlation (Pearson's correlation, $r = -0.481$, $p = 0.0233$), indicating that cells with lower baseline firing rates had greater deviations from baseline as a result of ultrasound application.

3.3.3 | The effects on motoneuron DE-3 are direct and persist during synaptic isolation

To determine whether fUS effects were specific to the targeted nerve, a subset (N = 4) of nerves tested were accompanied by simultaneous extracellular

recordings of DP nerves from adjacent ganglia. DE-3 neurons in neighboring ganglia receive common synaptic inputs, and frequently have similar firing patterns. 3 out of 4 tested nerves responded to fUS and no comparable effects were observable in the neighboring nerves (see simultaneously recorded traces in Fig. 4a), suggesting fUS effects were limited to targeted tissue.

To determine whether observed fUS actions on DE-3 were direct, or a consequence of activation of synaptically-coupled neurons that may have mechanosensitive properties, a subset of fUS-treated nerves (N = 10) were bathed in calcium-free saline. Calcium was replaced with equimolar manganese, which has been shown to block synaptic transmission in the leech, and which produces less rhythmic oscillatory activity than other replacement divalent cations (Angstadt and Friesen, 1991). This loss of synaptic activity is evidenced by the loss of post-synaptic potentials in intracellular DE-3 recordings (Fig. 4b). Rhythmic firing was observed in one of the ten nerves prior to FUS application, and the trial was aborted (final N = 9). A representative trace of fUS-induced inhibition in Ca^{2+}-free saline is shown in Fig. 4b. The mean baseline firing rate of DE-3 did not differ between conditions of normal saline and Ca^{2+}-free saline (3.42 Hz ± 3.93; for normal saline: 4.56 Hz ± 2.66; $t(9) = 0.675$, $p = 0.511$, Welch's *t*-test). We observed both excitatory (N = 1) and inhibitory (N = 6) responses to fUS within this subset, and a response rate (7/9 nerves, or 77.8%) matching our overall ultrasound sample shown in Fig. 3b, suggesting ultrasound's effects on DE-3 persist in the absence of synaptic input. Intriguingly,

we observed relatively more inhibition in this condition in comparison to the paradigm utilizing normal saline (results are summarized in Table 1), suggesting that some of the excitation we observed in the normal saline condition may have been due to the activation of synaptically coupled structures. The single excitatory case in the Ca^{2+}-free saline is consistent with the potential outlier cases we observed in control nerve experiments; thus, fUS applied to DE-3 without synaptic input achieves inhibition of firing activity, which is evident beyond spontaneous fluctuations.

3.3.4 l Heat mimics ultrasound's effects on DE-3

To determine the magnitude of fUS-associated tissue heating, we placed a thermocouple directly beneath and in contact with the DP nerve to measure changes in temperature during fUS application. FUS induced a temperature increase of 3.42 ± 0.20 °C (n = 3 thermocouple recordings).

Recognizing this increase in nerve temperature could be driving the inhibitory effects, we attempted to minimize the preparation's heating to determine whether effects persisted. We found that our wax substrate contributed to heating by minimizing thermal dissipation. We thus performed fUS trials on an additional 21 nerves on a latex substrate with the recording dish positioned over a large water bath to enable better dissipation of heat (see schematic in Fig. 5). One nerve was excluded from analysis due to high variability in baseline-firing rate. With this paradigm, the temperature increase

was limited to 0.3 °C. By greatly reducing heat in this manner, we reduced fUS modulation. Only 5 of 20 (25%) DE-3 motoneurons demonstrated more than a 20% change in firing rate during fUS application (all inhibited; mean inhibition = 50.9% ± 26.8%). Although the number of affected nerves did not differ significantly from control (Fisher's Exact Test, $p = 0.423$), a subset of nerves remained susceptible to fUS modulation despite minimal heating.

We attempted to control further for potential differences associated with our use of different substrates. Standing waves can occur when ultrasound reflects off a reflective surface in the direction of the transducer; reflective surfaces are those with a higher acoustic impedance than the surrounding medium, such as our transition from saline to wax. Reflected and emitted waves can summate, causing localized areas of heightened heat and pressure, which have been shown to impact neuronal responsiveness to fUS by increasing localized radiation force (Menz et al., 2019). Although we had attempted to control for the formation of standing waves by heavily pocking the wax substrate and angling the transducer, as has been shown to greatly reduce the neuromodulatory effects of standing waves (Menz et al., 2019), they nevertheless remained a possibility. To ensure our effects with the higher heat paradigm did not stem in part from higher pressures than those utilized in the lower heat, non-reflective latex dish paradigm, we doubled fUS absolute peak negative pressure to 1.3 MPa in 4 nerves in our low-heat latex dish paradigm. None of the 4 nerves responded to fUS, suggesting the purely mechanical effects

of ultrasound at this frequency, if present, were subtle as compared to thermal effects.

We next attempted to replicate the actions of fUS by inducing comparable fUS temperature increases in the DP nerve. We found that we could reliably induce a 2.10 ± 0.03 °C (n= 3) maximum heat increase in the media surrounding the DP nerve by aiming a 50 mW laser (with a fiber optic attachment) at the nerve for 30 seconds at the typical site of ultrasound application (see schematic in Fig. 6a). We applied the laser to 14 DP nerves from 6 animals. One nerve was excluded from analysis due to its high variability in firing rate. Of the remaining 13 nerves, 12 (92.3%) had mean firing rates that differed >20% from baseline during the 30 second laser application period. The laser produced a faster rate of heating than fUS; peak effects were observed 10 seconds into the stimulation and persisted until the end of heat application. Thus, the analysis window was shifted to include data collected during this period (20 seconds, equivalent to fUS and control analysis windows). Ten out of 12 responsive DE-3 motoneurons had decreased activity; this inhibition was dramatic (mean = 91.7% ± 20.5%). Two out of 12 were excited (mean = 50.3% ± 20.1% increase in firing). Representative traces of neuromodulatory effects are shown in Fig. 6b.

To ensure this laser-induced inhibition stemmed from heating versus a photic mechanism, we performed additional experiments with an alternative heating mechanism: a small insulated nickel-chromium (nichrome) wire coil connected to a direct current source positioned in the typical location of fUS

application (see schematic in Fig. 6c). Using the wire heating device, the maximum heat increase of the DP nerve was 4.86 ± 0.11 °C (N = 3). We tested 9 nerves with 30-second applications of heat. As with the laser, the wire heated more quickly than fUS, and we thus again shifted the analysis window to 40-60 seconds from trial onset to reflect peak effects. We found that 6/9 (67%) DE-3 motoneurons had mean firing rates that differed from mean baseline rates by more than 20%. Four of 6 DE-3 motoneurons were inhibited and half of these were completely suppressed (mean inhibition 85.7% ± 16.0%). The remaining two modulated nerves were excited; mean excitation = 29.6% ± 12.7%. Representative traces of the effects of the wire are shown in Fig. 6d.

In total, we observed both inhibition and excitation in response to our three stimuli, with a predominance of inhibitory cases. Stimuli ranged in temperature changes from 2.1 – 4.9 °C. In Fig. 7a, we plotted the firing rates of inhibitory trials for each stimulus that was averaged across trials against increases in temperature, and found a strong correlation for the fUS, laser, and wire trials (least-squares fit, R^2 = 0.69, 0.87 and 0.77, respectively). With respect to the low-heat ultrasound trials, the correlation between the mean firing rates of inhibitory trials and heating was low (R^2 = 0.11). The inhibition observed in these trials may have been due to natural variability in firing versus modulation; the baseline mean coefficient of variability in these trials (0.510 ± 0.208) was slightly higher than in the other ultrasound trials (0.425 ± 0.2315), though this difference was not significant (p = 0.222, Welch's *t*-test).

3.3.5 | Thermal neuromodulation may be influenced by the spatial spread of heating

Counter to expectations, the stimulus that generated the lowest heating, the laser, produced the most profound inhibition. While the laser had a sharper rate of heat increase than fUS, this rate was comparable to that of the wire (Fig. 7c and f); thus, the magnitude of modulation observed with the laser could not be attributed to the rate of heating alone. We thus investigated whether the area of tissue heated differed between the two types of thermal stimuli. To do so, we measured heat increases from a fixed thermocouple at incremental distances in the X and Y direction for all three stimuli. Interpolated plots depicting the spatial spread of heating for each stimulus are shown in Fig. 7g-i. While the wire and fUS had similar heating profiles, with peak heating occurring within a 5 mm radius from the center, the laser produced much more focused heating, with peak heating limited to a 1mm radius from the center. This restricted heating may have accounted for the relatively greater and less reversible inhibition observed with the laser as compared to the other stimuli. Results by stimulus are summarized in Table 1.

3.3.6 | Post-stimulus recovery of US and heat

Recovery from fUS and heat application was variable. The firing rates of 14/18 (77.8%) fUS-modulated DE-3 neurons returned to within 20% of baseline,

the benchmark that encompassed most of the variability in firing in control nerves. Recovery typically occurred quickly (mean time to recovery = 21.6 ± 16.9 seconds following the end of stimulation, or approximately 10 seconds after the end of the peak effect period). Excited nerves (N=4) recovered more slowly than inhibited nerves (N = 10) (29.3 ± 26.9 seconds versus 18.6 ± 11.7 seconds), though this difference was not significant (Welch's t-test, p = 0.494). Of the 4 nerves (all inhibited) that did not return to within 20% of baseline firing, 2/4 partially recovered (50.0% and 74.1% recovery). The remaining 2 nerves maintained greatly reduced firing rates for the remainder of the nerve's viability, with one case reaching a maximum of 29.0% of baseline firing rate 106 seconds after the end of the stimulus period, and the other case firing a single time 60 seconds after the end of the stimulus. These two minimally recovered nerves were also the most inhibited by fUS, with 95.1% inhibition and 100% inhibition, respectively.

Recovery rates for heat-only stimuli were similar, with 8/12 (66.7%) modulated nerves treated with the laser and 4/6 (66.7%) nerves treated with the wire returning to within 20% of baseline firing rate. Mean time to recovery with the laser was 18.8 ± 29.9 seconds (15.0 ± 47.4 s for excited nerves, 22.7 ± 27.4 s for inhibited nerves), and 2.75 ± 3.50 seconds (4.50 ± 4.95s for excited nerves, 1.00 ± 0.00 s for inhibited nerves) with the wire. As we observed with fUS, all nerves that failed to recover fully from heat application had been significantly inhibited (laser: 4/12 nerves, mean inhibition = 99.6% ± 0.00820; wire: 2/6

nerves, mean inhibition = 97.2% ± 0.0350). Three out of 4 irreversibly suppressed nerves treated with the laser failed to fire at all post-stimulus, as did 1 of the 2 nerves irreversibly suppressed with the wire; the other nerves occasionally spiked at rates far below baseline. All nerves that failed to recover were strongly inhibited by stimuli; however, not all strongly inhibited nerves failed to recover. Two nerves whose firing was completely suppressed (100%) by the laser fully recovered, suggesting total suppression need not be irreversible. Differences in recovery rates may have been due to subtle differences in the placement of the stimulus with respect to the nerve, or other stochastic factors beyond the scope of the present study.

3.3.7 l Heat induces conduction block in motoneuron DE-3

To determine whether the inhibitory effects of fUS were due to a broad hyperpolarization of DE-3, or from a local conduction block at the site of stimulus application, we performed intracellular somatic recordings of DE-3 in conjunction with application of the laser placed distally on the DP nerve. The laser was the most compact heat apparatus, and the most compatible with our intracellular electrode placement. Heat was applied between the somatic intracellular electrode and the distal suction electrode (see schematic in Fig. 8a). DE-3 activity could thus be measured on either side of the heat stimulus. Fig. 8b shows a representative simultaneous intracellular and extracellular recording of the DE-3 motoneuron with an inhibitory response with laser stimulation. Spikes initiated

near the soma as measured via our intracellular electrode failed to propagate to the distal electrode due to a presumed conduction block at the site of heat application.

3.3.8 l Local versus global heating biases the neuromodulation outcome

To determine whether a global temperature shift of a comparable magnitude over a similar time course (several seconds) could inhibit firing to the extent of focal heating, we raised the bath temperature by 2 °C through the rapid addition of heated saline. We found a moderate and short-lived increase in DE-3 firing associated with the addition of heated saline in the four nerves tested. This effect was comparable to excitatory effects observed in similar bath-heating experiments performed with this preparation (Romanenko et al., 2014a). We thus propose that non-noxious thermal inhibitory neuromodulation is only achievable with focused applications of heat, as summarized in Table 1 based on the combined results presented across our different fUS and heating experiments.

3.4 l Discussion

The data presented here systematically demonstrate the effects of 30 seconds of pulsed 960 kHz fUS on the axon of motoneuron DE-3, a uniquely identified cell located in the well-studied medicinal leech. A benefit of our paradigm was that response-type variability (i.e., excitatory versus inhibitory) was restricted to a single neuron and cell type, thus avoiding confounding outcomes

due to inconsistent access to different subtypes of cells and networks across various recording sessions. To the best of our knowledge, there have been no other studies investigating the modulatory effects of fUS on a single neuron within a functioning nervous system. These experiments have revealed that fUS targeting the axon can decrease spike firing of a neuron or nerve through a thermal mechanism. By chemically removing synaptic inputs -, we were able to conclude that fUS directly inhibits the targeted cell (Figs. 3 & 5). In contrast, neural excitation with fUS was difficult to achieve when synaptic or indirect inputs to the targeted motoneuron were removed, consistent with previous studies performed in intact brain preparations from mammalian species (Guo et al., 2018; Sato et al., 2018).

Because a potential mode of action for ultrasound neuromodulation has previously been proposed to be thermal (Lele, 1963; Ueda et al., 1977; Darrow et al., 2019), though not yet confirmed in a single cell within a functioning nervous system, we performed additional experiments with different heating modalities. We measured ultrasound-associated heating and replicated its comparable levels of heat with two stimuli, a 50 mW laser and a wire device. We determined that heat alone mimicked the effects of fUS. Furthermore, after significantly reducing fUS-associated heat to 0.3°C with a less insulating dish substrate, the rate of neuronal inhibition was reduced substantially from 14/22 nerves (64%) to 5/20 nerves (25%). These latter recordings may have reflected a natural variation in firing, as the mean firing rates during the inhibitory trials in this low heat

condition failed to correlate with changes in temperature (R^2 = 0.11), as was observed with the higher heat paradigms (R^2 = 0.82, 0.87 and 0.77 for higher heat fUS, laser, and wire, respectively). Despite using a fUS peak pressure higher than that reported in studies attributing fUS excitation effects to mechanical forces (e.g.,(Tyler et al., 2008; Tufail et al., 2010)), we also failed to obtain compelling evidence of non-thermal ultrasound excitation in our single cell preparation, as has been reported elsewhere (Tyler et al., 2008; Tufail et al., 2010; Yoo et al., 2011a; Kim et al., 2014; Kubanek et al., 2018).

The mechanisms underlying thermal inhibition, below the range of temperatures known to cause protein degeneration or necrosis (ca. 45°C in humans, or ca. 8°C above normal (Wang et al., 2014)), are not completely understood, but are believed to include changes in ion-channel-gating kinetics and conductances, leading to inactivation of voltage-gated sodium channels (Shapiro et al., 2012; Duke et al., 2013) or a loss in ion homeostasis (Robertson and Money, 2012). To investigate further how fUS can inhibit neural activity via a thermal mechanism, we performed additional heat experiments. As a proxy for fUS-associated heat, we utilized the laser, as it was the most compact stimulus, and thus the most compatible with placement of our intracellular recording electrode. During heat application, we observed a continuation of spikes recorded in the soma with a loss of spikes distal to the stimulus (Fig. 8), indicating that the inhibition we observed was due to a failure of spike conduction versus spike initiation. A potential mechanism for this conduction block is

‘spreading depression’, a conserved phenomenon reported in systems ranging from locusts to humans (Spong et al., 2016). Its molecular signature is a spike in extracellular potassium, causing disruption of ion concentration gradients (Kraio and Nicholson, 1978; Somjen, 2001; Ayata and Lauritzen, 2015). This loss of homeostasis has been shown to underlie conduction block and neuronal inhibition resulting from a range of environmental stressors, including hyperthermia, and may stem from a loss-of-function of the sodium-potassium ATPase pump (Wu and Fisher, 2000). Importantly, two earlier studies in rat brain found that ultrasound can induce spreading depression, resulting in effects reminiscent of pharmacologically raising extracellular potassium (Koroleva et al., 1986) and increasing temperature (Ueda et al., 1977). This mechanism could also explain the brief uptick in firing rate that preceded some of our inhibitory trials, particularly those utilizing the wire (the “hottest” stimulus in the present study), as evidenced by an initial increase in mean firing rate (Fig. 6F**)**; spreading depression-associated inhibition can be preceded by depolarization of the resting membrane potential (Pietrobon and Moskowitz, 2014), and by hyperexcitation (Rodgers et al., 2007).

Previous studies have proposed that non-thermal mechanisms underlie changes in neuronal fUS excitation or inhibition, such as intramembrane cavitation (Plaksin et al., 2014) or other mechanical effects (Kubanek et al., 2018; Prieto et al., 2018; Ye et al., 2018). Most hypotheses or computational models for cavitational actions assume an ultrasound frequency in the low hundreds of

kilohertz, which is thought to generate cavitational forces more effectively on the cell membrane (Gaertner, 1954; King et al., 2013; Kim et al., 2014). We opted, however, to use shorter wavelengths with a 960 kHz transducer as these parameters permitted a more precise targeting of neurons (Carovac et al., 2011), such as the DE-3 motoneuron and its associated nerve studied here. This frequency is below those used in some other studies attributing effects to mechanical forces (e.g., gating of voltage-gated ion channels), including a recent demonstration of activation of mouse sciatic nerve via 3.57 MHz ultrasound (Downs et al., 2018). We cannot rule out the possibility that other center frequencies or parameters (beyond those we tested in our experiments) may achieve mechanical-mediated neuronal excitation or inhibition. However, the companion paper published by Guo et al. tested the actions of ultrasound over a wide range of ultrasound parameters, in an *in vivo* mammalian preparation, and observed that ultrasound reliably inhibited neural activity directly via a thermal mechanism and found that excitatory responses were not typically observed. Together, these results from two independent studies across two different animal models (vertebrate versus invertebrate) and types of nerves (myelinated versus unmyelinated) demonstrate that the proposed mechanical actions of ultrasound on neural activity, if indeed present, are relatively minor and easily obscured by thermal mechanisms. Furthermore, these companion studies jointly provide strong evidence that ultrasound reliably inhibits nerves or axons via a thermal mechanism across a wide range of stimulation parameters.

The minority of DE-3 motoneurons excited by fUS and heat could have had different intrinsic membrane properties than those that were inhibited. Although motoneuron DE-3 has similar motor functions and synaptic connectivities across animals, these cells are not completely identical. Different ion channel types and densities are known to be associated with the same identified neuron (Prinz et al., 2004). More importantly, the relative frequency with which we observed excitation versus inhibition varied with the experimental paradigm, suggesting that the mode of heat application was a much more significant determinant in neuronal response type than differences in, perhaps, membrane properties. Notably, we observed the least amount of excitation in trials performed with fUS in Ca^{2+}-free saline (1/9 nerves) or with the laser heat stimulus (1/13 nerves), where the occurrence of excitatory cases was not different than that of the control trials (untreated nerves). The Ca^{2+}-free saline condition blocked activated sensory cells or other tissues from synaptically exciting DE-3. In addition, the laser paradigm yielded the most spatially restricted heating, thus limiting the contributions of other pathways that may have provided excitatory inputs to the targeted motoneuron when spatially broader heat stimuli were used. These data support the idea that excitation stems largely or entirely from circuit-level heating, while precise and targeted axonal heating results in inhibition (summarized in Table 1). This finding is further supported by our inability to generate inhibition via bath heating, as has been reported in the leech elsewhere (Romanenko et al., 2014a). Differences in the rate and magnitude of

inhibition—faster and more complete inhibition with heat-only versus fUS – may stem from the faster rate of heating (Fig. 6). The rise rate of tissue heating is a salient determinant of neuromodulation outcomes in other forms of thermal neuromodulation, including with infrared laser (Shapiro et al., 2012).

From a clinical perspective, various types of neural stimulation modalities have been shown to modulate neuronal activity safely and effectively, such as optical (Wells et al., 2007b) and millimeter wave technology (Pikov et al., 2010). Ultrasound, especially, has the advantages of delivering spatially restricted energy noninvasively to different regions in the brain and body, and it has a long history of safe clinical usage in subdermal imaging based on FDA guidelines (FDA, 2019; Pasquinelli et al., 2019). It is encouraging that 100% of the nerves we treated with fUS remained capable of generating DE-3 action potentials, with 78% of them returning to baseline firing rates within 20 seconds of the cessation of stimulus application. Only 2/14 modulated nerves maintained greatly reduced firing rates (<50% of baseline) following fUS treatment, indicating that fUS modulation is largely reversible. Future studies are now warranted to investigate the long-term safety of fUS for inhibiting neural activity via a thermal mechanism. The ability to suppress neuronal activity safely and reversibly will clearly have a significant clinical impact on a wide range of health disorders. The demonstration that fUS neural suppression occurs in mammalian myelinated nerves (see companion paper by Guo et al.) underscores the feasibility of this goal. Specifically, ultrasound neuromodulation may be most effective for treating

health disorders associated with excessive peripheral nerve activity, including peripheral neuropathies (St. John Smith, 2018) and spasticity (Raghavan, 2018). As we applied fUS to unmyelinated axons (leech neurons lack myelin), our results are most relevant to the future modulation of unmyelinated mammalian C-fibers. Because such cells are involved in the transmission of pain (Costigan and Woolf, 2000), our results underscore the great potential that fUS has in providing a novel non-pharmaceutical approach to treating neuropathic and inflammatory pain.

3.5 | Methods

3.5.1 | Animal preparation and recording substrates

Hermaphroditic adult leeches (*Hirudo verbana*) were obtained from Niagara Medical Leeches (Niagara, NY, USA) and housed at room temperature (22-24°C) in a large tank filled with pond water. Leeches were anaesthetized on ice (< 5 minutes) prior to dissection. For intact preparations (all fUS and control trials), leeches were pinned dorsal-side-up on a porous beeswax dish; dissections were minimal and limited to exposing the targeted dorsal posterior (DP) nerve, which contained the axon of the targeted motoneuron, DE-3. An overview of the neuroanatomy of the leech, the DE-3 motoneuron's spike profile, and experimental paradigm are shown in Fig. 1.

For isolated preparations (laser, wire, and low-heat fUS trials), we removed a portion of the dorsal nerve cord containing 3 segmental ganglia with

attached DP nerves. For laser and wire trials, we pinned the nerve cord dorsal-side-up on a silicone polymer surface (Sylgard, Dow Corning). Low-heat fUS trials were performed utilizing a latex-bottomed dish over a 500 mL bottle filled with a large sponge and deionized, degassed water (depth = 15 cm). All preparations were bathed in normal saline during dissection, and either normal or calcium-free saline during experimental trials. Normal saline (adapted from Nicholls and Baylor, 1968) was composed of (in mM): 115 NaCl, 4.0 KCl, 1.8 $CaCl_2$, 1.5 $MgCl_2$, 10.0 Glucose, and 10.0 Trizma pre-set crystals (pH 7.4). Calcium-free saline was prepared by replacing calcium with equimolar manganese as described (recipe from Olsen and Calabrese, 1996).

3.5.2 l Trial design

All trials were performed at room temperature (22-24°C), the temperature to which the animals were adapted. Trials were 90 seconds in duration: 30 seconds of baseline, 30 seconds of stimulus application, and 30 seconds of recovery; a sample trial is shown in Fig. 2a. Recovery periods were extended in trials in which nerves failed to return to within 25% of baseline firing rate. Control trials were equivalent in duration but did not include stimulus application.

3.5.3 l Electrophysiology

Extracellular DE-3 activity was recorded using a suction electrode placed on the distal end of the DP nerve; suction electrodes were made in-house, and

had a tip diameter of ca. 50 µm. Signals were amplified by a Model 1700 A-M Systems differential A-C amplifier, and digitized by an Axon CNS Digidata 1440A (Molecular Devices). Intracellular sharp recordings of DE-3 activity were performed using glass electrodes pulled to a resistance of 25 – 60 MΩ with a micropipette puller (Sutter Instrument Co., model P-87) and filled with 2 M potassium acetate. Signals were amplified by an IX2-700 dual intracellular preamp (Dagan Corp.), and digitized as previously described. All signals were recorded with the pClamp software package (Axon Instruments), and imported into MATLAB (MathWorks, Inc.) for analysis. Extracellular DE-3 activity was identified as the largest spontaneously active unit in the DP recording; somatic intracellular recordings were confirmed to be DE-3 by the cell's size and position, and the correspondence of intra- and extracellular spikes.

3.5.4 l Ultrasound

We applied 960 kHz fUS to DP nerves between the ganglion and the suction electrode recording site at the distal end of the DP nerve. Ultrasound was generated with a Sonic Concepts H-102MR transducer coupled with a focusing cone filled with degassed, deionized water. Waveforms were designed by an Agilent 33500B Series function generator and triggered by TTL pulses generated by an Axon CNS Digidata 1440A via pClamp software. Waveforms were amplified by an E&I 100W RF linear power amplifier (model 2100L), and impedance matched with a Sonic Concepts matching network. Ultrasound pulses

consisted of 290 cycles, and were 300 microseconds in duration. We applied 500 pulses per second at a 1 kHz pulse repetition frequency; pulse parameters are diagrammed in Fig. 2a.

Transducer output was characterized by hydrophone (ONDA HNR-0500) measurements in 0.25 mm increments in x, y, and z directions in a large tank filled with deionized, degassed water. Vertical and horizontal cross-sections of linearly interpolated hydrophone measurements (step size = 500 microns in x, y, and z directions; 309 total measurements) at peak amplitudes overlaid with scaled preparation dimensions are shown in Fig. 1d.

Absolute peak negative pressure was approximately 660 kPa. The transducer was attached to a micromanipulator and positioned such that its peak output was aligned with the center of the approximately 5 mm long DP nerve. The transducer was tilted at a 20° angle from vertical to reduce the potential for generation of standing waves.

3.5.5 l Heat measurement and apparatuses

For heat-only experiments, we utilized two methods of heat application, a 50 mW laser with a fiber optic cable attachment (SIMPLEX OS1-9, 125 µm diameter), and a coiled nickel-chromium wire device made in-house and powered by an adjustable direct current source.

In all experiments, the DP nerve was surrounded on all sides by saline. Due to the thinness of the nerve (approximately 50 µm in diameter) and the close

similarity of the specific heats and thermal conductivities of water and nervous tissue (Elwassif et al., 2006), we approximated nerve heating by measuring local saline temperature increases with a thermocouple (National Instruments model NIUSB-TC01) positioned underneath (in contact with) the DP nerve. Stimuli were applied as described for ultrasound and heat-only experiments. Thermocouple measurements were taken at a 1 Hz sampling rate and logged with NCBI thermologger software; data were imported into MATLAB ® (Mathworks,Natick, MA, USA) for plotting and analysis.

3.5.6 l Filtering

FUS application sometimes caused high-frequency artifact in DP recordings. The amplitude of the artifact was highly variable, and was not always resolved or ameliorated with the addition of a bath ground. A digital low-pass Butterworth filter (sampling frequency = 10 kHz; cutoff frequency = 1000 Hz; 6^{th} order) was effective in reducing high frequency artifact (see Fig. 2b for an example); for consistency, this filter was applied to all traces regardless of stimulus. Beyond high-frequency noise, ultrasound application onset and offset was sometimes associated with large-amplitude low-frequency baseline distortions. Affected traces were high-pass filtered with a digital Butterworth filter (fs = 10 kHz; fc = 200 kHz) to smooth the affected baseline. Residual high amplitude artifacts were digitally flattened prior to spike detection to avoid interference; this resulted in a small loss of information (0.5% in noisiest trace).

All digital filtering was performed in MATLAB using butter, and filter functions. In addition to filtering, we inverted extracellular traces for more intuitive viewing (the initial vertical deflection from baseline, corresponding to the rising phase of the action potential was made positive).

3.5.7 l Analysis

Data acquired by pClamp software were imported into MATLAB for all analyses. DE-3 spikes were identified via manually-adjusted thresholding; larger spikes attributed to other cell types (rare) were excluded from analysis via indexing to ensure accurate frequency calculations. DE-3 spikes were binned in 1-second bins for the duration of each trial to yield frequencies in Hz (see Fig. 2b). Spike frequencies during the stimulus and recovery periods were normalized to 30 second baseline means for comparison across trials. The rising phase of the DE-3 action potential was typically negative in our extracellular recordings; extracellular traces in all figures were inverted for more intuitive viewing. By convention, we have omitted vertical scale bars from extracellular traces due to our use of an AC-coupled amplifier.

3.6 l Figures and Tables

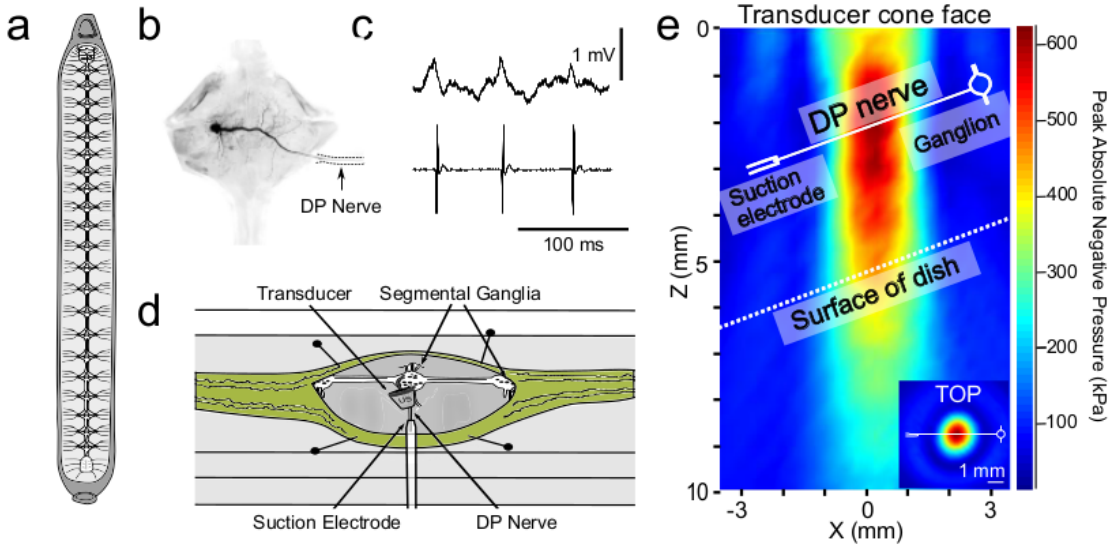

Figure 3.1. Schematic overview of the experimental preparation (medicinal leech, *Hirudo verbana*), and details of the ultrasound transducer and its placement. **(a)** Body of the leech dissected open to reveal the CNS, consisting of a cephalic ganglion, twenty-one individual segmental ganglia and a posterior compound ganglion, all interconnected by longitudinal connectives. **(b)** A single segmental ganglion (dorsal surface) showing the morphology of the left DE-3 motoneuron obtained by intracellular iontophoretic injection of Neurobiotin. Note: the axon exits the ganglion through the right dorsal posterior (DP) nerve (arrow). **(c)** Dual intracellular somatic (top) and extracellular DP nerve (bottom) recordings of spontaneous spiking in the DE-3 motoneuron. **(d)** Schematic of semi-intact preparation placed in the recording chamber (not to scale) and the positioning of the ultrasound transducer and suction electrode on the exposed DP nerve. **(e)** Pressures (in kPa) emitted from the face of the ultrasound transducer (upper graph). Hydrophone data (linearly interpolated) are shown at maximum intensity in relationship with the DP nerve and surface of the recording dish overlaid on scan. Ultrasound pressures are shown in vertical and horizontal (inset) cross section in relation to the ganglion (white circle, right) and suction electrode (white tube-shape, left). All proportions in e are depicted accurately.

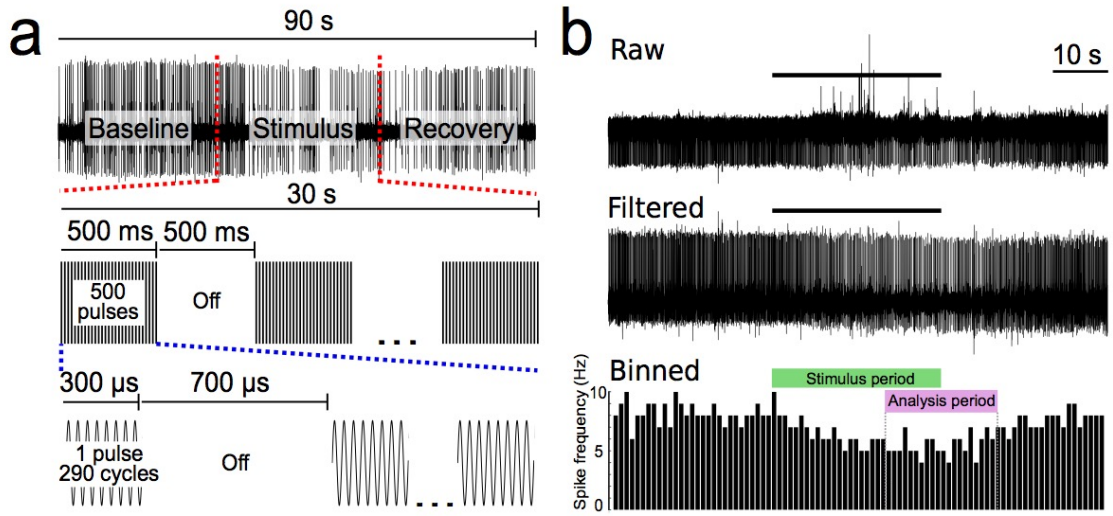

Figure 3.2. Ultrasound pulse parameters and trial design with an example response. **(a)** Each fUS application trial lasted 90 seconds in duration wherein 960 kHz pulsed ultrasound was applied for 30 seconds, preceded by a baseline period (30s) (example, top trace). Each ultrasound pulse was 300 μsec in duration (bottom trace), and was applied with a 1 kHz pulse repetition frequency with a 50% duty cycle (middle trace). **(b)** An example of extracellular DE-3 recorded spikes with the ultrasound-associated artifact (top trace). The same recording after filtering the data with a 6th-order low-pass Butterworth filter (frequency cutoff = 1000 Hz) (middle trace). Spike data from the filtered trace binned in 1 second intervals to yield spike frequency in Hz (bottom trace).The ultrasound application period is denoted by the stimulus period box; the analysis period is denoted by the analysis box.

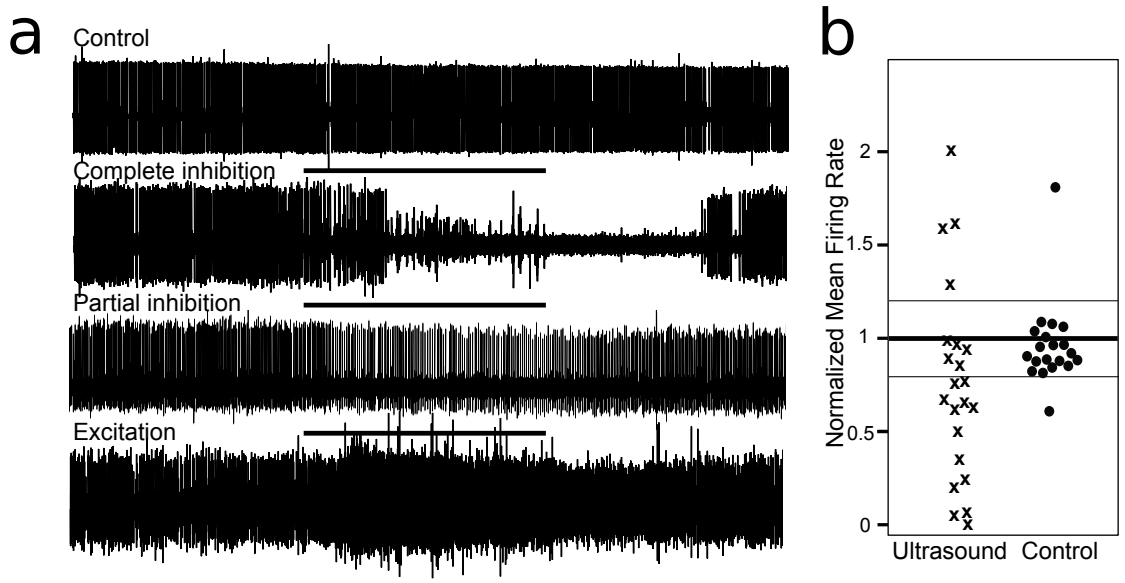

Figure 3.3. Ultrasound modulates the activity of motoneuron DE-3.
(a) Representative traces of DE-3 spiking activity in the absence of fUS (top trace) and in response to fUS applied for 30 sec (bar denotes application). The predominant response was a reduction in spike activity (two middle traces), and less frequently an increase in spiking activity (bottom trace). **(b)** Scatter plot of normalized mean firing rates during the analysis period of fUS application and in control trials. The mean of each trial in the study is represented as a single point. Thresholds for “excitatory” and “inhibitory” traces are 20% above and below baseline mean, as denoted by the thinner horizontal lines.

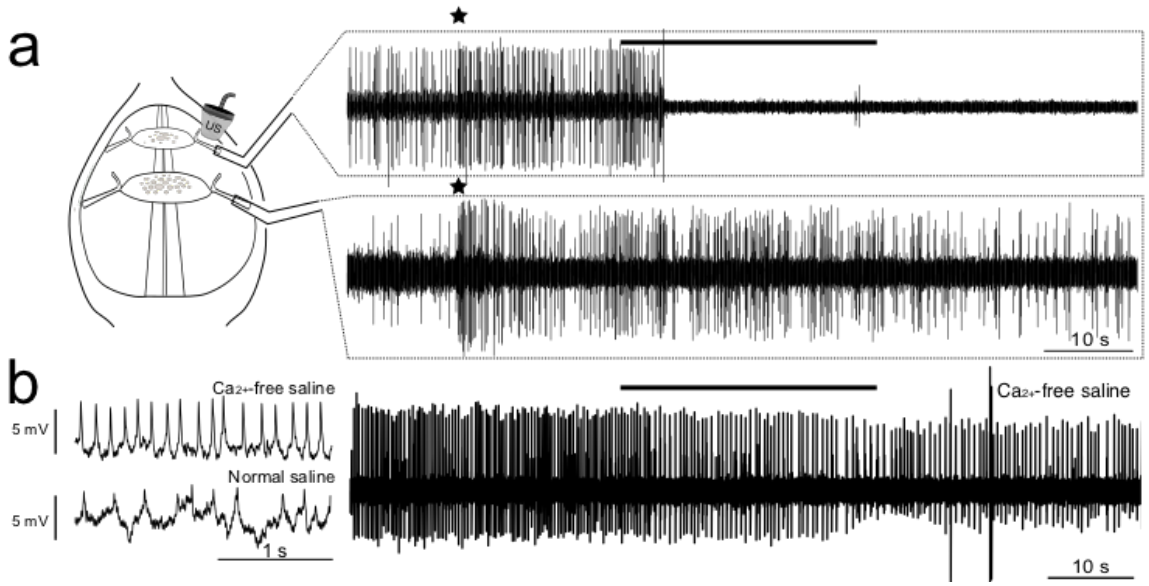

Figure 3.4. Experiments testing whether fUS affects the excitability of DE-3 locally and directly. **(a)** Because the DE-3 cells in adjacent ganglia often receive common synaptic inputs and are tightly coupled (Note: stars indicate an example of common response), we tested if fUS applied to a DE-3 axon in one ganglion would affect the DE-3 in the adjacent ganglion (diagram depicting dual DP recordings, left). Dual DE-3 recordings from the DP nerves (right) indicate that fUS inhibition is limited to the DE-3 targeted (upper trace). **(b)** Intracellular recordings of spontaneous DE-3 activity in Ca^{2+}-free saline (left, top) and normal saline (bottom, left), showing the reduction of post-synaptic potentials in the absence of Ca^{2+}. Blocking synaptic activity (via bathing in Ca^{2+} free saline) does not prevent fUS from inhibiting DE-3 activity (right trace).

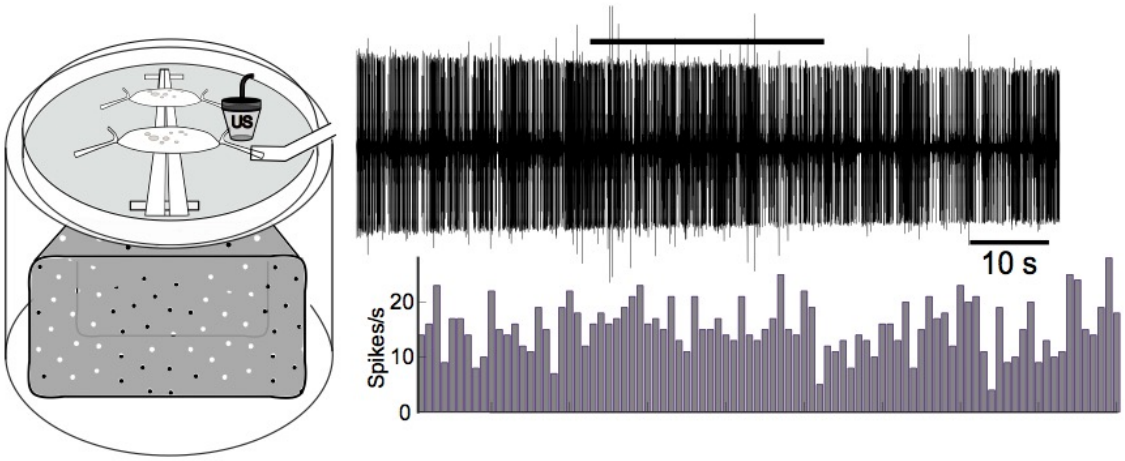

Figure 3.5. Ultrasound does not typically modulate neuronal activity in an ultralow-heat paradigm. **Left**: Schematic diagram demonstrating the placement of the latex-bottomed dish placed over a water reservoir filled with sponges. Schematic is not shown to scale; reservoir is approximately 10 cm in depth. **Right**: Representative trace of DE-3 firing during 30 sec of fUS (bar) using the latex dish paradigm (upper); Corresponding histogram of spike frequency (lower).

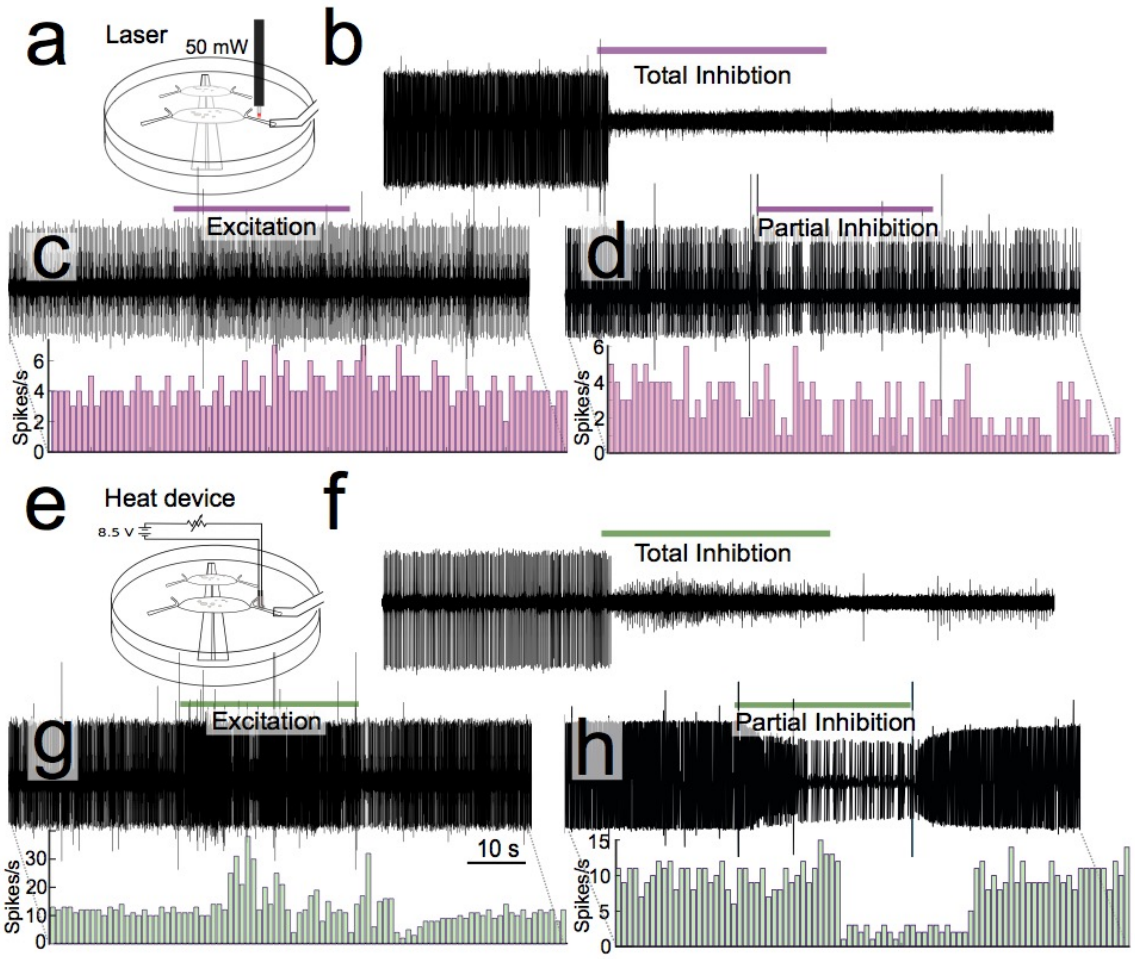

Figure 3.6. The effects of ultrasound can be mimicked by localized application of fUS-comparable heat. **(a) & (e)** Schematics of the laser tool and nichrome wire heating device shown respectively for heat application to the DP nerve. **(b)** Representative extracellular trace of DE-3 firing with 30 seconds (bar) of thermal stimulation using the laser (50 mW), resulting in total inhibition, the most frequent outcome. As with fUS, we also observed some excitation **(c)** and partial inhibition **(d)**. Similar results were obtained using the wire device, with representative traces showing predominantly total inhibition **(f)**, excitation **(g)**, and partial inhibition **(h)**.

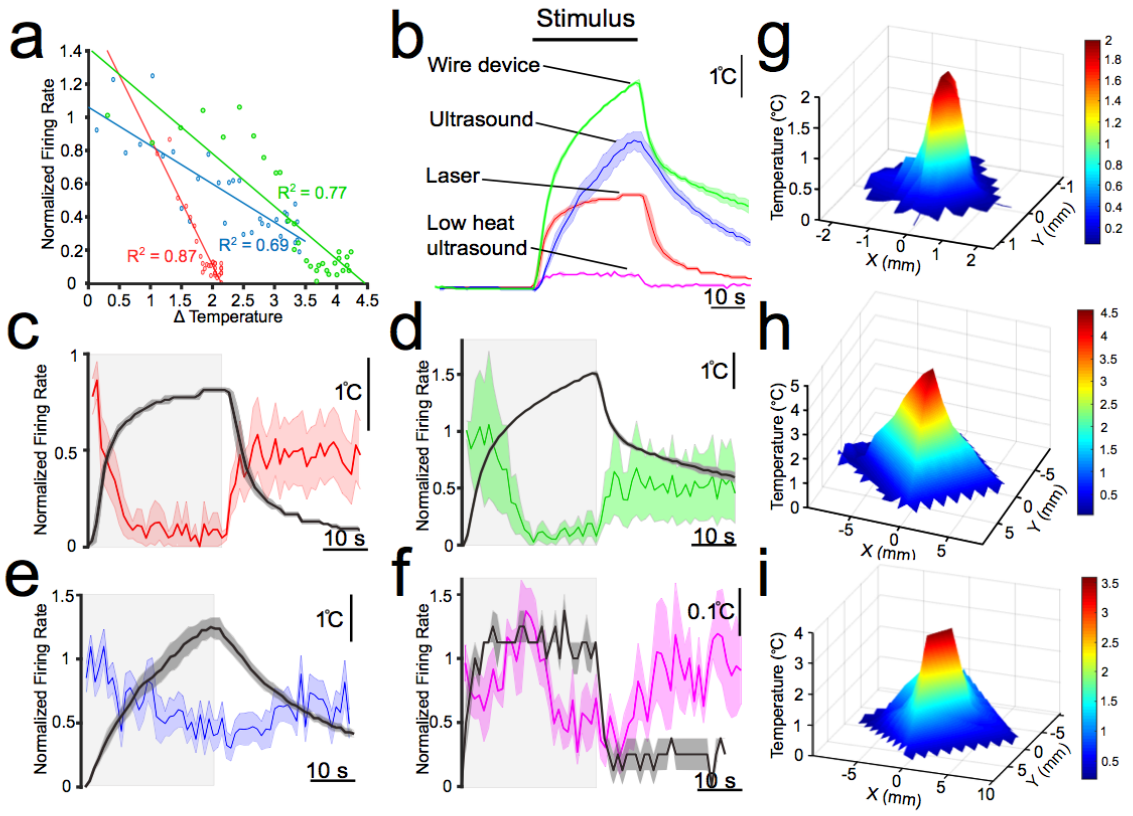

Figure 3.7. The effects of ultrasound can be mimicked by localized application of heat. **(a)** Normalized mean firing rates across inhibitory trials (ultrasound, laser, wire device) plotted against the corresponding increase in temperature. **(b)** Averaged thermocouple recordings (N = 3) for each stimulus type; central line = mean, shaded areas = ± SEM. **(c – f)** Averaged normalized firing rates across inhibitory trials. Shaded areas = SEM. Stimulus was applied during gray window. Thermocouple recordings are overlaid (mean = black line, gray shaded area = SEM). **(g – i)** Plots of spatial distribution of heat generated by thermocouple recordings of different stimuli in X and Y directions from center (position of nerve). Plots are linearly interpolated from measurements (mean of 2) taken at ¼ mm increments **(g)**, or 1 mm increments **(h, i)**; stimuli were attached to a notched micromanipulator to ensure accurate movement, thermocouple remained fixed. **(g)** Spatial distribution of heating generated by the laser. **(h)** Spatial distribution of heating generated by the wire device. **(i)** Spatial distribution of heating generated by fUS.

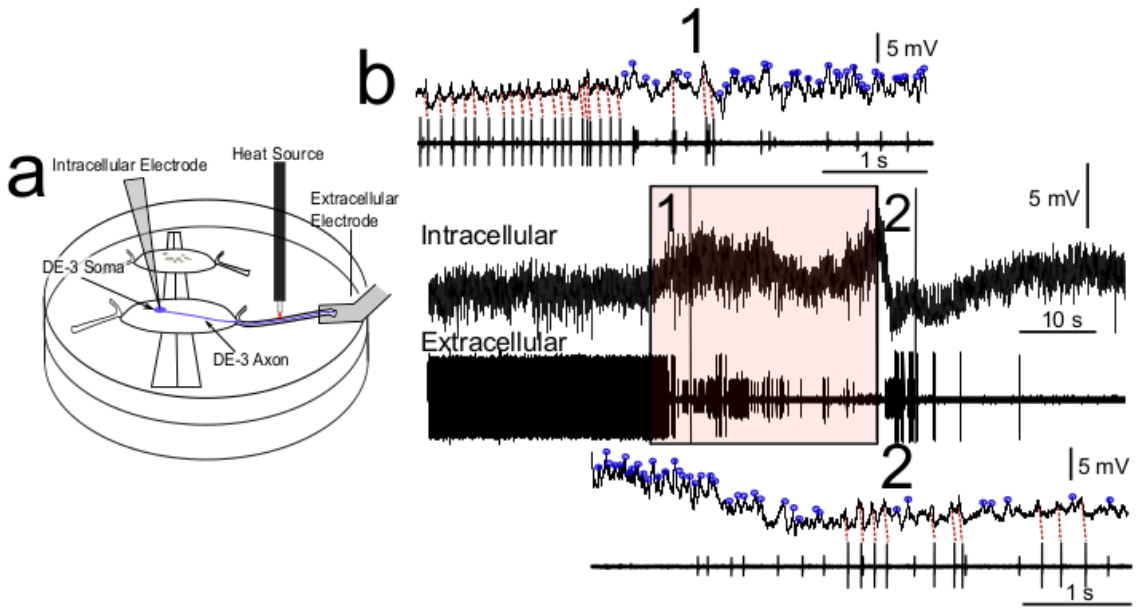

Figure 3.8. US-comparable heat blocks propagation of the DE-3 spike in the DP nerve. **(a)** Schematic showing the placement of heat delivery (laser) and the position of the dual intra- and extracellular DE-3 recording sites during heat application (red boxes). **(b)** Prior to laser heat application, the intracellular spike recorded in the soma of DE-3 (near the spike initiation zone) can be seen to correlate one-for-one with the extracellular DE-3 spike (Inset 1, expansion of first five seconds of stimulus). Upon heat delivery, however, the extracellular spike disappears despite the continuation of the intracellular spike, indicating a conduction block at the site of heat application between the spike initiation site and the distal nerve (Inset 2, expansion of five seconds immediately following stimulus application).

	Laser	Ca^{2+}-free fUS	fUS	Wire device	Bath heating	Control
Heat increase (°C)	2.1	3.4	3.4	4.9	2.0	0
Diameter of heat focus (mm)	1.2	6.8	6.8	8.5	n/a	n/a

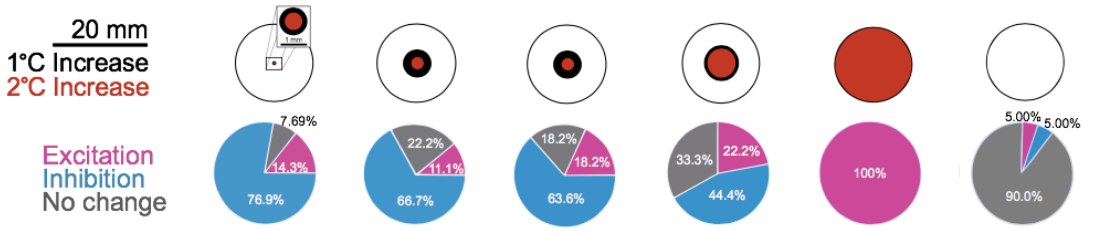

Table 3.1. Neuromodulatory effects were found to differ with respect to the spatial properties of stimuli. We observed a trend whereby a broader heat application (e.g. wire device, bath) elicited proportionally more excitation, whereas a more narrow heating, including the most focused heat source (i.e., the laser), produced more inhibition. FUS applied in the Ca^{2+}-free condition (blockage of synaptic communication) elicited relatively more neuronal inhibition compared to applications in regular saline. While the thermal properties in this condition were identical to those in the regular saline one, we observed less excitation, which was likely due to the reduction of network-level synaptic inputs that might increase neuronal activity.

CHAPTER 4

Focused ultrasound neuromodulation and the confounds of intracellular electrophysiological investigation

Publication Citation:
Collins and Mesce (2020) eNeuro [*in press*, full citation pending]

4.1 | Summary

Focused ultrasound can modulate neuronal activity noninvasively with high spatial specificity. In intact nervous systems, however, efforts to determine its enigmatic mode of efficacy have been confounded by the indirect effects of ultrasound on mechanosensitive sensory cells and the inability to target equivalent populations of cells with precision across preparations. Single-cell approaches, either via cultured mammalian neurons or tractable invertebrate neural systems, hold great promise for elucidating the cellular mechanisms underlying the actions of ultrasound. Here, we present evidence from the medicinal leech, *Hirudo verbana*, that researchers should apply caution when utilizing ultrasound in conjunction with single-cell electrophysiological recording techniques, including sharp-electrode intracellular recording. Although we found that ultrasound could elicit depolarization of the resting membrane potential of single neurons, a finding with precedent, we determined that this effect and others could be reliably mimicked via subtle manual displacement of the recording electrode. Because focused ultrasound is known to induce resonance of recording electrodes, we aimed to determine how similarly ultrasound-induced depolarizations matched those produced by micro movements of a sharp glass electrode, a phenomenon we believe can account for purported depolarizations

measured in this manner. Furthermore, we show that when clonally related homologous neurons, which are essentially isopotential, are impaled prior to the application of focused ultrasound, they show a statistically significant change in their membrane potential as compared to the homologous cells that received ultrasound with no initial impalement. Future investigations into ultrasound's cellular effects should attempt to control for potential electrode resonance or utilize alternative recording strategies.

4.2 | Significance statement

Interest in focused ultrasound (US) neuromodulation has soared in recent years, yet researchers have yet to agree on whether ultrasound excites or inhibits neuronal activity, or what mechanisms underly these effects. Basic investigations have attempted to clarify how US affects neuronal membrane properties to understand how it alters firing rates. Several groups have linked ultrasound-induced excitation to depolarization of the resting membrane potential, as measured with intracellular sharp electrodes or membrane patch methods. Here, we replicate this depolarization while recording with intracellular sharp electrodes, but find that the depolarizing effects of US can be replicated by small displacements of the recording electrode. We conclude that intracellular electrophysiological investigations of ultrasound's neuromodulatory effects are susceptible to artifacts introduced via electrode resonance.

4.3 I Introduction

Focused ultrasound (US) is currently under investigation as a promising noninvasive neuromodulation technology. Reports of the effects of US on nervous tissue date back 100 years (Harvey, 1929). Recently, the pace of US neuromodulation research has accelerated as other neuromodulatory technologies (e.g., those utilizing implantable devices) have proven to be therapeutic for the treatment of an ever-increasing array of neurological disorders. Uniquely among noninvasive technologies, US has the ability to deliver energy noninvasively to deep brain structures with high spatial specificity (Hynynen and Clement, 2007; Ai et al., 2016).

Despite evidence that US modulates neuronal activity in a wide range of animal systems, including humans (Legon et al., 2014, 2018), inconsistencies in reported outcomes persist with respect to the direction of its effects. Researchers have reported both US-induced neuronal excitation (e.g., Tyler et al., 2008; Tufail et al., 2010; Yoo et al., 2011; Kim et al., 2012, 2014; Downs et al., 2018) and inhibition (Fry et al., 1958; Rinaldi et al., 1991; Min et al., 2011; Legon et al., 2014, 2018; Kim et al., 2015). Furthermore, underlying mechanisms to account for the neuronal excitatory and inhibitory actions of US have been ascribed to being thermal (Lele, 1963; Colucci et al., 2009; Darrow et al., 2019), mechanical (direct or via US-induced cavitation) (Plaksin et al., 2014; Wright et al., 2017; Kubanek et al., 2018; Menz et al., 2019), or a combination of the two (Bachtold et al., 1998). Efforts to elucidate how US modulates neural activity have been

confounded by the US activation of mechanosensory structures, including auditory hair cells (Guo et al., 2018; Sato et al., 2018). To circumvent these and other complicating factors, we and other groups have examined how US influences neurons on a foundational level in tractable invertebrate systems (Wright et al., 2015, 2017; Yoo et al., 2017; Kubanek et al., 2018; Dedola et al., 2020), mammalian cell culture (Muratore et al., 2009; Qiu et al., 2019), or slice (Rinaldi et al., 1991; Bachtold et al., 1998; Tyler et al., 2008; Prieto et al., 2018).

Recently, we obtained evidence to support the idea that the direct effects of US on nerves at low intensities are largely inhibitory (Mesce and Newhoff, 2020; M. N. Collins, W. Legon and K. A. Mesce, unpublished observations). We obtained these results by studying a synaptically-isolated identified motoneuron in the well-studied medicinal leech, *Hirudo verbana*. This work stands in contrast to some other single-cell reports whereby US was found to induce neuronal excitation via depolarization of the resting membrane potential (Tyler et al., 2008; Lin et al., 2019a; Dedola et al., 2020). Because we used extracellular suction electrodes versus intracellular or patch electrodes to record action potentials from the axons of our identified neuron, we considered whether different recording methodologies might contribute to a phenomenon of excitation versus inhibition.

Here, we examined the effects of US on the resting membrane potentials of identified leech neurons, and asked whether the actions of US could be

influenced by the impalement of a sharp-glass electrode. As in vertebrate neurons, the rising and falling phases of its action potential are mediated by voltage-gated sodium and potassium channels, respectively (Kleinhaus, 1976; Kleinhaus and Prichard, 1976). This is important to note, as these channels have been implicated as actuators of US-induced neuromodulation, yet are not present in all animal models under investigation with US (e.g., *C. elegans* lacks voltage-gated sodium channels).

As our primary target, we chose the Retzius neuron, a serotonergic bilaterally-paired cell located on the ventral surface of all 21 segmental ganglia. This cell has been extensively studied since its discovery in 1891 (Carretta, 1988). Its large soma (50-80 μm diameter) has enabled its rapid identification and subsequent impalement during intracellular recording experiments. The two Retzius neurons per segmental ganglion are electrotonically coupled and nearly isopotential (Hagiwara and Morita, 1962; Eckert, 1963). To compare our findings with a recent intracellular investigation of US on leech nociceptive (N) cells (Dedola et al., 2020), we performed additional experiments on this cell type.

Specifically, we studied whether physical microadjustments of the intracellular electrode could mimic the depolarized state and related action potential parameters induced by US. We found that US-induced changes, including depolarization of the resting membrane potential, an increase in spike frequency, and attenuation of spike amplitude could be mimicked by brief, manual electrode displacements. Due to known US-induced electrode

resonance, the rapid depolarization of cells found to occur in neurons in response to US application during intracellular recording may be artifactual, as we have found here.

4.4 l Materials and Methods

4.4.1 l Animal preparation

We examined the effects of US and manual electrode displacement on Retzius neurons from the medicinal leech, *Hirudo verbana*. Retzius cells are present bilaterally in each of the leech's 21 segmental ganglia; a diagram of the leech nervous system and a single ganglion are shown in Fig. 1a & b. Retzius cells can be readily identified due to their large size and firing properties, enabling rapid entry and re-entry of the same cell. The resting membrane potential is typically -30 to -50 mV, and spikes are 20 to 50 mV in amplitude (Hagiwara and Morita, 1962; Eckert, 1963). The cell's soma and neurites are visible in a Neurobiotin cell fill in Fig. 1c.

We obtained hermaphroditic adult leeches from Niagara Medical Leeches (Niagara, NY, USA); they were housed at room temperature (22-24°C) in a large tank filled with pond water and anaesthetized on ice prior to dissection. Single leech ganglia were pinned ventral side up in a petri dish lined with 2 mm-thick SYLGARD™ (Dow Corning) and filled with leech saline (in mM: 115 NaCl, 4.0 KCl, 1.8 $CaCl_2$, 1.5 $MgCl_2$, 10.0 Glucose, and 10.0 Trizma pre-set crystals, all from Sigma Aldrich; recipe adapted from Nicholls and Baylor, 1968). A 5 mm

diameter circle of SYLGARD™ directly beneath the ganglion was removed, and the hole in the dish was sealed with a thin layer of latex.

4.4.2 l Intracellular recording

The somata of Retzius neurons were impaled with sharp electrodes made from borosilicate glass (1 mm outer diameter, 0.75 mm inner diameter) pulled to resistances of 25-40 MΩ on a micropipette puller (P-87, Sutter Instrument Co.); electrodes were filled with 2 M potassium acetate and 20 mM KCl (Cymbalyuk et al., 2002). Recordings were amplified (IX2-700 dual intracellular preamp, Dagan Corp.), digitized (Axon CNS Digidata 1440A, Molecular Devices), and bridge balanced. Data were acquired with pClamp software (Axon Instruments) and imported into MATLAB (R2018b, MathWorks, Inc.) for analysis.

The ultrasound transducer (Sonic Concepts H102-MR) was placed beneath the preparation (see schematic in Fig. 1d). The degassed, deionized water-filled focusing cone was sealed to the latex-covered dish opening with a drop of water, ensuring continuous transmission of energy from the transducer to the ganglion.

4.4.3 l Neurobiotin cell filling

The Retzius cell fill displayed in Fig. 1c was filled by iontophoretic injection of Neurobiotin (Vector Laboratories). Briefly, the tip of an intracellular recording electrode was filled with 5% Neurobiotin dissolved in 2 M KAc; the electrode was

then backfilled with 2 M KAc and 20 mM KCl. Following cell impalement, we injected 2 nA negative current for a duration of 20 minutes. The ganglion was incubated at room temperature for 45 minutes following iontophoretic injection to allow the dye to diffuse to distal structures. Following this incubation period, the ganglion was fixed in 4% paraformaldehyde (overnight at 4°C) and rinsed in iso-osmotic Millonig's buffer (all components from Sigma Aldrich, recipe from Puhl and Bigelow et al., 2018). Cells were permeabilized in 1% Triton in iso-osmotic buffer for 2 hours, and incubated overnight at 4°C in a 1:50 dilution of streptavidin conjugated to Cy3 (Jackson ImmunoResearch Laboratories, Inc.). The ganglion was then rinsed in iso-osmotic Millonig's buffer, dehydrated in ethanol, and mounted between glass coverslips using DEPEX mounting medium (VWR International). The filled Retzius cell was imaged on a Nikon A1 laser-scanning confocal microscope, and the resulting image was processed in ImageJ.

4.4.4 l Electrode displacement paradigm

For our electrode displacement paradigm (Fig. 1e), we rapidly raised and lowered the recording electrode by rotating the knob of our micromanipulator (Leitz joystick model, Leica Optical). Distance raised was tracked using marked notches on the fine-adjustment knob (each notch corresponds to a distance of 200 nm). The motion took ca. 2 seconds, the fastest time in which we could consistently raise and lower the electrode. As with our US trials, electrode displacement was induced following a 20 second baseline recording, and

subsequent trials had increased displacement until electrode impalement was lost.

4.4.5 l Ultrasound characterization and parameters

All US waveforms were designed by a waveform generator (Agilent 33500B Series) and triggered by a TTL pulse from our intracellular recording digitizer via pClamp software. Waveforms were amplified by a 100 W RF linear power amplifier (E&I, model 2100L) and impedance matched with a matching network (Sonic Concepts). Transducer output was characterized by hydrophone (ONDA HNR-0500) measurements in 0.5 mm increments in x, y, and z directions in a large tank filled with deionized, degassed water. Shown in Fig. 2c are the vertical and horizontal cross-sections of linearly interpolated hydrophone measurements (step size = 500 microns in x, y, and z directions; 309 total measurements) at peak amplitudes, which are overlaid with scaled preparation dimensions.

In our first paradigm (Figs. 3 & 4), US trials consisted of the application of a single tone of 960 kHz pulsed ultrasound for 100 ms following a 20 second baseline recording period. Pulses were 313 μs in duration and were delivered at a 1 kHz pulse repetition frequency. Peak pressures and intensities were increased sequentially in repeated trials until the electrode impalement was lost. Pulse parameters and the range of pressures and intensities used are described in Fig. 2.

In our second paradigm (Fig. 5), US trials consisted of a single tone of 960 kHz continuous (100% duty cycle) US applied for 300 ms. Peak pressures and intensities were increased sequentially in repeated trials until electrode impalement was lost.

In our third paradigm (Fig. 6), US trials consisted of a 20-minute application of 960 kHz pulsed ultrasound preceded by a baseline recording period of at least 20 seconds. A subsequent baseline recording was made after the ultrasound application. Ultrasound was applied for the first 10 seconds of every minute (tone duration = 10 s). Tones consisted of 313 μs pulses (pulse duration) pulsed at 1 kHz (pulse repetition frequency), yielding a duty cycle of ~30%. Ultrasound intensity and pressure were fixed at 4 W/cm^2 spatial peak pulse average intensity (I_{SPPA}) and 111 kPa, respectively.

4.4.6 l Statistics

All statistical tests save power analyses were performed in MATLAB. Data were tested for normality via Shapiro-Wilk tests. Comparisons of non-normally distributed data were performed via non-parametric Wilcoxon rank-sum tests; normally distributed data were compared via Welch's *t*-tests. All hypothesis tests were two-tailed with $\alpha = 0.05$. We quantified effect sizes [Cohen's d with correction for small sample sizes (Durlak, 2009)], and performed post-hoc power analyses. Power analyses were performed using G*Power 3.1 (Erdfelder et al., 2009). All statistical results are reported in Table 1.

4.5 l Results

4.5.1 l Ultrasound depolarizes Retzius neurons and alters spike frequency and waveform

For the first set of experiments, depicted in Figs. 3 and 4, we applied US as described to 14 leech ganglia while recording intracellularly from one of the bilateral Retzius cells (n = 14 Retzius cells). Data from 2/14 recordings were not included in analyses due to an unstable baseline (membrane potential rising rapidly prior to US application due to poor electrode impalement); final n = 12. US induced a dose-dependent rise in the resting membrane potential, with higher pressures yielding greater depolarization. As US pressure increased in subsequent trials, neurons typically showed increasing levels of depolarization until the cell was lost, as evidenced by a sharp, high amplitude increase in voltage consistent with partial or full loss of electrode impalement. Aggregated data demonstrating mean depolarization at ascending pressures are shown in Fig. 3a; only data from the five lowest pressures are displayed, as these were sufficient to induce effects and/or loss in most of the cells tested, and thus our sample sizes at higher pressures were low. Responses were highly variable with respect to the pressures at which cells were lost (mean = 110.38 kPa, SD = 56.22). The mean time to peak depolarization following the US onset was 1.19 s (SD = 1.43). At maximally depolarizing pressures prior to loss (mean = 77.69 kPa, SD = 51.54), cells were depolarized by an average of 3.73 mV (SD = 3.25).

We also observed changes in spike amplitude and spike frequency during peak depolarization (time from stimulus onset to beginning of a sustained period of repolarization towards baseline membrane potential). During peak depolarizations, most cells (n = 10/12) fired action potentials. Of these cells, mean spike amplitude (normalized to spike amplitude during 20 s baseline) was decreased (mean normalized spike amplitude = 0.88, SD = 0.20). Because changes in spike frequency were highly variable and the data were skewed, we have opted to report data dispersion versus mean and standard deviation. The median normalized spike frequency during the period of peak depolarization was 2.28; the interquartile range was 10.4. All data points are visible in Fig. 4b.

Despite our awareness of others achieving similar results with respect to US-induced depolarization (Dedola et al., 2020), several factors gave us pause with respect to the legitimacy of our data. First, we observed high variability in responses to our tested pressures, which was less expected in this system than others due to our use of the same identified neuron in all preparations. Second, The sharp upward deflections in membrane potential even during moderate US-induced depolarizations were reminiscent of what we observed when a cell recording was naturally lost due to stochastic factors, a phenomenon that can occur in gradations (partial versus full loss), with a clear reduction in spike amplitude in instances in which partial electrode impalement remains. US causes mechanical disturbance of targeted tissue and can cause electrode resonance that can result in loss of contact with the recorded neuron (Tyler et al., 2008).

We, like others, attributed cell loss resulting from US application to electrode resonance. We further suspected that US applications that fell below the pressure threshold to induce a full recording loss might induce a partial one, resulting in depolarization of the resting membrane potential and other reversible changes that, in isolation, could appear to be the cellular signatures of excitatory neuromodulatory processes.

4.5.2 l Electrode displacement mimics ultrasound-induced effects

To determine whether brief disruption of electrode placement could elicit effects comparable to US reliably, we performed trials in which we manually displaced the recording electrode in increasing increments while recording from Retzius cells in an additional 13 ganglia (n = 13 Retzius cells). The recording electrode was raised and lowered vertically in 2-second motions; displacement magnitude was standardized via notches on the micromanipulator knob corresponding to 200 nm distances. Data from one cell was not included in analyses due to an unstable baseline (final n = 12). Increasing displacements yielded dose-dependent depolarizations (see means of data aggregated across cells in Fig. 3a.). We observed high variability in the displacement magnitude necessary to lose cell impalement, with a mean of 3.93 μm (SD = 1.92). Time to maximum depolarization was also variable, occurring on average 4.34s (SD = 5.83) from the start of the displacement motion. At maximally depolarizing displacements, prior to cell loss (mean = 2.38 μm, SD = 1.42), cells depolarized

by an average of 3.62 mV (SD = 2.53). We also observed a reduction in spike amplitude and a reduction in spike frequency in the 10/12 cells that fired action potentials during the period of peak depolarization, similar to what we had observed with US. Mean normalized spike amplitude during peak US effects was 0.91 mV (SD = 0.16). Comparable to changes in spike frequency in the US condition, changes were highly variable and skewed, so we again opted to describe data dispersion versus mean and standard deviation. The median normalized spike frequency during the period of peak depolarization was 2.24; the interquartile range was 3.23. All data points are visible in Fig. 4b.

Both US and manual electrode displacement were found to depolarize cells up to a threshold that resulted in a loss of the intracellular recording; examples may be seen in Fig. 3b., in which traces show typical outcomes in a cell exposed to US at increasing pressures (upper; pink), and a cell subjected to electrode displacement (lower; green). Time to peak depolarization differed between the two conditions (see Fig. 3c and d); $Z= 2.6275$, $p=0.0086$[a]. This difference is consistent with the differential in stimulus application time (100 ms for US vs. 2 seconds for electrode displacement). We observed an increase in spike frequency and a decrease in spike amplitude in both US and electrode displacement conditions (Fig. 4a-d). Mean increase in spike frequency and decrease in spike amplitude at maximally depolarizing levels prior to loss did not differ significantly between US and electrode displacement (spike frequency: Z =

0.1890, p = 0.8501[b], Wilcoxon rank-sum test; spike amplitude: t(17.33) = 0.2777, p = 0.7843[c], Welch's *t*-test).

4.5.3 | The depolarizing effects of ultrasound and electrode displacement are common to nociceptive neurons

To assess whether our observed effects were applicable to other identified neurons in the leech, we performed an additional set of experiments on another cell type, the nociceptive (N) cell (Fig. 5a.). This cell was chosen due to its usage in a recent study in which US is reported to depolarize leech neurons in an intracellular paradigm (Dedola et al., 2020). We adjusted pulse parameters to mimic more closely those found to be effective in eliciting a response in N cells: we applied a single pulse of continuous US with a 300 ms pulse duration (Fig. 5b). We were unable to replicate fully the authors' paradigm as we were constrained by the higher center frequency of our ultrasound transducer (960 kHz vs. 490 kHz).

We applied US at ascending pressures to 6 N cells (n = 6) while recording intracellularly. Our first tested pressure was 20 kPa (root mean squared, the highest pressure used by Dedola et al. (2020)); we observed that 0/6 cells responded. Increasing pressures, however, were sufficient to elicit depolarization and, ultimately, loss of electrode impalement. At maximally depolarizing pressures prior to recording loss (mean = 49.3 kPa, SD = 30.5), mean

depolarization was 3.50 mV (SD = 4.11). A representative trace of this depolarization is displayed in Fig. 5c (upper).

We next assessed whether these effects could be mimicked by electrode displacement in a manner comparable to what we observed in Retzius cells. We again displaced the recording electrodes by ascending distances until the intracellular recording was lost. We observed a similar phenomenon, in which electrode deflections insufficient to compromise the recording resulted in small depolarizations. Maximal depolarization prior to loss of electrode impalement was achieved at 2.25 μm (SD = 0.99), and averaged 3.45 mV (SD = 3.45). A representative trace of this effect is displayed in Fig. 5c (lower).

4.5.4 l Ultrasound application following electrode impalement depolarizes Retzius neurons

Our results in both cell types raised concern as to whether US-induced changes in the resting membrane potential of neurons could be accurately assessed via intracellular recording during US application. We next sought to determine whether it was feasible to measure changes by comparing baseline characteristics from the same cell before and after ultrasound application. The large, physiologically robust, and easily identifiable nature of the Retzius neurons enabled re-entry into the same cell in 20-30 seconds following cessation of US application. We were concerned that the effects of a 100 ms application of pulsed US, as we had used in our previous experiment, would not persist for the time

taken to re-enter the cell. Assuming longer application times yielded more persistent effects, we dramatically increased the US application period to 20 minutes. Ultrasound parameters for these experiments are outlined in Fig. 6a.; the broader experimental design is outlined in Fig. 6b.

We found that Retzius neurons (n = 8) exposed to 20 minutes of ultrasound were depolarized from their pre-US baseline (mean change = 16.03 mV, SD = 8.29). Neurons re-entered after a 20-minute wait period with no ultrasound (control condition, n = 8) did not have a demonstrable change in membrane potential (mean change = 0.0625 mV, SD = 5.57). The change in membrane potential in the US vs. control conditions differed significantly (Z=100, p=1.554E-4[d], Wilcoxon rank-sum test). Intracellular traces recorded in the same cell before and after US application are shown for comparison in Fig. 6c.

Despite this compelling result, we were concerned that the depolarization we observed as a function of US application could still have resulted from electrode-associated artifactual effects, including creation of a leaking puncture in the cell membrane, or the introduction of cavitational nuclei. As a control, we performed a similar experiment in which we recorded from the contralateral Retzius neuron following US application instead of the same cell (see schematic in Fig. 6b, lower). The two Retzius neurons in each ganglion are electrically coupled and are known to be isopotential (Hagiwara and Morita, 1962; Eckert, 1963). Recording from the contralateral cell yielded an opportunity to estimate changes in membrane potential caused by US in an electrode-naïve cell.

Intriguingly, the depolarization we observed in the same-cell condition did not persist significantly in the contralateral condition ($p = 0.1605$, Wilcoxon rank-sum test), suggesting the stark depolarization we observed in the same-cell condition could have been influenced by the initial electrode impalement.

4.6 | Discussion

4.6.1 | Overview

We have demonstrated that US reliably produces a dose-dependent depolarization of the resting membrane potential of single leech Retzius neurons when applied during intracellular sharp-electrode recording. We found that these effects, however, are likely to be artifactual as they could be mimicked by the manual displacement of the recording electrode. US effects appeared to differ from manual electrode displacement only with respect to the time to achieve peak effects. We believe that this difference is simply due to the time course of the applied stimulus across the two paradigms; for example, US was delivered for 100 ms, while manual displacement and replacement of the electrode took longer (ca. 2 seconds). We also determined that even when the recording electrode was removed from the targeted neuron during US application, the baseline (i.e., first) impalement appeared to cause a sufficient leak current to affect the subsequent membrane properties of the Retzius cell when recorded after US application (Fig. 6). In contrast, by recording from the electrode-naïve contralateral Retzius neuron, which was impaled only once and after the US was

applied, we observed that US did not induce a statistically significant elevation in resting membrane potential.

We observed similar results, as discussed above, when targeting N cells, sensory neurons recently reported to depolarize during US application (Dedola et al., 2020). Utilizing one of the authors' employed pulse parameters (300 ms of continuous US), we observed depolarization of a comparable magnitude. Achieving this effect, however, required the use of higher pressures than the authors reported, which we attribute to our use of a higher US frequency. Higher frequencies (with lower wavelengths) generate less electrode resonance. As we suspect that electrode resonance is a primary driver of depolarization in intracellular paradigms, it follows that higher pressures may be required to elicit comparable depolarizations when working with higher US frequencies. Importantly, by briefly displacing the recording electrode, we were able to mimic the effects of US on the N cells as well.

We conclude that a nonspecific leak current most likely contributes to the US-induced depolarizations we observed. In leech neurons, it has been shown previously that sharp electrode impalement can affect nonspecific leak currents, having profound effects on the ability of some cells, for example, to exhibit endogenous bursting activity (Cymbalyuk et al., 2002).

4.6.2 | The confounds of electrode recording techniques

Ultrasound-induced electrode resonance is a commonly-reported problem, complicating efforts to asses US effects via whole-cell patch clamp (Tyler et al., 2008; Prieto et al., 2018) and two-electrode voltage clamp (Kubanek et al., 2016). Although these reports utilized different single-cell recording modalities, some of the electrophysiological signatures of neuromodulation following US onset resemble our own, characterized by a very steep initial depolarization that elicits action potentials (Tyler et al., 2008). This steep depolarization and increase in spike frequency were observed similarly in a recent intracellular sharp electrode study of the actions of US on a type of leech sensory neuron (Dedola et al., 2020). These authors also reported a US-associated reduction in spike amplitude, which is consistent with our US and electrode displacement data. We cannot rule out the possibility that US can induce a rapid depolarization, at certain US parameters and in some types of neurons across animal models, as suggested by prior work utilizing optophysiological techniques (Tyler et al., 2008; Qiu et al., 2019). We can, however, strongly posit that electrode resonance is a potent indirect driver of US-induced neuronal stimulation in the context of intracellular paradigms, especially in the leech.

Concerns of artifactual effects have been raised previously, when it was postulated that US-induced electrode resonance, particularly at sub-MHz frequencies, could introduce depolarizing leak currents in *Xenopus* oocytes (Kubanek et al., 2016). It remains unclear whether extracellular recordings are similarly prone to artifactual effects when combined with US. Minute movements

of an animal preparation or displacement of any type of electrode induced by ultrasound could cause a temporary reduction in electrode resistance, yielding an artifactual reduction in voltage as measured, for example, in the form of a reduced-amplitude single or compound action potential.

One additional concern in combining US with single-cell electrophysiological recording techniques is the potential to introduce cavitational nuclei. Ultrasound has been theorized to depolarize neurons through the rhythmic expansion and contraction of microbubbles in the cell membrane, altering membrane capacitance (Krasovitski et al., 2011; Plaksin et al., 2014). Electrode insertion could transport non-endogenous cavitational nuclei to the cell membrane from the surrounding media, facilitating US effects. Degassing the saline medium, as was done in our report, may limit the potential for artifactual cavitational effects. However, aerating bath disturbances caused by insertion and movement of the recording electrode remain potential considerations. The introduction of cavitational nuclei may be of particular concern with mammalian preparations that require continued oxygenation.

4.6.3 | Alternative approaches

Moving forward, reducing the confounds of electrode resonance will be important to achieve confidence in defining the cellular underpinnings of ultrasound's actions. Resonance can be reduced by separating the recording site from the site of US application (e.g., applying US to a neuron's axon while

recording from the soma). This is an imperfect solution, however, as distal changes to membrane properties may not be accurately reflected at the soma due to space clamp issues (Spruston and Johnston, 2008). Another potential means of reducing resonance is by increasing US frequency, thereby decreasing wavelength, a strategy with which other groups have found success (Prieto et al., 2018; Ye et al., 2018). Although this latter strategy may be effective in reducing resonance, it cannot eliminate it entirely, and there remains the potential for a resonating electrode to cause a leak at the site of electrode entry, increasing cell permeability to surrounding sodium-rich media and inducing artifactual depolarization. In addition, it remains unclear whether US at frequencies in the 10s of MHz range, as used in these studies, affect neural function in a manner comparable to US in the 100s of kHz range utilized in transcranial studies (e.g., Tufail et al., 2010; Min et al., 2011; Legon et al., 2014, 2018; Lee et al., 2016).

In conclusion, we are of the opinion that future investigations exploring the effects of US on single neurons should avoid simultaneous intracellular recording and ultrasound delivery. Investigations that incorporate extracellular or optical recording approaches may be better suited to control for the potential artifactual effects of electrode resonance, an idea already adopted by some other groups who have found success with optical alternatives to classical electrophysiological techniques, including the use of ion-indicator dyes (Tyler et al., 2008; Qiu et al., 2019).

4.7 l Figures and tables

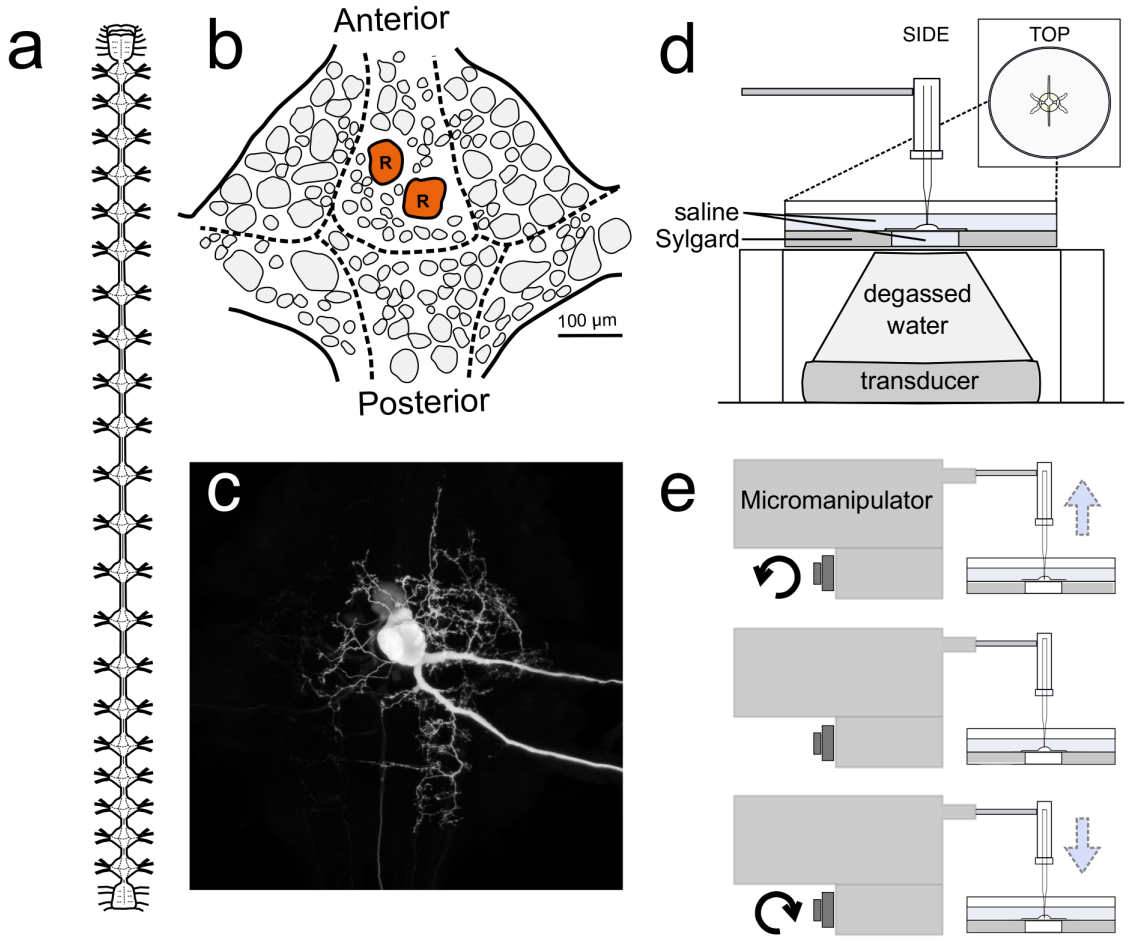

Figure 4.1. The medicinal leech and experimental design. **(a)** Diagram of the central nervous system of the leech, characterized by a ventral nerve cord interspersed with 21 segmental ganglia descending from a compound cephalic ganglion. **(b)** Schematic of the placement of neuronal somata on the ventral surface of a single ganglion. The bilateral Retzius cells are colored red and labeled “R”. **(c)** Neurobiotin fill of a Retzius cell showing its soma, neurites, and axons (a faintly labeled contralateral soma is present due to electrical coupling of the 2 cells). **(d)** Ultrasound paradigm demonstrating the positioning of the transducer, intracellular electrode and ganglion preparation. **(e)** Side view of the electrode displacement paradigm demonstrating the movement of the recording electrode.

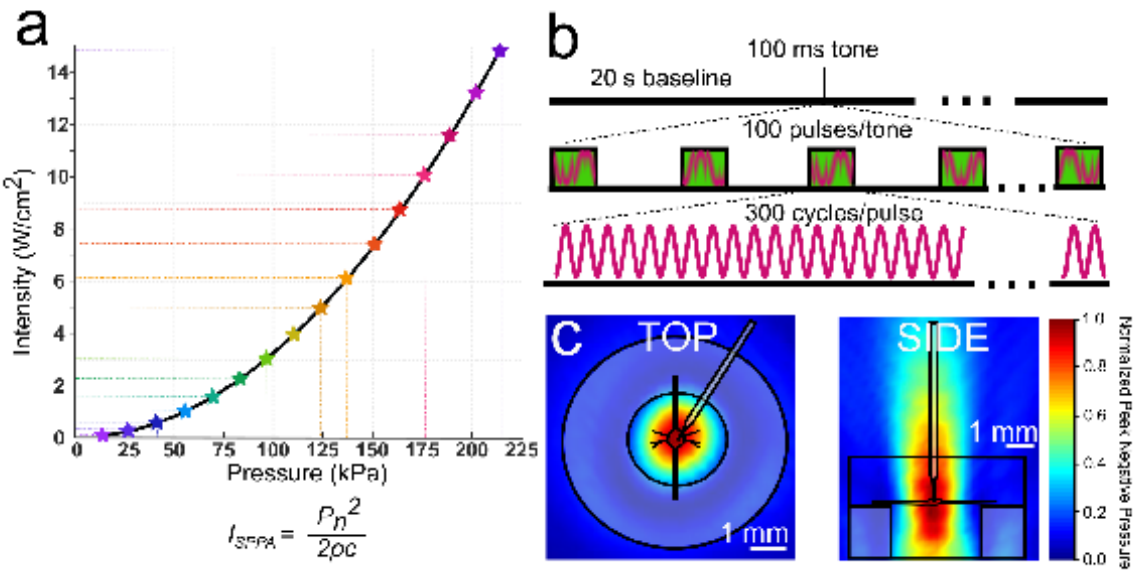

Figure 4.2. Ultrasound parameters. **(a)** In this graph, all the pressures utilized in this study and their corresponding intensities (spatial peak pulse average) are indicated. Intensities were calculated using the equation shown in **(a)** where P_n = pressure; Þ = density of nerve tissue, estimated to be 1.03 g/cm^3; c = speed of sound in saline medium, estimated to be 1507 m/s. **(b)** Ultrasound pulse parameters. 960 kHz ultrasound was applied for a single tone of 100 ms duration. Tones consisted of 100 pulses of 300 cycles of ultrasound (313 μs pulse duration). **(c)** Linearly interpolated pressure distribution maps overlaid with scale preparation, dish, and electrode.

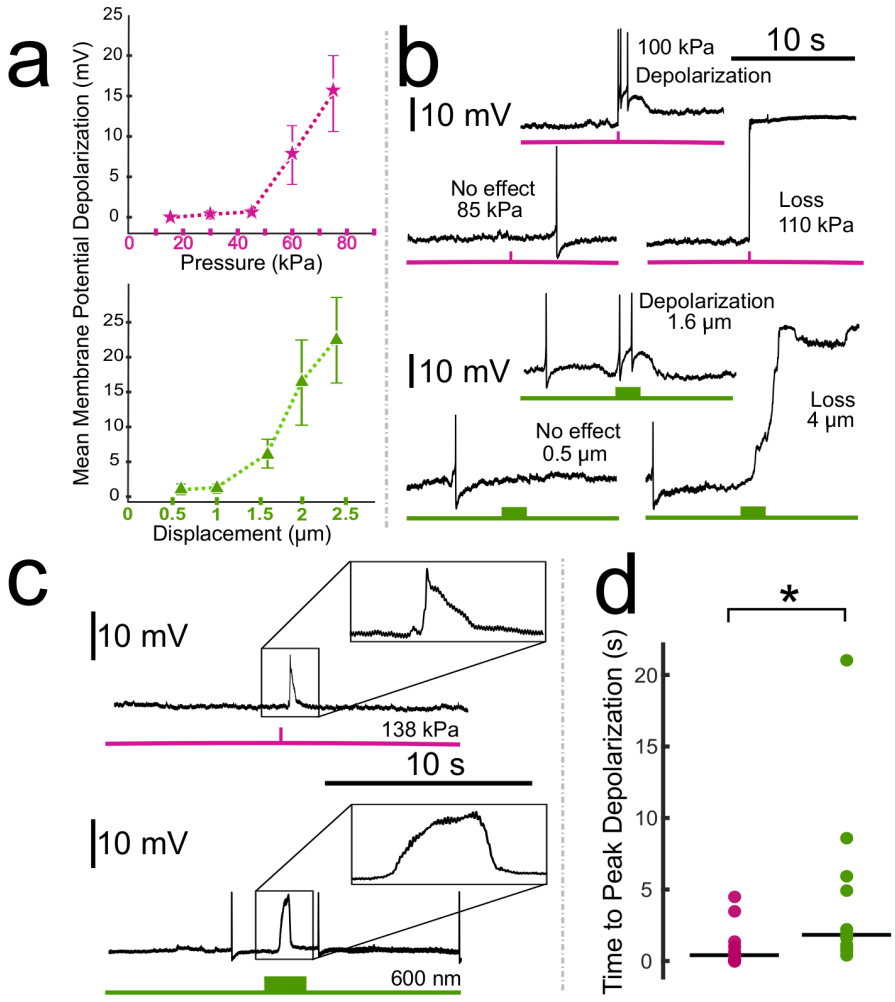

Figure 4.3. Comparison of the effects of ultrasound and electrode displacement on the resting membrane potential of Retzius neurons **(a)** Plots demonstrating changes in mean membrane potential in response to ultrasound applied at increasing pressures (upper plot, pink) and electrode displacements of increasing distance (lower plot, green), aggregated across preparations. Error bars denote standard error of the mean. **(b)** Intracellular recordings demonstrating effects of ultrasound applied at increasing pressures to the same cell (pink, upper); recordings demonstrating effects of electrode displacement at increasing distances on the same cell (green, lower). **(c)** Intracellular recordings demonstrating typical waveforms of depolarizations elicited by ultrasound (upper) and electrode displacement (lower). **(d)** Scatter plots comparing time to peak depolarization following start of ultrasound (pink) and electrode displacement (green). Horizontal lines denote medians. The difference between the two was significant (Z= 2.6275, p=0.0086, Wilcoxon rank-sum test).

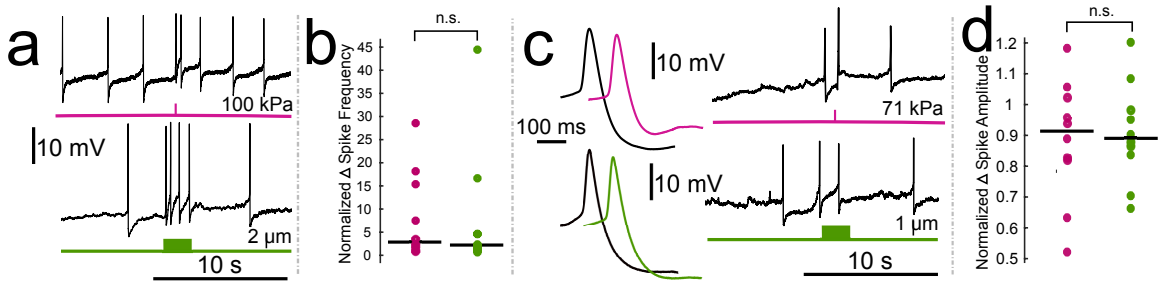

Figure 4.4. Comparison of the effects of electrode displacement on the spike frequency and amplitude of Retzius neurons. **(a)** Intracellular recordings demonstrating ultrasound (upper, pink) and electrode-displacement (lower, green) associated increase in spike frequency. **(b)** Scatter plots comparing the normalized change in spike frequency, during the period of peak effect, in ultrasound (pink) and electrode displacement (green) conditions. Horizontal lines denote medians. The difference between the two did not reach the threshold for significance (Z= 0.1890, p= 0.8501, Wilcoxon rank-sum test). **(c)** Intracellular recordings showing that ultrasound (pink) and electrode displacement (green) induce reductions in spike amplitude. Averaged spike waveforms (left) demonstrate reduction in spike amplitude (black waveforms = averaged from the 2 spikes prior to stimulus onset, pink and green waveforms = averaged from the 2 spikes fired during the peak effect period following ultrasound application and electrode displacement, respectively). **(d)** Scatter plots comparing normalized change in spike amplitude during peak effect period in ultrasound (pink) and electrode displacement (green) conditions. Horizontal lines denote medians. The difference between the two did not reach the threshold for significance (t(17.3329) = 0.2777 , p = 0.7845, Welch's *t*-test).

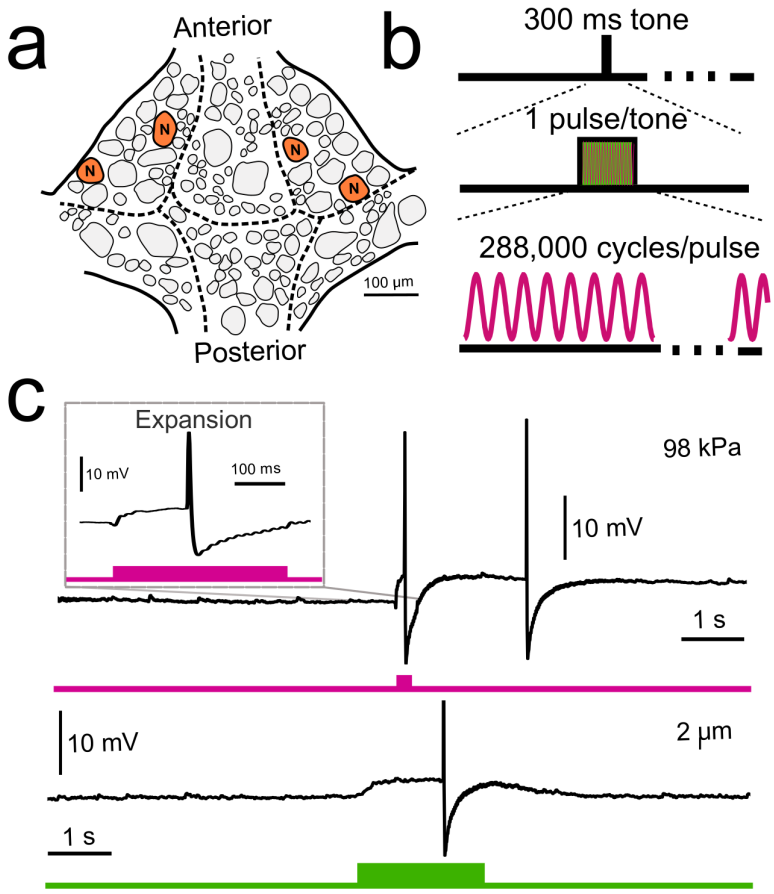

Figure 4.5. Ultrasound application and electrode displacement yield similar results when a different neuron (N cell) and different pulse parameters are used. **(a)** Schematic of ventral surface of a single leech ganglion with Nociceptive (N) neurons marked. **(b)** Ultrasound parameters applied to N cells. We applied one tone (300 ms duration) of continuous (vs. pulsed) ultrasound per trial. **(c)** Representative intracellular traces of N cell voltage during a trial of ultrasound application (upper, pink) and electrode displacement (lower, green). When upper trace is expanded (inset), the waveform closely resembles that observed in the electrode displacement paradigm. The difference in the duration of the ultrasound-induced depolarization can be attributed to the difference in stimulus duration.

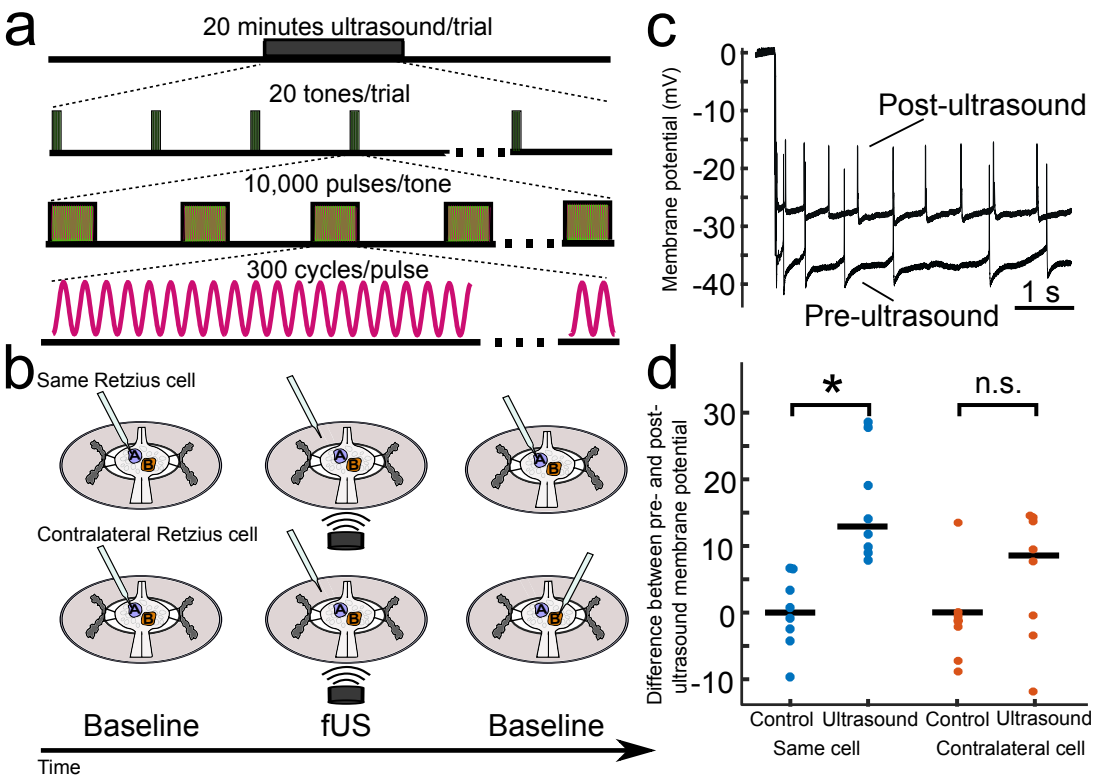

Figure 4.6. Retzius neuron membrane potential following extended ultrasound application is influenced by prior sharp electrode impalement. **(a)** Schematic of extended ultrasound application. Pulsed ultrasound was applied for a 20-minute duration. Tones were delivered the first 10 seconds of each minute (tone duration = 10 s, tone frequency = 0.167 Hz). Tones consisted of 10,000 pulses of 300 cycles of 960 kHz ultrasound (pulse repetition frequency = 1 kHz, pulse duration = 312.5 μs). Pressure applied was 111 kPa in all trials. **(b)** Schematics of trial design for extended application paradigm. Upper: Retzius neuron was impaled (blue) and resting membrane potential was recorded. The recording electrode was then removed (middle cartoon) and ultrasound was applied for 20 minutes. Following ultrasound application, the electrode was re-inserted into the same Retzius cell for a second baseline recording. Lower: In a different preparation, the electrode was inserted into the Retzius cell (blue) to record the resting membrane potential. As in the previous experiment, the electrode was removed prior to 20 minutes of ultrasound application (middle cartoon). After application, the contralateral Retzius cell (orange) was impaled to record baseline activity; this cell was thus not previously impaled. **(c)** Intracellular recordings taken from the same Retzius cell before and after extended application of ultrasound demonstrating post-ultrasound depolarization of the resting membrane potential. **(d)** Scatter plots comparing differences between pre- and post-ultrasound membrane potential in the same cell (blue) and contralateral cell (orange). Control paradigms replaced the ultrasound application period with a waiting period of equivalent time. Membrane potentials of the ultrasound-treated and

control groups differed significantly (Wilcoxon rank-sum test, p = 1.55e-4) when the same Retzius cell was re-impaled. However, the ultrasound and control groups did not differ significantly (Wilcoxon rank-sum test, p = 0.1605) when the contralateral cell was recorded.

	Data Structure	Type of test	Result	Effect size	Power
a	Non-normal US condition: W(11) = 0.7185, p= 0.0018 ED condition: W(11) = 0.6417, p= 4.38e-04	Wilcoxon rank-sum test	Z= 2.6275, p=0.0086	d = 1.3018	0.8438
b	Non-normal US condition: W(9) = 0.7890, p= 0.0141 ED condition: W(9) = 0.5623, p= 2.6799e-04	Wilcoxon rank-sum test	Z= 0.1890, p= 0.8501	d = 0.0135	0.0501
c	Normal US condition: W(9) = 0.9659 , p= 0.8508 ED condition: W(9) = 0.9713 p= 0.9027	Welch's *t*-test	t(17.3329) = 0.2777, p = 0.7845	d = 0.0343	0.0506
d	Non-normal US condition: W(7) = 0.8499, p=0.0951 Control condition: W(7) = 0.9543 p=0.7547	Wilcoxon rank-sum test	Z=100, p=1.554E-4	d = 3.613	0.99
e	Non-normal US condition: W(7) = 0.8802, p=0.189 Control condition: W(7) = 0.8802, p=0.0274	Wilcoxon rank-sum test	p=0.1605	d = 1.3432	0.68

Table 4.1. Description of statistical tests reported in Results. Letters (leftmost column) correspond to p-values of statistical tests as reported in Results. The data structure, test type, result, effect size, and statistical power of these tests are described. Results of Shapiro-Wilk test for normality of data in ultrasound (US) and electrode displacement (ED) conditions (α=0.05) are reported under "Data Structure." Normally distributed data were compared with Welch's *t* test, and non-normal data were compared with the nonparametric Wilcoxon rank-sum test. Effect sizes were calculated as Cohen's d with correction for small sample sizes as described by Durlak (2009).

CHAPTER 5
Conclusions and prospects for future research

5.1 | Introduction

Focused ultrasound (US) neuromodulation is an emerging therapy with the potential to modulate neuronal activity noninvasively with high spatial specificity. The pace of US neuromodulation research has accelerated dramatically in recent years as research evidence mounts of the therapeutic benefits of implantable neuromodulatory devices in the treatment of an ever-increasing array of neurological disorders. US could present an appealing alternative to invasive technologies, sparing patients the risks and expenses of surgery, while maintaining millimeter-level precision (Hynynen and Clement, 2007) in targeting, which is not presently possible with other noninvasive therapies.

Despite strong apparent clinical potential, US neuromodulation has yet to bridge the gap between the laboratory and the clinic, and has yet to be proven therapeutic in the context of neurological disease. Perhaps more pressingly, the precise disorders for which this technology is best suited remain a matter of debate. Though US's neuromodulatory effects have been under investigation for nearly a century (Harvey, 1929), there remains persistent variability in the direction of reported effects. Researchers have described both neuronal excitation (e.g., Kim et al. 2012; King et al. 2013; Kubanek et al. 2018; Lin et al. 2019; Menz et al. 2013; Qiu et al. 2019; Tufail et al. 2010; Tyler et al. 2008;

Wright et al. 2015; Yoo et al. 2011) and inhibition (e.g., Colucci et al. 2009; Darrow et al. 2019; Deffieux et al. 2013; Lee et al. 2015; Legon et al. 2014, 2018; Min et al. 2011; Yoo et al. 2017) in response to US application. The appropriate clinical applications for this technology will be in contexts in which one of these outcomes can be produced reliably and repeatably, and in the absence of deleterious effects (e.g. tissue damage).

Much of the variability in reported effects may stem from the use of different experimental paradigms. Factors that may bias effect direction include model system (e.g., mammalian vs. non-mammalian), targeted location (e.g., transcranial vs. peripheral, or somata versus nerves), and US parameters (frequency, amplitude, and pulse parameters). Outcomes in vertebrate systems may be further influenced by the incidental activation of sensory structures including auditory hair cells, which have been shown to influence cortical activity independent of the US target (Guo et al., 2018; Sato et al., 2018). Finally, the recording modality used to measure US-induced effects may impact observations; it may be hard to assess basic effect direction when recording across a population of neurons, and single-cell electrophysiology may be prone to excitation-mimicking artifacts (Chapter IV).

Here, we reflect on how these and other factors may have yielded opposing outcomes, and offer a unifying thermal mechanism that can be exploited to bias effect direction for eventual clinical usage. This synthesis will be

couched in our own observations of the actions of this technology on single neurons in a tractable invertebrate model, the medicinal leech, *Hirudo verbana*.

5.2 | Proposed mechanisms of ultrasound neuromodulation

US has been demonstrated to induce a wide range of bioeffects on targeted tissue, both neural and non-neural. These effects can be categorized broadly as mechanical or thermal. Mechanical effects refer to those induced by mechanical pressure, and include the activation of stretch-sensitive ion channels via tissue stretch (Zhao et al., 2016b); the generation of shear waves in some body solids including kidney stones (Zhu et al., 2002); and cavitation, the formation and pulsation of microbubbles (Wu and Nyborg, 2008). Thermal effects in turn are those induced by tissue absorption of US energy as heat, which is known to have a litany of effects on body tissues including nervous tissue, including increasing the gating kinetics of ion channels and accelerating metabolic processes (Janssen, 1992; Sminia et al., 1994).

Several early papers utilizing high intensity US reported neuromodulation accompanied by significant heating (> 10 °C) and, consequentially, significant tissue damage (Barnard et al., 1955; Lele, 1963; Ueda et al., 1977). Modern neuromodulation applications utilize much lower intensities, typically those falling within the range of intensities permissible for non-ophthalmic diagnostic use (spatial-peak pulse-average intensity of ≤ 190 W/cm^2; (FDA, 2019)). US-induced tissue temperature increases at these intensities are considerably lower, and are

typically measured or estimated to be ≤ 3 °C (Pasquinelli et al., 2019), with some studies reporting less than 0.1 °C (Tufail et al., 2010; Kim et al., 2012, 2019; Yoo et al., 2018).

In light of the negligible temperature increases reported by most neuromodulation researchers, observed effects on neural activity are most often attributed to mechanical actions, including direct gating of ion channels (Kubanek et al., 2016, 2018; Lin et al., 2019a; Qiu et al., 2019), or modulation of membrane capacitance via cavitation (Plaksin et al., 2014; Saffari et al., 2017; Vion-Bailly et al., 2017; Wright et al., 2017) or radiation force (Prieto et al., 2018; Menz et al., 2019).

By contrast, reports attributing effects to tissue heating are published less frequently, and typically describe US parameters that generate temperature increases of 2 °C (Darrow et al., 2019) or higher (Colucci et al., 2009). To achieve these temperatures, these paradigms utilize application times in the tens of seconds, as opposed to the hundreds of milliseconds range employed by most researchers who attribute effects to mechanical actions.

In our laboratory, we have examined the effects of US on single, identified neurons in an effort to elucidate the technology's enigmatic neuromodulatory mechanism. It has been our observation, across thousands of trials in hundreds of preparations, that mechanical effects, if present, are subtle and easily obscured by thermal actions. There are several potential rationales that could account for our failure to observe evidence of mechanically induced US

neuromodulation, which will be discussed below. Among them are our use of a potentially atypical model system (the leech), the limited parameters that we have employed, or a broad resistance of most neuronal cell types (non-sensory) to US mechanical modulation of membrane properties.

5.3 l Contribution of the leech model to our failure to mechanically modulate neural activity

A major goal of US neuromodulation studies across model systems is to generate knowledge that can eventually be leveraged for the development of human therapies. Consequentially, most intact studies have explored effects on mammalian models, as these animals' neural physiology closely resembles our own. The leech, an annelid, poses many benefits for usage in basic studies of US's actions, including the ability to examine effects on single identified neurons, but its nervous system, like that of all invertebrates, is an imperfect proxy for mammalian systems. Thus, it could be argued that our results diverge from those observed in mammals because of intrinsic differences between vertebrate and invertebrate nervous systems.

First, it must be noted that invertebrate and vertebrate neurons share many more similarities than differences. Much of our current understanding of vertebrate neurophysiology was first described in invertebrates, including the ion currents that govern the generation of the action potential (Hodgkin and Huxley, 1952), and the cellular basis of learning and memory (Walters et al., 1979;

Glanzman, 1995). The action potential of the leech, too, is governed by a rising phase meditated by voltage-gated sodium channels (Na_V), and a falling phase mediated by voltage-gated potassium channels (K_V) (Kleinhaus, 1976; Kleinhaus and Prichard, 1976). This must be noted, as Na_V channel types have been implicated in neuronal response to US (Tyler et al., 2008; Kubanek et al., 2016; Prieto et al., 2018), yet these channels are not expressed by all invertebrates, including *C. elegans*, another system used in investigations of US mechanisms (Zhou et al., 2017; Kubanek et al., 2018). Other classes of ion channels hypothesized to be mechanically activated by US, including two-pore potassium channels (Kubanek et al., 2016; Zhao et al., 2017), transient receptor potential (TRP) channels (Ibsen et al., 2015), and voltage-gated calcium channels (Tyler et al., 2008; Tufail et al., 2010), are expressed in leech as reported in the recently published transcriptome (Northcutt et al., 2018). The authors did not explicitly specify the presence of two other types of ion channels that have been hypothesized to underlie US's mechanical effects in other systems. These are members of the degenerin/epithelial Na^+ channel (DEC/ENaC) family, which have been reported to underlie behavioral responses to US in C. elegans (Kubanek et al., 2018), and Piezo channels, which have also been reported to respond to US (Prieto et al., 2018; Qiu et al., 2019). Expression of DEC/ENaC in the leech is highly likely, as this channel family is broadly conserved across all major animal lineages (Moroz et al., 2014; Lynagh et al., 2018). Similarly, Piezo channels, though not described in the transcriptome, are almost certainly

expressed in the leech, as conservation of related channels extends to organisms as distantly related to mammals as plants and protozoa (Coste et al., 2010). It is thus unlikely that our failure to observe mechanical modulation of neural activity stems from a lack of expression of channels necessary to actuate the effect.

Leeches and other invertebrate nervous systems also differ from those in mammals with respect to glial cells. Invertebrates lack myelinating glia (oligodendrocytes and Schwann cells), and thus their axons differ anatomically and physiologically from most axons in mammalian systems, a distinction that could underlie our inability to mechanically elicit spikes when targeting a leech nerve (Chapter III). Ion channel distribution in myelinated axons is highly concentrated to nodes of Ranvier, whereas unmyelinated axons have more diffuse distribution (Waxman and Murdoch Ritchie, 1985). Nodes of Ranvier, sites of Na_V density of over 1,200 channels per square micron, are interspersed along myelinated axons at distances approximately 100x axonal diameter (Poliak and Peles, 2003). Most cortical axons are around 500 nm in diameter (Liewald et al., 2014), yielding node spacing of approximately 50 μm. Focused US foci, on the order of hundreds of microns to several millimeters in diameter, thus stimulates dozens of nodes in aggregate, as opposed to a singular site of concentrated channels. The extent to which the stimulation of many sites of concentrated channels as opposed to a comparable area of membrane with more uniformly distributed channels contributes to differential outcomes is difficult

to predict. This distinction loses relevance, however, when considering that (1) unmyelinated axons are known to innervate the CNS and the periphery of mammals (Liewald et al., 2014), and (2) ion channels in unmyelinated axons in mammals and invertebrates alike are reported to exhibit patterns of clustering to increase the efficiency of action potential conduction in a strategy similar to clustering at nodes of Ranvier (Freeman et al., 2016).

The aforementioned differences outline potential ways in which our model system may have contributed to differences in our observations and those reported in the literature, none of which are specific to the leech, but rather stem from our use of an invertebrate versus a vertebrate system. Yet, US-associated effects in invertebrates have been widely reported in systems including crabs (Saffari et al., 2017; Wright et al., 2017), crayfish (Lin et al., 2019a), nematodes (Zhou et al., 2017; Kubanek et al., 2018), and the leech's distant cousin, the earthworm (Wahab et al., 2012; Yoo et al., 2017). Without exception, each of these studies has cited nonthermal mechanical actions as the drivers of their observed neuromodulation. The likelihood that the leech is intrinsically unresponsive to mechanical US is unlikely, particularly in light of its effects in similar species.

5.4 | Parameter-associated limitations as a contributor to our lack of mechanical modulation

Key factors in US neuromodulation paradigms are the specific US parameters, which include characteristics that define the US waveform and its consequential bioeffects including frequency and amplitude (pressure, measured in Pa), and pulse parameters including pulse duration (PD) and pulse repetition frequency (PRF), which further influence US intensity and heat output. Our frequency, 960 kHz, is higher than most used in transcranial applications (e.g., 250 kHz in monkeys (Yang et al., 2018), 350 kHz in rats (Kim et al., 2015), and 500 kHz in mice (Mehić et al., 2014)). Higher frequencies, however, generate less cavitation, and 960 kHz may thus be too high to generate proposed excitatory cavitational effects (Krasovitski et al., 2011; Plaksin et al., 2014). Although cavitational effects have been visualized via electron microscopy in cells treated with 1 MHz US (Krasovitski et al., 2011), a comparable frequency (1.1 MHz) was found insufficient to generate cavitation-induced *de novo* action potentials in a paradigm similar to our own (peripheral nerve in crab) (Wright et al., 2017).

Another parameter that may have influenced our ability to mechanically modulate neural activity is our US pressure. We applied pulses with 660 kPa amplitude (peak rarefactional pressure) to the dorsal posterior (DP) nerve to modulate the activity of motoneuron DE-3 (Chapter III). Estimating nerve tissue to have a density of 1.03 g/cm^3 (Mendez et al., 1960), and assuming the speed of sound in saline is approximately 1507 m/s at 22 °C (Goss and O'Brien, 1979), this pressure yields a spatial peak pulse average intensity (I_{SPPA}) of 140 W/cm^2.

This intensity approaches, but does not exceed, the FDA limit for diagnostic use (190 W/cm^2) (FDA, 2019). The maximum pulse amplitude applied to neuronal somata in our intracellular study (Chapter IV) was 225 kPa (I_{SPPA} = ~ 16 W/cm^2), though most recordings were lost due to electrode resonance at pressures ≤ 100 kPa (I_{SPPA} = ~ 3 W/cm^2).

The pulse energies applied in our studies (Chapter 2: I_{SPPA} = 140 W/cm^2; Chapter 3: max I_{SPPA} = 16 W/cm^2) are well in excess of those used in most US neuromodulation studies, particularly transcranial studies (e.g., Yoo et al. 2018 [4.2 W/cm^2]; Kim et al. 2019 [up to 61.5 mW/cm^2]; Tufail et al. 2010 [211.7 mW/cm^2]; Lee et al. 2015 [up to 14.3 W/cm^3]; Legon et al. 2014 [29.3 W/cm^3]). In our nerve study (Chapter III), comparable intensities were insufficient to modulate the activity of the spontaneously-firing DE-3 neuron, nor evoke spikes from any of the other neurons whose axons pass through the DP nerve. This is consistent with others' findings that peripheral nerves require much greater energy to cause an effect as compared to central tissue. Authors Wright et al. (2017) averaged intensities used to modulate peripheral nerves across studies, and calculated a mean intensity of 59 W/cm^2 used in peripheral studies, versus 3 W/cm^2 in CNS studies. Notably, though our intensity was more than twice the average used to modulate peripheral nerve activity, we failed to observe results until pulse durations were lengthened to generate significant tissue heating.

In our intracellular study, we applied short pulses of US at increasing pressures and intensities until we observed what we believe to be electrode

resonance-induced depolarization of the resting membrane potential of identified neurons. At our lowest pressure tested (~14 MPa, I_{SPPA} = 63 mW/cm^2), parameters with which others have reported successful stimulation (Kim et al., 2019), none of the 12 impaled neurons in our study responded, either via changes in the voltage of the resting membrane potential, or by increasing neuronal firing. The full complement of parameters used in this study ran the gamut of those reported in the majority of transcranial studies (Pasquinelli et al., 2019), using intensities ranging from 63 mW/cm^2 to 16 W/cm^2, pulse durations from 100-300 ms, and both pulsed (30% duty cycle) and continuous US. Despite extensive attempts, the only modulation we were able to generate was artifactual, and resulted from US-induced electrode resonance, which could be compellingly replicated by micro-displacements of the recording electrode.

Despite our use of intensities in excess of what many other groups have found sufficient to modulate neuronal activity, it may be the case, paradoxically, that we did not go high *enough* to generate true mechanical effects. Work by other groups has revealed that mechanical neuromodulation may require the use of extremely high pressures, up to an order of magnitude greater than ours. In a preparation comparable to ours employed in Chapter 2 (invertebrate nerve), and using a comparable US frequency (1.1 MHz vs. our 960 kHz), Wright et al. (2017) were unable to modulate nerve activity using short pulses (negligible heating), even at extremely high intensities (4.2 kPa, 475 W/cm^2). At a lower frequency (670 kHz), the authors were able to evoke compound action potentials

starting at a threshold of 169 W/cm^2. This lower frequency and high intensity correlated with inertial cavitation activity, which was reported to be the primary actuator of neural activation, but which caused significant damage in a minority of nerves tested. Recent publications by another group exploring the effects of US in mammalian systems also reported the need for extremely high energy to modulate peripheral nerve activity. Pressures of 11.8 MPa and 30 MPa, respectively, were used to elicit motor responses during stimulation of sciatic nerve in mice (Kim et al., 2020; Lee et al., 2020). With respect to the myriad publications describing activation of the cortex in mammals with much lower US intensities, perhaps modulation is not readily possible in the leech system at comparable intensities, even when targeting somata (Chapter 3). However, it is much more plausible that prior reports of neuronal activation in mammalian systems were influenced by incidental activation of sensory structures or other confounds, as will be discussed in the following section.

5.5 | Limitations of prior studies

The multimodal nature of US has apparently obscured attempts to elucidate its core neuromodulatory mechanisms, as exemplified by continued discourse regarding its core mode of efficacy, even after a century after it was first demonstrated to modulate neural tissue (Harvey, 1929). In recent years, new variables have come to light that may indirectly bias cellular responses to US,

confounding attempts to clarify the mechanisms underlying US's effects, as well as the direction of these effects (neuronal excitation or inhibition).

In 2018, two studies demonstrated that US causes widespread but indirect cortical activation by activating auditory hair cells in the cochlea (Guo et al., 2018; Sato et al., 2018). The first study, by authors Guo et al., revealed that US activated the primary auditory cortex (A1) and primary sensory cortex in guinea pigs. This activation occurred even when targeting such distant structures as the eyeball, and was mediated indirectly by the cochlea and eliminated by the severance of the auditory nerve or the removal of cochlear fluids. The second study, by authors Sato et al., found that US applied to the visual cortex induced broad cortical activation originating in A1 as measured via wide-field calcium imaging, and elicited motor responses consistent with a startle reflex evoked by audible sound; both effects were dampened by chemical deafening. These studies have important implications for the interpretation of prior transcranial studies, especially those that describe the elicitation of motor responses (for example, Kamimura et al. 2016; Kim et al. 2019; King et al. 2013; Li et al. 2016; Ye et al. 2016).

A more recent study demonstrated that auditory-evoked motor responses to US could be attenuated by reshaping the US waveform, and that motor effects persisted in genetically deaf mice (Mohammadjavadi et al., 2019). It remains possible, however, that mechanosensitive ion channels localized to sensory systems beyond the cochlea contributed to the effects observed in this and other

studies, regardless of whether these systems were the primary target of stimulation. US has been shown to excite neurons of the salamander retina by radiation force (Menz et al., 2013, 2019; Jiang et al., 2018), and can directly activate ion channels widely expressed in sensory neurons, including Piezo1 (Prieto et al., 2018; Qiu et al., 2019) and an invertebrate ion channel of the degenerin/ENaC/ASIC ion channel family (Kubanek et al., 2018).

Beyond the confounds posed by incidental activation of sensory systems, our lab recently showed that some recording modalities may influence US neuromodulation outcomes (Chapter IV). We found that experiments incorporating single-cell intracellular sharp recordings are vulnerable to depolarizing US-induced electrode resonance. Similar issues have been reported in other single-cell paradigms, including two-electrode voltage clamp in *Xenopus* oocytes (Kubanek et al., 2016), and patch clamp in mammalian cortical neurons (Tyler et al., 2008). Importantly, depolarization induced via US in leech neurons, as previously reported (Dedola et al., 2020) and reproduced by us, could be fully replicated by micromovements of the recording electrode. The effects of US on spike frequency and amplitude were similarly reproducible. This finding challenges the conclusions of studies that have utilized single cell electrophysiology to assess underlying US mechanisms, which have universally reported excitation/depolarization of the resting membrane potential, and have universally attributed such results to mechanical effects (Tyler et al., 2008; Prieto et al., 2018; Dedola et al., 2020).

Ultimately, we failed to observe evidence of mechanically-mediated US neuromodulation, despite targeting both somata and peripheral nerves, and modulating parameters including pressure, pulse duration, duty cycle, and (to a limited extent) frequency. Parameters that failed to yield significant (> 1 °C) tissue heating (e.g., short pulses) failed to modulate peripheral nerve activity (Chapter III), and effects elicited in neuronal somata appeared artifactual (Chapter IV). Possibly, the mechanical actions of US exerted more subtle effects that could have become perceptible over the course of hours or days, beyond the feasible recording window of our study. Regardless, we remain convinced that the actions of US on non-mechanosensory neurons, at moderately low intensities (within FDA-allowable range for diagnostic use), are predominantly thermal. We are of the opinion that thermal neuromodulatory effects can be achieved more reliably and efficiently than mechanical effects; embracing and exploiting a thermal mechanism will thus likely expediate US technology's transition from the lab to the clinic.

Our position would change should evidence mount that certain cortical and other CNS neurons are, indeed, preferentially susceptible to mechanical modulation due to their expression of mechanosensitive ion channels, including subtypes of Piezo and TRP channels, which may be mechanically activated by US (Prieto et al., 2018; Yoo et al., 2020). Though these channels are expressed in cortical and other CNS tissue, it remains unclear whether their expression is

sufficient to enable modulation of desirable neural targets, or whether increasing channel conductance is clinically desirable, as discussed below.

Piezo2 is highly expressed in dorsal root ganglion neurons, though Piezo1 and 2 mRNAs in brain are significantly lower than in other body tissues (Coste et al., 2010). Potentially further limiting these channels' utility as a target, Piezo channels may play a significant role in pain pathology. Piezo2 is colocalized to nociceptors, and upregulation is hypothesized to contribute to hyperalgesia and allodynia (Volkers et al., 2014). Both Piezo1 and 2 are expressed in trigeminal sensory neurons, and excessive and repetitive activation of these channels is believed to contribute to migraine (Pietra et al., 2020).

TRP channels believed to be stimulated by US may face similar limitations, e.g. TRPC1, one of the TRP channels recently implicated in mechanically-mediated neuronal response to US (Yoo et al., 2020). While this channel does have widespread expression in the brain (Riccio et al., 2002), regions in which it is most highly expressed may not be especially clinically useful as a target for US stimulation; e.g., the cerebellum. Furthermore, increasing activation of TRPC1 channels may pose clinical risks. US has been shown to excite primary cortical neurons through a cascade initiated by a US-induced TRPC1-mediated calcium conductance (Yoo et al., 2020). Though not observed in association with ultrasound, increased neuronal calcium conductance can induce necrosis or apoptosis as a result of glutamate-induced excitotoxicity (Lau and Tymianski, 2010). Notably, increased calcium

conductance via TRPC1 has been implicated as a primary actuator of glutamate-induced cell death (Narayanan et al., 2008).

Limitations in the expression patterns of canonical mechanosensitive ion channels in nervous tissues, and potential risks inherent in significantly increasing the activity of these ion channels, underscore the constraints associated with pursuing purely mechanically-mediated US neuromodulation. The following section highlights the likely mechanisms underlying thermal US neuromodulation, and emphasizes its potential clinical attributes while weighing its possible risks.

5.6 l Heat as a valuable and versatile actuator of ultrasound neuromodulation

Tissue absorbs US energy as heat, which is a well-established neuromodulator in its own right (Janssen, 1992). US-induced tissue heating can be potentiated by manipulation of parameters by increasing frequency, increasing duty cycle in pulsed applications, increasing stimulus durations, and increasing intensity. US at parameters that maximize thermal effects, e.g. high-intensity focused ultrasound (HIFU), is destructive, and has been used clinically to lesion noninvasively tumors of the prostate, uterus, and brain (Evans et al., 2007).

Some of the earliest investigations of US's effects on neural firing utilized HIFU, and produced modulation replicable by increasing preparation

temperature. US was found to block conduction of impulses in the peripheral nerves of earthworms, cats, monkeys, and humans at parameters that induced temperature increases of ≥ 17 °C (mammalian preparations) or ≥ 6 °C (earthworm), which could be replicated by focused heating of the nerves (Lele, 1963). In a cortical study, US-induced temperature increases of ≥ 7.5 °C in rats caused modulation in the form of spreading depression, a phenomenon characterized by a period of neuronal depolarization followed by hyperpolarization (Ueda et al., 1977). In both studies, however, this thermal modulation was not without consequence. In the first study, nerve conduction block was accompanied by hemorrhage, ulceration, and significant skin damage when examined during transcutaneous applications (Lele, 1963); in the second study, cortical heating caused severe necrosis of neurons and glia at the US focus (Ueda et al., 1977).

While HIFU continues to present therapeutic opportunities in some neurological capacities (e.g., lesioning the ventral intermediate nucleus of the thalamus to treat essential tremor (Lipsman et al., 2013), or temporarily disrupting the blood-brain barrier to permit localized drug delivery (Mesiwala et al., 2002)), nondestructive low intensity applications (LIFU) are of primary interest to US neuromodulation researchers, as these applications present an opportunity to mimic noninvasively the effects of clinically successful electrical stimulation devices (deep brain stimulation devices, etc.) without the risks of surgery. LIFU applications, which typically employ parameters that fall within the FDA-approved

limits for diagnostic applications (FDA, 2019), can be used to generate moderate levels of tissue heating, which can nonetheless significantly impact neural firing.

5.7 | US-induced hyperthermia: what is safe?

Significant hyperthermia can have devastating effects on the nervous system. In humans treated with whole-body hyperthermia for cancer, systemic temperature increases of up to 3 °C can be tolerated for several hours without demonstrable loss of organ function, while increases of 5-6 °C for 30-60 minutes can cause significant injury to the brain including hemorrhage, edema, and necrosis (Sharma and Hoopes, 2003). Similar effects have been observed in other mammals, in which the maximum tolerated thermal dose for brain exposures of 15 – 60 min was 41 – 43 °C, which corresponded to an increase above normal body temperature of approximately 3 – 5 °C in the animals studied (cats, dogs, monkeys) (Haveman et al., 2005). Greater temperature increases may be tolerable for acute exposure times, although infrared laser experiments in rats resulted in irreversible damage following 46 °C heating of cortical neurons for 30 seconds (Xia and Nyberg, 2019).

The effects of hyperthermia on nerves are less well studied. In rodents, the maximum tolerated thermal dose for spinal cord exposures of ≤ 60 min is 42 – 43 °C, or approximately 5 – 6 °C above normal body temperature (Haveman et al., 2005). There is evidence that peripheral nerves may be able to withstand greater increases in temperature without a demonstrable loss of function, with

susceptibility of individual axons to thermal effects, including conduction block, being at least partially dependent on axon diameter and/or myelination. In cat tibial nerve, impulse conduction in myelinated A fibers was blocked after 110 minutes at 46.5 °C (7 – 8 °C higher than normal), or for 10 minutes at 51 °C. Conduction block of smaller, unmyelinated C fibers required longer heating durations, and was more reversible (Klumpp and Zimmerman, 1980). Axon diameter-dependent susceptibility to thermal effects including conduction block has also been documented in the infrared (Lothet et al., 2017) and ultrasound (Lele, 1963; Kim et al., 2020) literature. This has held true in our own observations of the thermal effects of US and other heating modalities on the firing properties of unmyelinated axons in the leech DP nerve, in which the stimulus duration necessary to inhibit impulses was inversely proportional to spike amplitude, a correlate of axon diameter in extracellular recordings (unpublished data, Fig 1).

As with other neuromodulatory heating modalities, e.g. infrared (Richter et al., 2011), the range of temperatures that can effectively modulate neural activity without inducing damage may be low, which has been argued to be a constraint on the pursuit of safe, primarily thermally-mediated US neuromodulation therapies (Tyler et al., 2018). While we are optimistic that continuing technological developments in phased US array transducers (Kim et al., 2019), frequency modulation (Mehić et al., 2014), and incorporation of US imaging (Darrow et al., 2019; Kim et al., 2020) will enable targeted, noninvasive tissue

heating with sufficient precision, we acknowledge that the margin of error is low. Safe, effective temperature ranges will vary by target tissue type (central versus peripheral, gray versus white matter), and by exposure durations, with greater temperature increases permissible over shorter durations.

In our studies on leech nerve, US-induced temperature increases of 3.6 °C were sufficient to modulate neuronal activity significantly (Chapter III). While this temperature increase is nontrivial, it is unlikely to cause significant damage over short durations, particularly in peripheral nerves, as indicated by the aforementioned human and animal studies. In addition, we were able to generate more dramatic effects with only 2 °C as applied by a 50 mW laser, a heating modality with faster heating kinetics and a sharper focus. These latter variables, which should be taken into consideration when designing parameters for thermal US, may have a greater impact on the direction and extent of neuromodulation than smaller (1 – 2 °C) differences in the magnitude of tissue heating, as will be discussed in greater detail in the following sections.

5.8 l Factors that influence response direction and magnitude

In our study of the effects of 960 kHz US on the firing rate of a spontaneously-firing identified motoneuron in the medicinal leech, we found that short pulses (100-300 ms in duration) were insufficient to modulate neural activity (Chapter IV), but very long exposures, on the order of 30 seconds, could induce reliable neuromodulation (Chapter III). These long durations facilitated the

generation of significant tissue heating. In an attempt to determine whether the US-induced neuromodulatory effects on an identified motoneuron were thermal, we replicated the US-associated heating, which we estimated raised the temperature of our nerve by approximately 3.5 °C, with two heating modalities: a 50 mW laser and a nickel-chromium wire device that heated when connected to a direct current source. The laser heated tissue by approximately 2 °C, and the wire device heated by approximately 4.5 °C.

Like US, both heating modalities induced compelling neuronal excitation and inhibition, suggesting that net tissue temperature increase (2 °C vs 4.5 °C) was not the sole determinant of any given neuromodulation outcome. For example, differences with respect to the percentage of trials that yielded each effect (Fig. 2) has suggested that intrinsic differences in the spatial or temporal thermal gradients of the two conditions can induce different bioeffects on our targeted nerve. In fact, these spatial and temporal gradients may be of greater significance than total temperature, at least within this 2.5 °C range. We observed relatively more inhibition with the 2 °C laser than the 4.5 °C wire device, a finding contrary to a more commonly reported trend of higher heat stimuli inducing inhibition, and lower heat stimuli inducing excitation. This finding suggests that spatial and temporal gradients are, in fact, the primary determinants of thermal neuromodulation outcomes within this range of temperatures.

5.8.1 | The neuromodulatory effects of moderate heating: the INS connection

The mild-to-moderate increases in temperature observed in our leech nerve study can significantly impact neurophysiology. Much of what is currently understood about the neuromodulatory effects of non-noxious heat on nervous tissue derives from the infrared/optical literature. Like US, infrared neural stimulation (INS) generates spatially restricted heating of nervous tissue, and can induce both excitation and inhibition of neural activity (Cayce et al., 2014). INS enacts modulation through an as-yet poorly understood mechanism, but one that is believed to be photothermal, as opposed to photochemical or photomechanical (Zhao et al., 2016a). Due to the relative wealth of INS studies compared to thermally-focused US neuromodulation studies, this literature will be called upon frequently to contextualize our hypothesized neuromodulatory mechanisms in the following sections.

5.8.2 | Thermal effects on neural activity at moderate temperatures: the spatial component

The leech, like all invertebrates, is an exothermic animal whose body temperature fluctuates with changes in environmental temperature. The animal's nervous system maintains functionality across rapid shifts in temperature that can range in the tens of degrees; for example, when transitioning from land to water. Exothermic animals have evolved adaptations to maintain neural circuit

activity across a wide range of body temperatures, which have been described extensively in the crab, *Cancer borealis*, whose stomatogastric ganglion (STG) is among the best characterized neural networks in any animal system. The STG produces a pyloric rhythm mediated by the orderly activation of select neurons (Marder and Bucher, 2007). Although pyloric rhythm frequency increases with increasing temperature, the phase relationships governing this rhythm are maintained by compensatory changes in input conductance, synaptic currents, transient outward currents, and hyperpolarization-activated inward currents (Tang et al., 2010). This feeding-related circuit thus maintains relatively normal functionality across temperature changes of at least 15 °C (Tang et al., 2010; Soofi et al., 2014). Studies of temperature compensation in other invertebrates and exothermic vertebrates have reported similar findings, in which neural circuit frequencies increase upon exposure to increases in environmental temperature, but circuit functionality persists due to complementary temperature coefficients (Q_{10}s) of opposing processes (Robertson and Money, 2012).

Given the leech's ability to maintain neural firing across significant environmental temperature changes, owing presumably to similar compensation mechanisms to those described in similar organisms (Robertson and Money, 2012), we were initially surprised that artificial temperature increases as low as 2 °C could cause the dramatic modulation of neural activity we observed in our study (Chapter III). One key difference between our heating modalities and those employed in most studies examining temperature compensation is the spatial

gradient of the temperature increase. Most studies have examined the effects of global heating on neural function, typically via bath heating (e.g., Soofi et al. 2014; Tang et al. 2010), whereas our heating modalities generated spatially restricted heating ranging from a 1.2 mm diameter (laser) to an 8.5 mm diameter (wire device), with US heating a 6.8 mm diameter area of tissue (Chapter III; see Fig 2). In a series of control studies, we also heated the bath temperature, enabling us to compare the effects of localized heating to global heating. We observed a strong trend whereby broader heating patterns were associated with a greater propensity towards an excitatory response, while more spatially restricted heating was biased towards an inhibitory response. The greater bias towards neural excitation with broader heating, including our exclusively excitatory results during bath heating [which mirrored results of prior bath heating experiments in leech (Romanenko et al., 2014b)], were reminiscent of reported increases in neural activity in response to global temperature increases reported in a wide range of exothermic animals (Robertson and Money, 2012). Importantly, the robustness of neural circuit activity seen in exothermic animals, in response to changes in environmental temperature, likely evolved in the context of systemic changes in temperature, versus spatially restricted changes, which these animals would not have routinely encountered. It is thus possible that the neuronal inhibition we observed in our study, which resulted from temperature increases of < 5 °C (far below the level at which temperature compensation in similar systems typically fails; Robertson and Money 2012),

were a consequence of a localized failure of homeostatic mechanisms, which did not evolve to sustain highly localized changes in temperature. Consistent with our findings, US applications that produce broader heating may facilitate increases in neuronal activity, while applications with sharper foci may be likelier to inhibit firing.

5.8.3 l Thermal effects on neural activity at moderate temperatures: the temporal component

Our nerve study compared the effects of US to comparable heating induced by a laser and a wire device (Chapter III). While the magnitude of tissue heating generated by US fell between the two other heating modes, the rate of temperature increase differed markedly. The laser and wire device heated rapidly, with the first degree of temperature increase achieved at a rate of 0.35 °C /s and 0.46 °C/s respectively, as compared to a rate of 0.17 °C/s with US (Fig 2). These differing temporal gradients are reflected in our neuromodulation data, with the peak modulation period (defined as the period of maximal difference in firing rate over baseline) occurring earlier in the laser and wire device trials in comparison to the US trials (peak effects began 10 seconds after the onset of the 30 second stimulus application for the laser and wire device, and 20 seconds after the onset of the stimulus in the US trials). The faster rate of heating of the two heat-only stimuli may also have enhanced the magnitude of the modulation achieved, defined as the mean firing rate during the peak modulation period

normalized to the baseline firing rate. We observed more dramatic inhibition of motoneuron firing with our rapidly heating modes, with a mean reduction of firing of 92% and 86% in our inhibitory laser and wire device trials, respectively, as compared to a mean reduction in firing of 43% in our inhibitory US trials.

As mentioned previously, thermal neuromodulation, particularly, thermally-mediated neuronal inhibition at sub-noxious temperatures, may result from a localized failure of the homeostatic mechanisms that normally maintain neuronal functionality across a much wider range of temperatures. Given these observations, it is possible that temperature-related compensatory mechanisms fail more readily in instances during the initiation of more rapid heating, or that these mechanisms are more readily outcompeted by thermally-mediated changes in the physiological metrics underlying neuromodulatory effects. The precise changes that have been proposed to underlie such effects are outlined in the next sections.

5.9 l Potential molecular mechanisms of thermal neuromodulation

Temperature increases below the range at which significant tissue damage (e.g. protein denaturation) occurs have been proposed to modulate neuronal activity through several mechanisms, including: increased membrane capacitance, and changes in ion conductance, which are argued to affect neuronal excitability via depolarization or hyperpolarization of the resting membrane potential. These processes are not mutually exclusive, and the net

neuromodulatory outcome of tissue heating via ultrasound or other thermal stimuli may be dependent on the interaction of these mechanisms, whose relative contributions may be weighted by factors including the magnitude of temperature increase, spatial and temporal heating gradients, and the intrinsic characteristics of the target tissue (e.g., the types of ion channels expressed and thermal diffusion rates).

5.9.1 | Modulation of membrane capacitance

Localized heating via INS has been proposed to excite neuronal activity by increasing membrane capacitance (Zhao et al., 2016a). This mechanism has also been proposed as an effector of US's thermal effects on neuronal activity (Kamimura et al., 2020), and may be mediated by heat-induced membrane dimensional changes and displacement currents (Plaksin et al., 2018). Experimentally, short pulses of INS have been shown to increase the membrane capacitance of mammalian HEK cells and artificial bilayers, and to depolarize *Xenopus* oocytes though a presumably related mechanism, which operates independently of the presence of voltage-gated ion channels (Shapiro et al., 2012).

While there exists compelling evidence to support a capacitance modulation-based mechanism in INS, the relevance of this mechanism to US applications remains unclear. INS studies have typically used short pulse durations that generate rapid and significant tissue heating (e.g., 10 ms pulses of

up to 22 °C of heating; Shapiro et al. 2012). In fact, it has been reported that the reliability of INS-evoked potentials begins to wane with pulse durations longer than 10 ms due to heat diffusion (Wells et al., 2007a).

Achieving significant temperature increases on the order of milliseconds requires a very steep temperature gradient. One report of the modeled actions of INS on nerves revealed an inverse relationship between the rate of temperature increase and the magnitude of heating necessary to evoke action potentials (Fribance et al., 2016). In this model, rapid increases in temperature sufficient to depolarize neurons and elicit action potentials via increases in membrane capacitance required a 6.6-11.2 °C increase in < 3 ms, though lower temperatures were sufficient with faster heating kinetics (Fribance et al., 2016). Conservatively, this equates to a 2,200 °C/s heating rate required to elicit firing through a membrane capacitance-mediated mechanism. This *vastly* exceeds the heating rate generated by US in our nerve study, as well as that of our heat-only modalities (Chapter III). Given this orders-of-magnitude difference, it is unlikely that heat-induced increases in membrane capacitance were a primary actuator of the minority of US trials in which we observed excitation, and may explain why other groups who have used US to thermally modulate neural activity have failed to evoke activity in a manner comparable to what has been reported in the INS literature (e.g., Darrow et al. 2019). It is possible that future thermal US neuromodulation applications could utilize parameters sufficient to elicit the rapid, significant heating necessary to evoke activity by increasing membrane

capacitance, although the high intensities required may pose substantial safety risks.

5.9.2 | Thermal gating of ion channels

Heat can also modulate neuronal activity by altering ion conductances. The temperature sensitivity of biological processes can be quantified by Q_{10} values, which describe the ratio of the rate of the process at two temperatures separated by 10 °C. With respect to ion channels, this can refer to the rate of channel gating or channel conductance. All ion channels have some degree of thermosensitivity, as channel gating is temperature dependent, yet ion channels are not typically considered thermosensitive unless they have a $Q_{10} \geq 2$ (Hille, 2001).

One class of ion channels frequently implicated in a neuronal response to heat is TRP, a family of cation-nonspecific ion channels with well-characterized roles in mediating responses to sensory stimuli including changes in temperature (Clapham, 2003). Highly thermosensitive TRP channels, such as members of the vanilloid (TRPV) subfamily, can have Q_{10}s ≥ 20 (Clapham, 2003). TRPV channels are highly expressed in thermosensitive sensory neurons of the dorsal root ganglia (DRG), and are also reportedly found in most CNS tissues including the cortex, where they may regulate neuronal responses to changes in osmolarity and pH in addition to temperature (Kauer and Gibson, 2009). These channels have been explored as effectors of INS. Infrared increases single-

channel activity of TRPV channels expressed in *Xenopus* oocytes (Yao et al., 2009). TRPV4 channels have been shown to mediate INS-evoked potentials in vestibular and retinal ganglia neurons (Albert et al., 2012), and TRPV1 channels in sensory fibers of the vagus nerve are necessary for infrared photostimulation (Rhee et al., 2008). The contribution of TRPV channels to thermal neuromodulation in non-sensory tissues is less clear, though one study of the effects of INS on cultured hippocampal primary neurons demonstrated an indifference of effects to Ruthenium Red, a non-specific TRPV channel blocker (Feyen et al., 2016). Given their well-established responsiveness to thermal stimuli, TRPV channels are likely activated upon stimulation with heat-generating US or other heating modalities, introducing depolarizing Na^+ and Ca^{2+} currents in neurons. The net thermal neuromodulation outcome, however, will be highly dependent on the extent to which TRP channels are expressed in target tissues, and whether their actions are enhanced or counteracted by the activation of other thermosensitive ion channels.

Other classes of ion channels implicated in thermal neuromodulation are the voltage-sensitive ion channels, including Na_V and K_V. Experimentally, increased temperature is associated with an increase in the rate constants of ion conductances mediated by these channels at the Nodes of Ranvier of myelinated nerves (Frankenhaeuser and Moore, 1963). Increases in the gating kinetics of these channels are consistent with established heat-induced neurophysiological changes beyond net increases or decreases in neuronal firing. These include

reductions in spike width and amplitude, and increases in conduction velocity (Hodgkin and Katz, 1949b; Haveman et al., 2004), which have been reported in the INS (Xia and Nyberg, 2019) and thermal US literature (Tsui et al., 2005). Whether these channels are the primary effectors of thermally-mediated changes in firing rates at the moderately low temperatures (< 5 °C) used in our study (Chapter III) and others (e.g., Darrow et al. 2019), however, is less clear.

Mechanically-increased Na_V conductance has been proposed to underlie US-induced excitation (Tyler et al., 2008; Tufail et al., 2010), and US has been shown to directly increase heterologously-expressed Na_V conductance (Kubanek et al., 2016). A more recent study showed that Na_V was not readily mechanically activated at parameters sufficient to activate mechanosensitive Piezo1 channels (43 MHz, up to 90 W/cm^2 I_{SPPA}), but Na_V could be activated thermally (Prieto et al., 2018). Though not exceptionally thermosensitive ($Q_{10} \leq 1.5$), increases in temperature steadily increase Na_V conductance (Milburn et al., 1995), which could sufficiently depolarize neurons to elicit firing. Na_V may thus contribute to increased firing in the minority of our thermal US trials that resulted in excitation (Chapter III).

Na_V-mediated effects could also underlie thermal inhibition. INS researchers have proposed that infrared's inhibitory effects, which include axonal conduction block, which we observed in our study during US-mimicking laser-induced heating (Chapter III, Fig. 3), may be driven by prolonged inactivation of Na_V (Peterson and Tyler, 2014). Recent work has shown, however, that INS-

induced conduction block persists in the presence of the Na_V blocker tetrodotoxin (TTX) (Ganguly et al., 2019a), suggesting Na_V channels are not the primary mediators of heat-induced reductions in firing rates. These channels may nonetheless effect other neurophysiological changes, including the reduction of spike amplitudes, which have been shown in primary cortical neurons to be mediated primarily by the increased inactivation of Na_V (Yu et al., 2012). This is consistent with our own data, in which we sometimes observed stimulus-induced truncation of spike waveforms regardless of the effects on firing rate, suggesting that this truncation is enacted independently of the mechanisms driving reductions in firing rate (unpublished data, Fig 3).

Rather than a Na_V-mediated mechanism, there exists compelling evidence that heat-induced conduction block is primarily caused by an increased potassium conductance. Hyperthermia elicits a rapid increase in extracellular potassium in invertebrate and mammalian systems, and thermal conduction block may be mimicked by artificially increasing extracellular potassium (Wu and Fisher, 2000; Money et al., 2009). Recent studies suggest a primary source of this increased potassium conductance may be K_V. Although TTX was not found to affect heat-induced conduction block in nerves in *Aplysia*, the phenomenon was shown to be greatly reduced by tetraethylammonium (TEA), a K_V antagonist (Ganguly et al., 2019a). Additional modeling work has demonstrated that thermal conduction block is likely a K_V-mediated phenomenon in which rapid channel

activation and increased channel conductance hyperpolarizes neurons (Ganguly et al., 2019b).

Although heat-induced increased K_V conductance is likely a primary contributor to conduction block, the contribution of these channels to other forms of thermal inhibition is less clear. We collected limited data with a high-heat (~ 10 °C) transducer compatible with intracellular recording that revealed inhibition driven by global hyperpolarization versus conduction block (unpublished data, Fig 4). While these data should be interpreted with caution given the potential for US-induced electrode resonance artifact in intracellular paradigms (Chapter IV), there exists in the literature support for this alternative mechanism, particularly in cases of more profound temperature increase (e.g., ≥ 10 °C). Consistent with our results, which were generated with broader, slower, and higher-magnitude US-associated heating than our conduction block-inducing laser, bath heating in *Aplysia* hyperpolarizes neurons by a typical rate of 1-2 mV/°C (Carpenter, 1967). This hyperpolarization, which is consistent with increased potassium conductance, may be in part a function of increased K_V activation. It may also be driven or potentiated by a separate, but complementary, potassium conductance through two-pore K^+ channels (K2P).

K_{2P} are voltage independent leak channels that assist in the maintenance of the resting membrane potential (Enyedi and Czirják, 2010). Ultrasound increases conductance of the K_{2P} TREK-1, TREK-2, and TRAAK (Kubanek et al., 2016), potentially via a thermal mechanism (Prieto et al., 2020). Many subtypes

of K_{2P} are thermosensitive, including TREK and TRAAK, which are expressed widely in both the central and peripheral nervous systems (Schneider et al., 2014). Thus, thermal US-induced increased conductance of these channels would hyperpolarize neurons, bringing the membrane potential closer to the K^+ equilibrium potential to inhibit neuronal firing.

Voltage-gated and ion-activated calcium channels may also contribute to thermally-mediated US neuromodulation. In our studies, however, both neuronal excitation and inhibition persisted when the preparation was bathed in Ca^{2+}-free saline (Chapter III). This does not preclude the potential for Ca^{2+} influx-mediated modulation or potentiation of effects, but it does suggest that calcium channels were neither the primary initiators not effectors of thermal neuromodulation in our heating paradigms.

Finally, heat may also increase conductance of ligand-gated ion channels by facilitating synaptic vesicle release from presynaptic terminals (Wang et al., 2014). Increases in temperature lower energetic barriers to SNARE protein-mediated fusion of synaptic vesicles to neuronal cell membranes (Gao et al., 2012). Thermal effects on synaptic transmission may be further potentiated by cationic TRPV channels, which are reportedly present on presynaptic terminals in several brain regions (Kauer and Gibson, 2009). The neuromodulatory outcome of thermal US-induced increased synaptic activity would be dependent on whether released neurotransmitters were excitatory or inhibitory.

5.9.3 | A summary of the mechanisms underlying thermal neuromodulation

As the preceding sections attest, the thermal actions of US on neurons are likely multimodal. The direction and magnitude of the resultant neuromodulation is likely reliant on a complex interplay of changes in membrane capacitance, ion channel conductance, and membrane potential. These effects, which may be complementary or opposing, are likely further influenced by additional modulating factors beyond the scope of this review. These include long term effects, such as changes in neuronal gene expression, which may be initiated by Ca^{2+} influx (West et al., 2001), a known bioeffect of US stimulation (Tyler et al., 2008; Zhou et al., 2017; Yoo et al., 2020).

With respect to clinical applications, it is unlikely that a single, “one size fits all” US therapy will comparably modulate neuronal activity across tissue types, given intrinsic differences in ion channel expression and distribution present in, for example, axons versus neuronal somata. Responses will also vary dependent on the types of connective tissue surrounding neuronal targets, which may influence the rate and magnitude of heat generated due to associated factors including thermal diffusion rates (Wells et al., 2007a). Similarly, the actions of glia will likely prove significant in determining the type and duration of heat-induced neuromodulation, particularly in inhibitory contexts, wherein effects correlate with an increase in extracellular potassium. The extent to which $[K^+]_o$ is elevated as a consequence of heating will be dependent, in part, on rates of astrocytic uptake (Walz, 2000). This is of particular relevance for cortical US

applications, as sharp increases in $[K^+]_o$ can elicit spreading depression, a phenomenon associated with migraine and other neurological disorders (Ayata and Lauritzen, 2015), which have been reported to occur in response to high-heat cortical US applications (Ueda et al., 1977; Koroleva et al., 1986).

Despite heat's complicated array of actions on the nervous system, patterns in neural responses to heat are apparent (based on our own studies and those of other groups) and may be used to inform the design of thermal US neuromodulation therapies biased to generate a desired response, be it neuronal excitation or inhibition. Within the range of temperatures used in our study (2 – 4.5 °C, which are tolerable over durations < 1 hour in mammalian systems; Haveman et al. 2005), US parameters that yield broader heating may promote an excitatory response, which may be driven by the activation of thermosensitive sensory structures in surrounding tissue or broad increases in the kinetics of circuit-mediating ion channels with complementary Q_{10}s (Tang et al., 2010) and potentiated by increased Na_V conductance. Importantly, finer US foci may inhibit neurons through the localized induction of hyperpolarizing potassium currents through K_V and K_{2P} channels. In contrast, adjusting US parameters to promote sharper temporal gradients in heating, which mimic those of INS, may more readily enable excitation with finer foci.

5.10 | Future experiments needed to optimize effects

Future work is needed to refine US parameters to reliably induce the aforementioned thermal bioeffects in intact mammalian systems, and eventually in humans. In addition, longer term studies should be employed to assess whether neurons incur US-associated damage that may not be immediately apparent and establish whether thermal US exposure induces changes in gene expression. Studies should also examine the effects of thermal US on glial cells, which may contribute significantly to various neuromodulatory outcomes. Finally, there remains great potential to use US as a *bimodal* neuromodulatory technology. Clearly, future research should explore the ways in which mechanical effects can potentiate thermal effects, and vice versa, e.g., in tissues expressing both mechanosensitive and thermosensitive ion channels.

5.11 | Potential clinical uses for thermal US neuromodulation

We are optimistic that US parameters designed to generate thermal actions can produce significant and reliable neuromodulation in humans. Given a scenario in which both excitatory applications (with a broader spatial or sharper temporal heating profile) and inhibitory applications (with a more focused profile) are proven safe and effective, there are myriad potential clinical uses for this technology in the treatment of neurological disorders. Chief among these potential uses are for those disorders whose pathology is, in part, characterized by aberrant increases or decreases in neuronal activity.

5.11.1 l Diseases characterized by excessive neuronal firing

In our leech nerve studies, we most commonly observed neuronal inhibition (Chapter III). Human transcranial studies have also reported neuronal inhibition, typically in the form of suppression of evoked potentials (Legon et al., 2014, 2018b). Thermal US may thus have potential for the treatment of neurological disorders associated with excessive neuronal firing.

One distinct disorder in which thermal US therapies could provide clinical benefits is neuropathic pain. Chronic pain is estimated to affect 1/6 of individuals, and frequently originates from neuropathic origins, including lesions on nerves of the CNS or PNS, which are associated with a multitude of diseases including metabolic disease (e.g., diabetic neuropathy), autoimmune disease (e.g., multiple sclerosis), stroke, traumatic brain injury, and cancer (Campbell and Meyer, 2006). Although the pathophysiology of neuropathic pain is incompletely understood, it is linked to excessive spontaneous firing of primary sensory and other neurons (Campbell and Meyer, 2006). Thermal US could inhibit this excessive firing, providing non-pharmacological relief. One potential site to deliver therapy would be the DRG. Electrical stimulation of the DRG has been shown to reduce neuronal excitability, and has been used to treat pain disorders including phantom limb pain, postherpetic neuralgia, complex regional pain syndrome, and others (Harrison et al., 2018). Additional sites of thermal US stimulation that might also confer relief are the dorsal columns of the spinal cord, which have resulted similarly in pain relief when electrically manipulated. The use

of noninvasive US in lieu of implanted electrical wires would eliminate major risks associated with the use of these devices, including lead migration, lead malfunction, battery failure, infection, surgical injury, and scarring (Eldabe et al., 2016). Thermal US could also be explored as an alternative to traditional anesthetics for acute pain associated with minor surgical interventions.

Another disorder that could benefit from inhibitory thermal US delivery is epilepsy, which is characterized by excessive synchronous firing originating from a seizure focus. US has been shown to inhibit pharmacologically-induced seizures in rats (Min et al., 2011) and monkeys (Zou et al., 2020). Although the authors of these studies did not report significant US-associated tissue heating, thermal effects may have, indeed, contributed to seizure suppression.

5.10.2 | Diseases characterized by excessive neuronal firing

Increasing neuronal firing is a desired clinical outcome in many neurological disorders. Excitatory thermal US could increase the activity of neural circuits impaired in neurodegenerative disease, including relevant motor circuitry in Parkinson's disease (DeLong and Wichmann, 2007). US-induced neuronal excitation and facilitation of synaptic vesicle release could also enhance learning and memory, and potentially offset dysfunction of these processes in disorders including Alzheimer's disease. Increasing the activity of brain areas associated with response inhibition of inappropriate behaviors (e.g., the anterior cingulate

cortex and orbital frontal cortex) could reduce drug-seeking behavior in addiction (Lubman et al., 2004).

There are also many potential peripheral applications. Activation of the vagus nerve could help treat numerous disorders associated with inflammation through the activation of the cholinergic anti-inflammatory pathway (Pavlov et al., 2003). US, like electrical stimulation, could help restore motor function in paralyzed limbs or provide sensory feedback for limb prostheses (Günter et al., 2019).

In short, we have only begun to scratch the surface of what therapies may be possible with thermally-mediated US neuromodulation. Future studies will determine which of the aforementioned applications, and others, may be performed safely and effectively.

5.11 | Conclusion

In our studies of individual neurons, axons and fiber bundles in a well-studied animal model, the medicinal leech, we are confident that the cellular mechanism underlying ultrasound neuromodulation is tissue heating. We have come to this conclusion due to the ease with which this modulation could be replicated with comparable heating alone, the seeming absence of modulation in low-heat conditions, and the extensive available literature supporting the ability of heat to induce similar neuromodulatory results to those we observed. Much of the current evidence supporting nonthermal ultrasound stimulation, at low

intensities, is indirect and/or potentially confounded by incidental activation of synaptically coupled sensory structures, making it difficult to achieve a fully accurate picture of nonthermal US excitation. We agree that US can mechanically activate canonical mechanosensitive ion channels traditionally associated with mechanosensory neurons (e.g., members of Piezo, TRP, ASIC families), but the clinical implications of this modulation will be dependent on whether such channels are sufficiently expressed in desirable neural targets that are not primarily sensory. We are of the opinion that thermal US applications, which we believe modulate activity via actions on ubiquitously expressed voltage-gated and leak channels, are likelier to be more versatile and reliable than mechanical applications. Given the profound modulation we and others have observed at temperatures safe for brief exposures (< 5 °C), thermal US neuromodulation certainly merits extensive future study as a potential therapy for the treatment of neurological disorders and disease.

5.13 l Figures

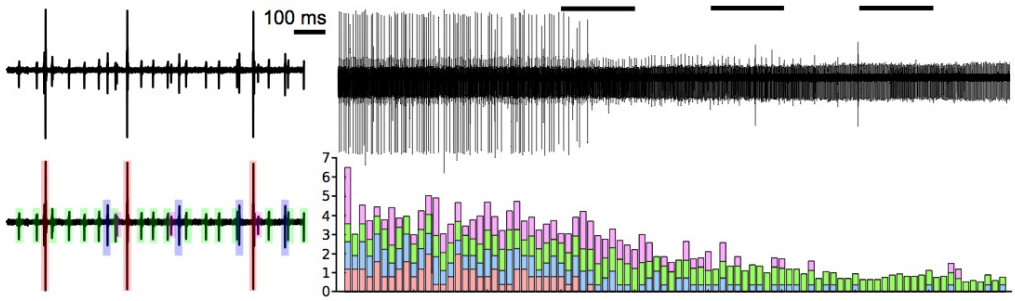

Figure 5.1. Ultrasound inhibits larger fibers prior to smaller fibers. Left: Enlargement of baseline of extracellular nerve recording, demonstrating the presence of 4 units. Right, upper: extracellular nerve recording during three 10 second applications of 960 kHz ultrasound (300 μs pulses, 500 kHz pulse repetition frequency, 1 MPa), denoted by the black bars. Right, lower: histogram of spikes per second during the extracellular recording, demonstrating that larger spikes (pink, blue) are inhibited prior to smaller spikes (green).

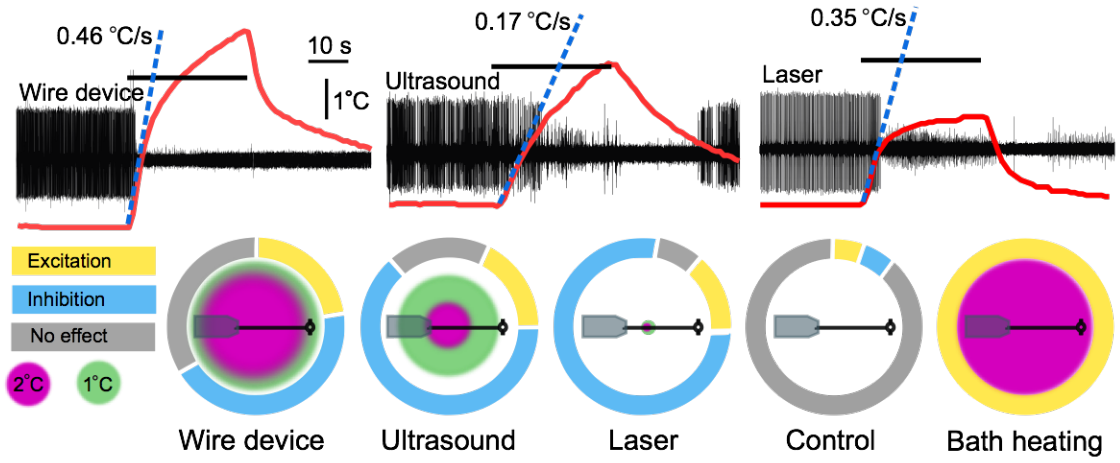

Figure 5.2 A comparison of the thermal effects of a wire device, ultrasound, a 50 mW laser, and bath heating. Upper traces (adapted from Chapter III) are extracellular leech nerve recordings that demonstrate inhibition of an identified motoneuron (largest unit) induced by 30 second applications of the three stimuli. Overlaid on the traces are thermocouple recordings demonstrating the height and rate of heating of each apparatus. Lower charts demonstrate the spatial profile of the different heating apparatuses overlaid on a scale depiction of a leech ganglion and nerve connected to a suction electrode. Surrounding these depictions are modified pie charts demonstrating the relative proportion of trials in our leech nerve study (Chapter III) that resulted in excitation, inhibition, or no effect.

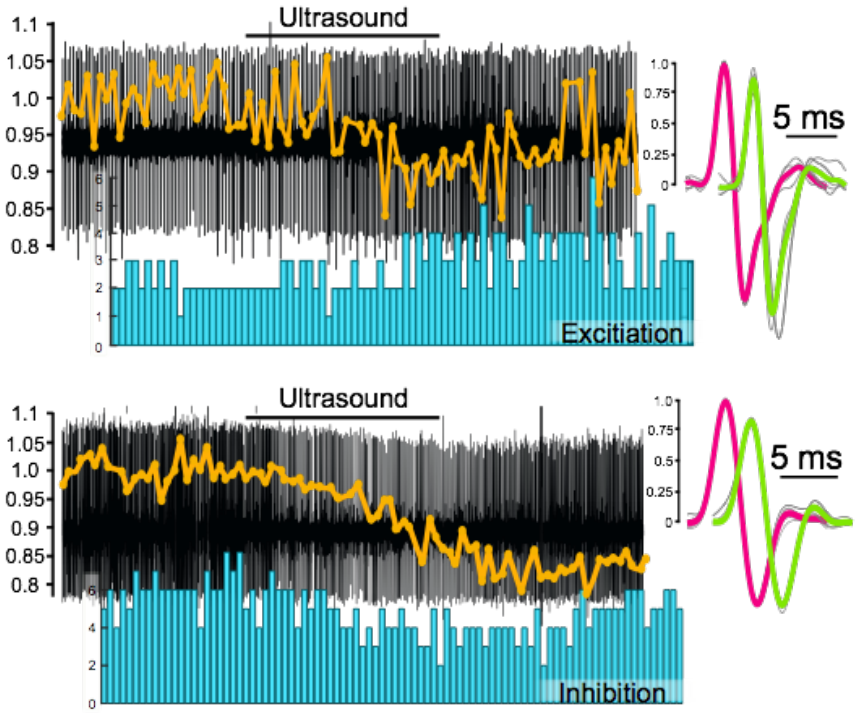

Figure 5.3. Thermal ultrasound reduces spike amplitude independent of effects on firing rate. Representative extracellular recordings of ultrasound trials that resulted in excitation (top), and inhibition (bottom). Overlaid on electrophysiological traces (orange) are normalized spike amplitudes (averaged in 1 second bins), demonstrating a reduction in firing rate during ultrasound application. Below traces are histograms of the number of spikes per second to facilitate visualization of change in firing rate. Right: comparison of 5 spikes before (gray, overlaid with pink average) and immediately after (gray, overlaid with green average) ultrasound application, demonstrating a reduction in spike amplitude. Scales are normalized to the peak amplitude of the pre-ultrasound average waveforms.

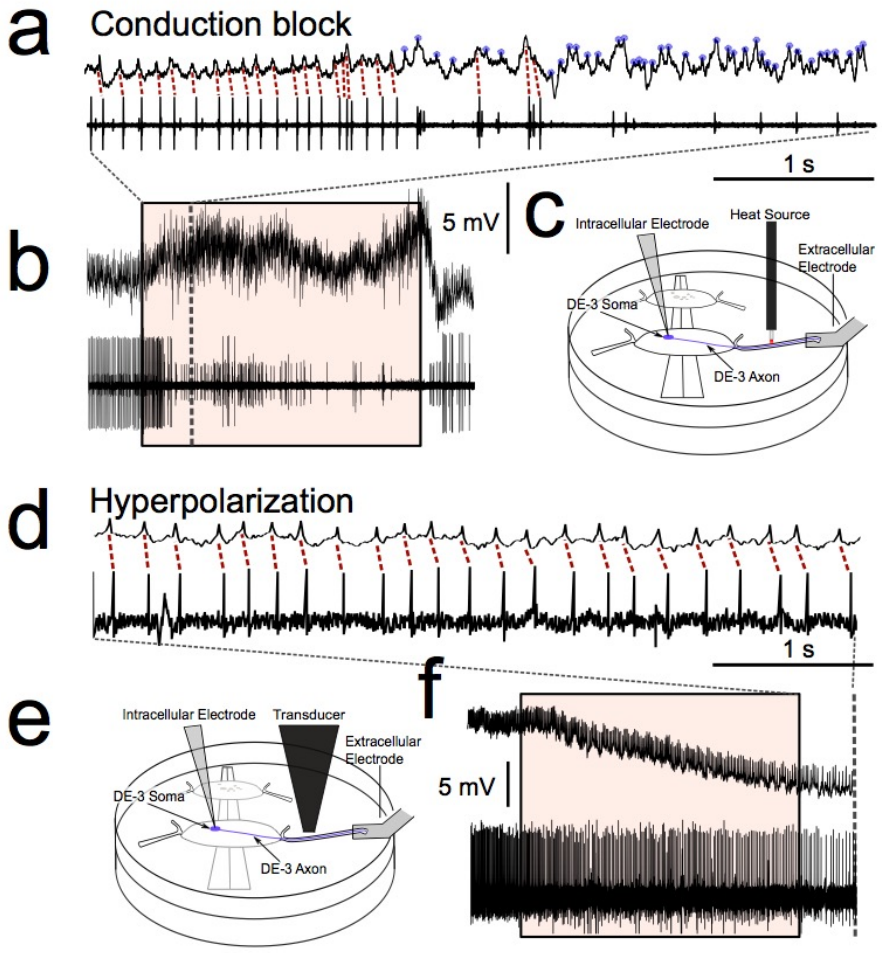

Figure 5.4 Heat can inhibit neuronal activity via conduction block or global hyperpolarization. A-C and E are adapted from Chapter III. **(a)** Expansion of dashed box over traces in B, in which intracellular spikes (upper trace) are matched 1:1 with extracellular spikes (lower trace) until conduction block occurs, at which time intracellular spikes continue (blue circles) but are no longer matched with extracellular spikes. **(b)** Simultaneous intra- and extracellular recordings of the leech motoneuron DE-3, including 30 seconds of localized heating with a 50 mW laser (applied during red box). **(c)** Schematic of experiment, in which an intracellular electrode is inserted into the soma of the motoneuron DE-3 while a suction electrode at the distal end of the nerve records extracellular potentials. The laser is applied between the two recording sites. **(d)** Expansion of dashed box over traces in F, in which we observe that even during maximal inhibition, intra- and extracellular-spikes are still matched 1:1. **(e)** Schematic of experiment, which is identical to that in C, but the laser is replaced with a 1 MHz (300 μs pulses, 500 kHz pulse repetition frequency, 1 MPa) ultrasound transducer. **(f)** Simultaneous intra- and extracellular recordings of DE-3, in which slowing of the firing rate corresponds to an approximately 10 mV hyperpolarization of the resting membrane potential.

REFERENCES

Ai L, Bansal P, Mueller JK, Legon W (2018) Effects of transcranial focused ultrasound on human primary motor cortex using 7T fMRI. BMC Neurosci 19:56.

Ai L, Mueller JK, Grant A, Eryaman Y, Legon W (2016) Transcranial focused ultrasound for BOLD fMRI signal modulation in humans. In: Proceedings of the Annual International Conference of the IEEE Engineering in Medicine and Biology Society, EMBS, pp 1758–1761.

Albensi BC, Oliver DR, Toupin J, Odero G (2007) Electrical stimulation protocols for hippocampal synaptic plasticity and neuronal hyper-excitability: Are they effective or relevant? Exp Neurol 204:1–13.

Albert ES, Bec JM, Desmadryl G, Chekroud K, Travo C, Gaboyard S, Bardin F, Marc I, Dumas M, Lenaers G, Hamel C, Muller A, Chabbert C (2012) TRPV4 channels mediate the infrared laser-evoked response in sensory neurons. J Neurophysiol 107:3227–3234.

Anderson TP, Wakim KG, Herrick JF, Bennet WA, Krusen FH (1951) An experimental study of the effects of ultrasonic energy on the lower part of the spinal cord and peripheral nerves. Arch Phys Med Rehabil 32:71–83.

Angstadt JD, Friesen WO (1991) Synchronized oscillatory activity in leech neurons induced by calcium channel blockers. J Neurophysiol 66:1858–1873.

Au W (2004) The sonar of dolphins. Acoust Aust.

Ayata C, Lauritzen M (2015) Spreading depression, spreading depolarizations, and the cerebral vasculature. Physiol Rev.

Azhari H (2010) Basics of Biomedical Ultrasound for Engineers.

Baader a P (1997) Interneuronal and motor patterns during crawling behavior of semi-intact leeches. J Exp Biol.

Bachtold MR, Rinaldi PC, Jones JP, Reines F, Price LR (1998) Focused ultrasound modifications of neural circuit activity in a mammalian brain. Ultrasound Med Biol 24:557–565.

Barbeau H, Rossignol S (1987) Recovery of locomotion after chronic spinalization in the adult cat. Brain Res 412:84–95.

Bargmann CI (1998) Neurobiology of the Caenorhabditis elegans genome. Science (80-).

Barnard JW, Fry WJ, Fry FJ, Krumins RF (1955) Effects of high intensity ultrasound on the central nervous system of the cat. J Comp Neurol 103:459–484.

Beauparlant J, Van Den Brand R, Barraud Q, Friedli L, Musienko P, Dietz V, Courtine G (2013) Undirected compensatory plasticity contributes to neuronal dysfunction after severe spinal cord injury. Brain 136:3347–3361.

Benfenati V, Toffanin S, Bonetti S, Turatti G, Pistone A, Chiappalone M, Sagnella A, Stefani A, Generali G, Ruani G, Saguatti D, Zamboni R, Muccini M (2013) A transparent organic transistor structure for bidirectional stimulation and recording of primary neurons. Nat Mater 12:672–680.

Blackshaw SE (1993) Stretch receptors and body wall muscle in leeches. Comp Biochem Physiol -- Part A Physiol 105:643–652.

Blackshaw SE, Thompson SW (1988) Hyperpolarizing responses to stretch in sensory neurones innervating leech body wall muscle. J Physiol 396:121–137.

Borgmann A, Hooper SL, Büschges A (2009) Sensory feedback induced by front-leg stepping entrains the activity of central pattern generators in caudal segments of the stick insect walking system. J Neurosci 29:2972–2983.

Boscardin E, Alijevic O, Hummler E, Frateschi S, Kellenberger S (2016) The function and regulation of acid-sensing ion channels (ASICs) and the epithelial Na+channel (ENaC): IUPHAR Review 19. Br J Pharmacol:2671–2701.

Briggman KL, Abarbanel HDI, Kristan WB (2005) Optical imaging of neuronal populations during decision-making. Science (80-) 307:896–901.

Briggman KL, Kristan WB (2006) Imaging dedicated and multifunctional neural circuits generating distinct behaviors. J Neurosci 26:10925–10933.

Briggman KL, Kristan WB (2008) Multifunctional Pattern-Generating Circuits. Annu Rev Neurosci 31:271–294.

Briggman KL, Kristan WB, González JE, Kleinfeld D, Tsien RY (2015) Monitoring Integrated Activity of Individual Neurons Using FRET-Based Voltage-Sensitive Dyes. Adv Exp Med Biol 859:149–169.

Brodfuehrer PD, Burns A (1995) Neuronal factors influencing the decision to swim in the medicinal leech. Neurobiol Learn Mem 63:192–199.

Brodfuehrer PD, Thorogood MSE (2001) Identified neurons and leech swimming behavior. Prog Neurobiol 63:371–381.

Cacciatore TW, Brodfuehrer PD, Gonzalez JE, Jiang T, Adams SR, Tsien RY, Kristan WB, Kleinfeld D (1999) Identification of neural circuits by imaging coherent electrical activity with FRET-based dyes. Neuron 23:449–459.

Cacciatore TW, Rozenshteyn R, Kristan WB (2000) Kinematics and modeling of leech crawling: Evidence for an oscillatory behavior produced by propagating waves of excitation. J Neurosci 20:1643–1655.

Campbell JN, Meyer RA (2006) Mechanisms of Neuropathic Pain. Neuron

52:77–92.

Cang J, Friesen WO (2002) Model for intersegmental coordination of leech swimming: Central and sensory mechanisms. J Neurophysiol 87:2760–2769.

Cang J, Yu X, Friesen OW (2001) Sensory modification of leech swimming: Interactions between ventral stretch receptors and swim-related neurons. J Comp Physiol - A Sensory, Neural, Behav Physiol 187:569–579.

Carovac A, Smajlovic F, Junuzovic D (2011) Application of Ultrasound in Medicine. Acta Inform Medica 19:168.

Carpenter DO (1967) Temperature effects on pacemaker generation, membrane potential, and critical firing threshold in Aplysia neurons. J Gen Physiol 50:1469–1484.

Carretta M (1988) The retzius cells in the leech: A review of their properties and synaptic connections. Comp Biochem Physiol -- Part A Physiol 91:405–413.

Carrier L, Brustein E, Rossignol S (1997) Locomotion of the hindlimbs after neurectomy of ankle flexors in intact and spinal cats: Model for the study of locomotor plasticity. J Neurophysiol 77:1979–1993.

Cayce JM, Friedman RM, Chen G, Jansen ED, Mahadevan-Jansen A, Roe AW (2014) Infrared neural stimulation of primary visual cortex in non-human primates. Neuroimage 84:181–190 Available at: http://dx.doi.org/10.1016/j.neuroimage.2013.08.040.

Cayce JM, Friedman RM, Jansen ED, Mahavaden-Jansen A, Roe AW (2011) Pulsed infrared light alters neural activity in rat somatosensory cortex in vivo. Neuroimage 57:155–166 Available at: http://dx.doi.org/10.1016/j.neuroimage.2011.03.084.

Cha J, Heng C, Reinkensmeyer DJ, Roy RR, Edgerton VR, De Leon RD (2007) Locomotor ability in spinal rats is dependent on the amount of activity imposed on the hindlimbs during treadmill training. J Neurotrauma 24:1000–1012.

Chakravarthy K, Nava A, Christo PJ, Williams K (2016) Review of Recent Advances in Peripheral Nerve Stimulation (PNS). Curr Pain Headache Rep 20.

Cheung EYY, Ng TKW, Yu KKK, Kwan RLC, Cheing GLY (2017) Robot-Assisted Training for People With Spinal Cord Injury: A Meta-Analysis. Arch Phys Med Rehabil 98:2320-2331.e12.

Chevassus-Au-Louis N, Baraban SC, Gaïarsa JL, Ben-Ari Y (1999) Cortical malformations and epilepsy: New insights from animal models. Epilepsia.

Christensen AP, Corey DP (2007) TRP channels in mechanosensation: Direct or indirect activation? Nat Rev Neurosci 8:510–521.

Chu PC, Liu HL, Lai HY, Lin CY, Tsai HC, Pei YC (2015) Neuromodulation

accompanying focused ultrasound-induced blood-brain barrier opening. Sci Rep 5.

Clapham DE (2003) TRP channels as cellular sensors. Nature 426:517–524.

COGGESHALL RE, FAWCETT DW (1964) THE FINE STRUCTURE OF THE CENTRAL NERVOUS SYSTEM OF THE LEECH, HIRUDO MEDICINALIS. J Neurophysiol 27:229–289.

Collins CA, Rojas E (1982) Temperature Dependence of the Sodium Channel Gating Kinetics in the Node of Ranvier. Q J Exp Physiol 67:41–55.

Colucci V, Strichartz G, Jolesz F, Vykhodtseva N, Hynynen K (2009) Focused Ultrasound Effects on Nerve Action Potential in vitro. Ultrasound Med Biol 35:1737–1747 Available at: https://www.ncbi.nlm.nih.gov/pmc/articles/PMC3624763/pdf/nihms412728.pdf.

Constans C, Mateo P, Tanter M, Aubry JF (2018) Potential impact of thermal effects during ultrasonic neurostimulation: Retrospective numerical estimation of temperature elevation in seven rodent setups. Phys Med Biol 63.

Coste B, Mathur J, Schmidt M, Earley TJ, Ranade S, Petrus MJ, Dubin AE, Patapoutian A (2010) Piezo1 and Piezo2 are essential components of distinct mechanically activated cation channels. Science (80-) 330:55–60.

Costigan M, Woolf CJ (2000) Pain: Molecular mechanisms. J Pain 1:35–44.

Crisp KM, Gallagher BR, Mesce KA (2012) Mechanisms contributing to the dopamine induction of crawl-like bursting in leech motoneurons. J Exp Biol 215:3028–3036.

Crisp KM, Klukas KA, Gilchrist LS, Narty AJ, Mesce KA (2002) Distribution and development of dopamine- and octopamine-synthesizing neurons in the medicinal leech. J Comp Neurol 442:115–129.

Crisp KM, Mesce KA (2003) To swim or not to swim: Regional effects of serotonin, octopamine and amine mixtures in the medicinal leech. J Comp Physiol A Neuroethol Sensory, Neural, Behav Physiol 189:461–470.

Crisp KM, Mesce KA (2004) A cephalic projection neuron involved in locomotion is dye coupled to the dopaminergic neural network in the medicinal leech. J Exp Biol 207:4535–4542.

Crisp KM, Mesce KA (2006) Beyond the central pattern generator: Amine modulation of decision-making neural pathways descending from the brain of the medicinal leech. J Exp Biol 209:1746–1756.

Cymbalyuk GS, Gaudry Q, Masino MA, Calabrese RL (2002) Bursting in leech heart interneurons: Cell-autonomous and network-based mechanisms. J Neurosci 22:10580–10592.

Darrow DP, O'Brien P, Richner TJ, Netoff TI, Ebbini ES (2019) Reversible neuroinhibition by focused ultrasound is mediated by a thermal mechanism. Brain Stimul 12:1439–1447.

Dedola F, Severino FPU, Meneghetti N, Lemaire T, Cafarelli A, Ricotti L, Menciassi A, Cutrone A, Mazzoni A, Micera S (2020) Ultrasound Stimulations Induce Prolonged Depolarization and Fast Action Potentials in Leech Neurons. IEEE Open J Eng Med Biol 1:23–32.

Deffieux T, Younan Y, Wattiez N, Tanter M, Pouget P, Aubry JF (2013) Low-intensity focused ultrasound modulates monkey visuomotor behavior. Curr Biol 23:2430–2433.

Delmas P, Coste B (2013) Mechano-gated ion channels in sensory systems. Cell 155:278.

DeLong MR, Wichmann T (2007) Circuits and circuit disorders of the basal ganglia. Arch Neurol 64:20–24.

Deng Z-D, Lisanby SH, Peterchev A V (2013) Stimulation : Simulation Comparison of 50 Coil Designs. Brain Stimul 6:1–13.

Downs ME, Lee SA, Yang G, Kim S, Wang Q, Konofagou EE (2018) Non-invasive peripheral nerve stimulation via focused ultrasound in vivo. Phys Med Biol 63.

Drew T, Prentice S, Schepens B (2004) Cortical and brainstem control of locomotion. Prog Brain Res 143:251–261.

Duan X, Gao R, Xie P, Cohen-Karni T, Qing Q, Choe HS, Tian B, Jiang X, Lieber CM (2012) Intracellular recordings of action potentials by an extracellular nanoscale field-effect transistor. Nat Nanotechnol 7:174–179.

Duke AR, Jenkins MW, Lu H, McManus JM, Chiel HJ, Jansen ED (2013) Transient and selective suppression of neural activity with infrared light. Sci Rep 3.

Durlak JA (2009) How to select, calculate, and interpret effect sizes. J Pediatr Psychol.

Eastwood AL, Goodman MB (2012) Insight into DEG/ENaC channel gating from genetics and structure. Physiology 27:282–290.

Eckert R (1963) Electrical interaction of paired ganglion cells in the leech. J Gen Physiol 46:573–587.

Edgerton VR, Tillakaratne NJK, Bigbee AJ, de Leon RD, Roy RR (2004) PLASTICITY OF THE SPINAL NEURAL CIRCUITRY AFTER INJURY. Annu Rev Neurosci 27:145–167.

Eisenhart FJ, Cacciatore TW, Kristan WB (2000) A central pattern generator underlies crawling in the medicinal leech. J Comp Physiol - A Sensory, Neural, Behav Physiol 186:631–643.

Eldabe S, Buchser E, Duarte R V. (2016) Complications of spinal cord stimulation and peripheral nerve stimulation techniques: A review of the literature. Pain Med (United States) 17:325–336.

Elhelf IAS, Albahar H, Shah U, Oto A, Cressman E, Almekkawy M (2018) High intensity focused ultrasound: The fundamentals, clinical applications and research trends. Diagn Interv Imaging 99:349–359 Available at: https://doi.org/10.1016/j.diii.2018.03.001.

Enyedi P, Czirják G (2010) Molecular background of leak K+ currents: Two-pore domain potassium channels. Physiol Rev 90:559–605.

Erdfelder E, FAul F, Buchner A, Lang AG (2009) Statistical power analyses using G*Power 3.1: Tests for correlation and regression analyses. Behav Res Methods.

Esch T, Mesce KA, Kristan WB (2002) Evidence for sequential decision making in the medicinal leech. J Neurosci 22:11045–11054.

Evans KD, Weiss B, Knopp M (2007) High-intensity focused ultrasound (HIFU) for specific therapeutic treatments a literature review. J Diagnostic Med Sonogr 23:319–327.

Falgairolle M, Puhl JG, Pujala A, Liu W, O'Donovan MJ (2017) Motoneurons regulate the central pattern generator during drug-induced locomotor-like activity in the neonatal mouse. Elife 6.

Fan RJ, Friesen WO (2006) Characterization of central axon terminals of putative stretch receptors in leeches. J Comp Neurol 494:290–302.

Fan RJ, Marin-Burgin A, French KA, Otto Friesen W (2005) A dye mixture (Neurobiotin and Alexa 488) reveals extensive dye-coupling among neurons in leeches; physiology confirms the connections. J Comp Physiol A Neuroethol Sens Neural Behav Physiol 191:1157–1171.

FDA (2019) Marketing Clearance of Diagnostic Ultrasound Systems and Transducers- Guidance for Industry and Food and Drug Administration Staff. US Dep Heal Hum Serv Food Drug Adm Cent Devices Radiol Heal:18–34 Available at: https://www.fda.gov/regulatory-information/search-fda-guidance-documents/marketing-clearance-diagnostic-ultrasound-systems-and-transducers%0Ahttps://www.regulations.gov%0Ahttps://www.fda.gov/media/71100/download.

Feng H, Dong W, Chai N (2014) A bionic micro sucker actuated by IPMC. In: IEEE International Conference on Orange Technologies, ICOT 2014, pp 223–226.

Fenno L, Yizhar O, Deisseroth K (2011) The Development and Application of Optogenetics. Annu Rev Neurosci.

Ferguson JE, Boldt C, Puhl JG, Stigen TW, Jackson JC, Crisp KM, Mesce KA, Netoff TI, Redish AD (2012) Nanowires precisely grown on the ends of microwire electrodes permit the recording of intracellular action potentials within deeper neural structures. Nanomedicine 7:847–853.

Feyen P, Colombo E, Endeman D, Nova M, Laudato L, Martino N, Antognazza MR, Lanzani G, Benfenati F, Ghezzi D (2016) Light-evoked hyperpolarization and silencing of neurons by conjugated polymers. Sci Rep 6:1–14.

Florez-Paz DM, Tong C-K, Hoffman BU, Lee SA, Konofagou EE, Lumpkin EA (2018) Focused Ultrasound Evoked Responses in Dorsal Root Ganglion Neurons (DRG) and HEK293 Cells. Biophys J 114:673a.

Foley JL, Little JW, Vaezy S (2008) Effects of high-intensity focused ultrasound on nerve conduction. Muscle and Nerve 37:241–250.

Frankenhaeuser B, Moore LE (1963) The effect of temperature on the sodium and potassium permeability changes in myelinated nerve fibres of Xenopus laevis. J Physiol 169:431–437.

Freeman SA, Desmazières A, Fricker D, Lubetzki C, Sol-Foulon N (2016) Mechanisms of sodium channel clustering and its influence on axonal impulse conduction. Cell Mol Life Sci 73:723–735.

Fribance S, Wang J, Roppolo JR, de Groat WC, Tai C (2016) Axonal model for temperature stimulation. J Comput Neurosci 41:185–192.

Friesen WO, Kristan WB (2007) Leech locomotion: swimming, crawling, and decisions. Curr Opin Neurobiol 17:704–711.

Friesen WO, Poon M, Stent GS (1978) Neuronal control of swimming in the medicinal leech. IV. Identification of a network of oscillatory interneurones. J Exp Biol 75:25–43.

Fromherz P, Offenhäusser A, Vetter T, Weis J (1991) A neuron-silicon junction: A Retzius cell of the leech on an insulated-gate field-effect transistor. Science (80-) 252:1290–1293.

Fry FJ, Ades HW, Fry WJ (1958) Production of reversible changes in the central nervous system by ultrasound. Science (80-) 127:83–84.

Fry WJ (1953) Action of Ultrasound on Nerve Tissues a Review. J Acoust Soc Am 25:1–5.

Fry WJ, Wulff VJ, Tucker D, Fry FJ (1950) Physical Factors Involved in Ultrasonically Induced Changes in Living Systems: I. Identification of Non-Temperature Effects. J Acoust Soc Am 22:867–876.

Gaertner W (1954) Frequency Dependence of Ultrasonic Cavitation. J Acoust Soc Am 26:977–980.

Galvan A, Wichmann T (2008) Pathophysiology of Parkinsonism. Clin

Neurophysiol.

Ganguly M, Ford JB, Zhuo J, McPheeters MT, Jenkins MW, Chiel HJ, Jansen ED (2019a) Voltage-gated potassium channels are critical for infrared inhibition of action potentials: an experimental study. Neurophotonics 6:1.

Ganguly M, Jenkins MW, Jansen ED, Chiel HJ (2019b) Thermal block of action potentials is primarily due to voltage-dependent potassium currents: A modeling study. J Neural Eng 16.

Gao Y, Zorman S, Gundersen G, Xi Z, Ma L, Sirinakis G, Rothman JE, Zhang Y (2012) Single reconstituted neuronal SNARE complexes zipper in three distinct stages. Science (80-) 337:1340–1344.

Gaudry Q, Kristan WB (2009) Behavioral choice by presynaptic inhibition of tactile sensory terminals. Nat Neurosci 12:1450–1457.

Gavrilov LR, Gersuni G V., Ilyinski OB, Tsirulnikov EM, Shchekanov EE (1977a) A study of reception with the use of focused ultrasound. I. Effects on the skin and deep receptor structures in man. Brain Res 135:265–277.

Gavrilov LR, Gersuni G V., Ilyinsky OB, Tsirulnikov EM, Shchekanov EE (1977b) A study of reception with the use of focused ultrasound. II. Effects on the animal receptor structures. Brain Res 135:279–285.

Gilchrist LS, Mesce KA (1997) Coactivation of putative octopamine- and serotonin-containing interneurons in the medicinal leech. J Neurophysiol 78:2108–2115.

Glanzman DL (1995) The cellular basis of classical conditioning in Aplysia californica - it's less simple than you think. Trends Neurosci.

Gordon IT, Whelan PJ (2008) Brainstem modulation of locomotion in the neonatal mouse spinal cord. J Physiol 586:2487–2497.

Gorman BYALF, Marmor MF (1970) Temperature dependence of the sodium-potassium permeability ratio of a molluscan neurone. J Physiol 210:919–931.

Goss SA, O'Brien WD (1979) Direct ultrasonic velocity measurements of mammalian collagen threads. J Acoust Soc Am 65:507–511.

Granzow B, Friesen WO, Kristan WB (1985) Physiological and morphological analysis of synaptic transmission between leech motor neurons. J Neurosci 5:2035–2050.

Gray J, Lissmann HW, Pumphrey RJ (1938) The Mechanism of Locomotion in the Leech (Hirudo Medicinalis Ray). J Exp Biol 15:408–430.

Grider J, Manchikanti L, Carayannopoulos A, Sharma ML, Balog CC, Harned ME, Grami V, Justiz R, Nouri K, Hayek SM, Vallejo R, Christo PJ (2016) Effectiveness of spinal cord stimulation in chronic spinal pain: A systematic review. Pain Physician.

Grillner S (2006) Biological Pattern Generation: The Cellular and Computational Logic of Networks in Motion. Neuron 52:751–766.

Grillner S (2011) Control of Locomotion in Bipeds, Tetrapods, and Fish. In: Comprehensive Physiology.

Grillner S, Wallén P (2002) Cellular bases of a vertebrate locomotor system - Steering, intersegmental and segmental co-ordination and sensory control. Brain Res Rev 40:92–106.

Günter C, Delbeke J, Ortiz-Catalan M (2019) Safety of long-term electrical peripheral nerve stimulation: Review of the state of the art. J Neuroeng Rehabil 16:1–16.

Guo H, Hamilton M, Offutt SJ, Gloeckner CD, Li T, Kim Y, Legon W, Alford JK, Lim HH (2018) Ultrasound Produces Extensive Brain Activation via a Cochlear Pathway. Neuron 98:1020-1030.e4.

Haar G ter (2011) Ultrasonic imaging: safety considerations. Interface Focus 1:686–697.

Hagiwara S, Morita H (1962) Electrotonic transmission between two nerve cells in leech ganglion. J Neurophysiol 25:721–731.

Harley CM, Reilly MG, Stewart C, Schlegel C, Morley E, Puhl JG, Nagel C, Crisp KM, Mesce KA (2015) Compensatory plasticity restores locomotion after chronic removal of descending projections. J Neurophysiol 113:3610–3622.

Harrison C, Epton S, Bojanic S, Green AL, FitzGerald JJ (2018) The Efficacy and Safety of Dorsal Root Ganglion Stimulation as a Treatment for Neuropathic Pain: A Literature Review. Neuromodulation 21:225–233.

Harvey EN (1929) the Effect of High Frequency Sound Waves on Heart Muscle and Other Irritable Tissues. Am J Physiol Content 91:284–290.

Harvey EN, Loomis AL (1928) High frequency sound waves of small intensity and their biological effects. Nature.

Haveman J, Sminia P, Wondergem J, van der Zee J, Hulshof MCCM (2005) Effects of hyperthermia on the central nervous system: What was learnt from animal studies? Int J Hyperth 21:473–487.

Haveman J, Van Der Zee J, Wondergem J, Hoogeveen JF, Hulshof MCCM (2004) Effects of hyperthermia on the peripheral nervous system: A review. Int J Hyperth 20:371–391.

Heinrich R (2002) Impact of descending brain neurons on the control of stridulation, walking, and flight in orthoptera. Microsc Res Tech 56:292–301.

Hille B (2001) Ion channels of excitable membranes. Sunderland, MA: Sinauer.

Hodgkin AL, Huxley AF (1952) A quantitative description of membrane current and its application to conduction and excitation in nerve. J Physiol 117:500–

544.

Hodgkin AL, Katz B (1949a) Resting potential Temperature has little effect on the resting potential , as may be seen from the. J Physiol:240–249.

Hodgkin AL, Katz B (1949b) The effect of temperature on the electrical activity of the giant axon of the squid. J Physiol 109:240–249.

Huang Y, Jellies J, Johansen KM, Johansen J (1998) Development and pathway formation of peripheral neurons during leech embryogenesis. J Comp Neurol 397:394–402.

Humphries MD, Gurney K, Prescott TJ (2007) Is there a brainstem substrate for action selection? Philos Trans R Soc B Biol Sci 362:1627–1639.

Husch A, van Patten GN, Hong DN, Scaperotti MM, Cramer N, Harris-Warrick RM (2012) Spinal cord injury induces serotonin supersensitivity without increasing intrinsic excitability of mouse V2a interneurons. J Neurosci 32:13145–13154.

Hynynen K, Clement G (2007) Clinical applications of focused ultrasound - The brain. Int J Hyperth 23:193–202.

Ibsen S, Tong A, Schutt C, Esener S, Chalasani SH (2015) Sonogenetics is a non-invasive approach to activating neurons in Caenorhabditis elegans. Nat Commun 6.

Ilham SJ, Chen L, Guo T, Emadi S, Hoshino K, Feng B (2018) In vitro single-unit recordings reveal increased peripheral nerve conduction velocity by focused pulsed ultrasound. Biomed Phys Eng Express 4.

Ivanenko YP, Cappellini G, Solopova IA, Grishin AA, MacLellan MJ, Poppele RE, Lacquaniti F (2013) Plasticity and modular control of locomotor patterns in neurological disorders with motor deficits. Front Comput Neurosci.

Janssen R (1992) Thermal influences on nervous system function. Neurosci Biobehav Rev 16:399–413.

Jiang Q, Li G, Zhao H, Sheng W, Yue L, Su M, Weng S, Chan LLH, Zhou Q, Humayun MS, Qiu W, Zheng H (2018) Temporal neuromodulation of retinal ganglion cells by low-frequency focused ultrasound stimulation. IEEE Trans Neural Syst Rehabil Eng 26:969–976.

Johnson RL, Wilson CG (2018) A review of vagus nerve stimulation as a therapeutic intervention. J Inflamm Res.

Jones G, Holderied MW (2007) Bat echolocation calls: Adaptation and convergent evolution. Proc R Soc B Biol Sci.

Juan EJ, González R, Albors G, Ward MP, Irazoqui P (2014) Vagus nerve modulation using focused pulsed ultrasound: Potential applications and preliminary observations in a rat. Int J Imaging Syst Technol 24:67–71.

Juvin L, Simmers J, Morin D (2005) Propriospinal circuitry underlying interlimb coordination in mammalian quadrupedal locomotion. J Neurosci 25:6025–6035.

Kamimura H, Wang S, Chen H, Wang Q, Aurup C, Acosta C, Carneiro A, Konofagou E (2015) Pupil dilation and motor response elicitation by ultrasound neuromodulation. In: 2015 IEEE International Ultrasonics Symposium, IUS 2015.

Kamimura HAS, Conti A, Toschi N, Konofagou EE (2020) Ultrasound neuromodulation: Mechanisms and the potential of multimodal stimulation for neuronal function assessment. Front Phys 8:1–9.

Kamimura HAS, Wang S, Chen H, Wang Q, Aurup C, Acosta C, Carneiro AAO, Konofagou EE (2016) Focused ultrasound neuromodulation of cortical and subcortical brain structures using 1.9 MHz. Med Phys 43:5730–5735.

Kanada A, Giardina F, Howison T, Mashimo T, Iida F (2019) Reachability Improvement of a Climbing Robot Based on Large Deformations Induced by Tri-Tube Soft Actuators. Soft Robot 6:483–494.

Kaplan JH (2002) Biochemistry of Na,K-ATPase. Annu Rev Biochem 71:511–535.

Kauer JA, Gibson HE (2009) Hot flash: TRPV channels in the brain. Trends Neurosci 32:215–224.

Kawahara AY, Barber JR (2015) Tempo and mode of antibat ultrasound production and sonar jamming in the diverse hawkmoth radiation. Proc Natl Acad Sci U S A.

Khraiche ML, Phillips WB, Jackson N, Muthuswamy J (2017) Sustained elevation of activity of developing neurons grown on polyimide microelectrode arrays (MEA) in response to ultrasound exposure. Microsyst Technol 23:3671–3683.

Kiehn O (2006) LOCOMOTOR CIRCUITS IN THE MAMMALIAN SPINAL CORD. Annu Rev Neurosci 29:279–306.

Kim H, Chiu A, Lee SD, Fischer K, Yoo SS (2014) Focused ultrasound-mediated non-invasive brain stimulation: Examination of sonication parameters. Brain Stimul 7:748–756.

Kim H, Kim S, Sim NS, Pasquinelli C, Thielscher A, Lee JH, Lee HJ (2019) Miniature ultrasound ring array transducers for transcranial ultrasound neuromodulation of freely-moving small animals. Brain Stimul 12:251–255 Available at: https://doi.org/10.1016/j.brs.2018.11.007.

Kim H, Park MY, Lee SD, Lee W, Chiu A, Yoo SS (2015) Suppression of EEG visual-evoked potentials in rats through neuromodulatory focused ultrasound. Neuroreport 26:211–215.

Kim H, Taghados SJ, Fischer K, Maeng LS, Park S, Yoo SS (2012) Noninvasive Transcranial Stimulation of Rat Abducens Nerve by Focused Ultrasound. Ultrasound Med Biol 38:1568–1575.

Kim MG, Kamimura HAS, Lee SA, Aurup C, Kwon N, Konofagou EE (2020) Image-guided focused ultrasound modulates electrically evoked motor neuronal activity in the mouse peripheral nervous system in vivo. J Neural Eng 17:026026.

King RL, Brown JR, Newsome WT, Pauly KB (2013) Effective parameters for ultrasound-induced in vivo neurostimulation. Ultrasound Med Biol 39:312–331.

Kleinhaus AL (1976) Divalent cations and the action potential of leech Retzius cells. Pflügers Arch Eur J Physiol 363:97–104.

Kleinhaus AL, Prichard JW (1976) Sodium dependent tetrodotoxin-resistant action potentials in a leech neuron. Brain Res 102:368–373.

Klumpp D, Zimmerman M (1980) Irreversible differential block of A- and C-fibres following local nerve heating in the cat. J Physiol 298:471–482.

Koroleva VI, Vykhodtseva NI, Elagin VA (1986) Cortical and subcortical spreading depression in rats produced by focused ultrasound. Neurophysiology 18:43–48.

Kraio RP, Nicholson C (1978) Extracellular ionic variations during spreading depression. Neuroscience 3:1045–1059.

Krasovitski B, Frenkel V, Shoham S, Kimmel E (2011) Intramembrane cavitation as a unifying mechanism for ultrasound-induced bioeffects. Proc Natl Acad Sci U S A 108:3258–3263.

Kristan WB, Calabrese RL, Friesen WO (2005) Neuronal control of leech behavior. Prog Neurobiol 76:279–327.

Kristan WB, Skalak R, Wilson RJA, Skierczynski BA, Murray JA, Eisenhart FJ, Cacciatore TW, Chiel HJ, Beer RD (2000) Biomechanics of Hydroskeletons: Studies of Crawling in the Medicinal Leech. In: Biomechanics and Neural Control of Posture and Movement, pp 206–220.

Kristan WB, Stent GS, Ort CA (1974) Neuronal control of swimming in the medicinal leech. J Comp Physiol.

Kubanek J, Shi J, Marsh J, Chen D, Deng C, Cui J (2016) Ultrasound modulates ion channel currents. Sci Rep 6.

Kubanek J, Shukla P, Das A, Baccus SA, Goodman MB (2018) Ultrasound elicits behavioral responses through mechanical effects on neurons and ion channels in a simple nervous system. J Neurosci 38:3081–3091.

Kupfermann I, Weiss KR (1978) The command neuron concept. Behav Brain Sci 1:3–10.

Kupfermann I, Weiss KR (2001) Motor program selection in simple model systems. Curr Opin Neurobiol 11:673–677.

Lapointe NP, Rouleau P, Ung RV, Guertin PA (2009) Specific role of dopamine D1 receptors in spinal network activation and rhythmic movement induction in vertebrates. J Physiol 587:1499–1511.

Lau A, Tymianski M (2010) Glutamate receptors, neurotoxicity and neurodegeneration. Pflugers Arch Eur J Physiol 460:525–542.

Lee CH, Chen CC (2018) Roles of ASICs in nociception and proprioception. In: Advances in Experimental Medicine and Biology, pp 37–47.

Lee SA, Kamimura HAS, Burgess MT, Konofagou EE (2020) Displacement imaging for focused ultrasound peripheral nerve neuromodulation. IEEE Trans Med Imaging:1–1.

Lee W, Lee SD, Park MY, Foley L, Purcell-Estabrook E, Kim H, Fischer K, Maeng LS, Yoo SS (2016) Image-Guided Focused Ultrasound-Mediated Regional Brain Stimulation in Sheep. Ultrasound Med Biol 42:459–470.

Lee YF, Lin CC, Cheng JS, Chen GS (2015a) High-Intensity Focused Ultrasound Attenuates Neural Responses of Sciatic Nerves Isolated from Normal or Neuropathic Rats. Ultrasound Med Biol 41:132–142.

Lee YF, Lin CC, Cheng JS, Chen GS (2015b) Nerve conduction block in diabetic rats using high-intensity focused ultrasound for analgesic applications. Br J Anaesth 114:840–846.

Legon W, Ai L, Bansal P, Mueller JK (2018a) Neuromodulation with single-element transcranial focused ultrasound in human thalamus. Hum Brain Mapp 39:1995–2006.

Legon W, Bansal P, Tyshynsky R, Ai L, Mueller JK (2018b) Transcranial focused ultrasound neuromodulation of the human primary motor cortex. Sci Rep 8:1–14 Available at: http://dx.doi.org/10.1038/s41598-018-28320-1.

Legon W, Sato TF, Opitz A, Mueller J, Barbour A, Williams A, Tyler WJ (2014) Transcranial focused ultrasound modulates the activity of primary somatosensory cortex in humans. Nat Neurosci 17:322–329 Available at: http://dx.doi.org/10.1038/nn.3620.

Lehmann JF (1953) The Biophysical Mode of Action of Biologic and Therapeutic Ultrasonic Reactions. J Acoust Soc Am 25:17–25.

Lele PP (1963) Effects of focused ultrasonic radiation on peripheral nerve, with observations on local heating. Exp Neurol 8:47–83.

Li GF, Zhao HX, Zhou H, Yan F, Wang JY, Xu CX, Wang CZ, Niu LL, Meng L, Wu S, Zhang HL, Qiu WB, Zheng HR (2016) Improved Anatomical Specificity of Non-invasive Neuro-stimulation by High Frequency (5 MHz) Ultrasound. Sci Rep 6:1–11.

Liewald D, Miller R, Logothetis N, Wagner HJ, Schüz A (2014) Distribution of axon diameters in cortical white matter: an electron-microscopic study on three human brains and a macaque. Biol Cybern 108:541–557.

Lin JW, Yu F, Müller WS, Ehnholm G, Okada Y (2019a) Focused ultrasound transiently increases membrane conductance in isolated crayfish axon. J Neurophysiol 121:480–489.

Lin X, Qiu Y, Song L, Chen S, Chen X, Huang G, Song J, Chen X, Yang H (2019b) Ultrasound activation of liposomes for enhanced ultrasound imaging and synergistic gas and sonodynamic cancer therapy. Nanoscale Horizons 4:747–756.

Lipsman N, Schwartz ML, Huang Y, Lee L, Sankar T, Chapman M, Hynynen K, Lozano AM (2013) MR-guided focused ultrasound thalamotomy for essential tremor: A proof-of-concept study. Lancet Neurol 12:462–468 Available at: http://dx.doi.org/10.1016/S1474-4422(13)70048-6.

Liu FH, Pei-Sun M, Chen JP, Zhu J, Yao Q (2002) Locomotion characteristics of an SMA-actuated micro robot simulating a medicinal leech in a pipeline. J Robot Syst 19:245–253.

Lothet EH, Shaw KM, Lu H, Zhuo J, Wang YT, Gu S, Stolz DB, Jansen ED, Horn CC, Chiel HJ, Jenkins MW (2017) Selective inhibition of small-diameter axons using infrared light. Sci Rep 7:1–8.

Lubman DI, Yücel M, Pantelis C (2004) Addiction, a condition of compulsive behaviour? Neuroimaging and neuropsychological evidence of inhibitory dysregulation. Addiction 99:1491–1502.

Lynagh T, Mikhaleva Y, Colding JM, Glover JC, Pless SA (2018) Acid-sensing ion channels emerged over 600 Mya and are conserved throughout the deuterostomes. Proc Natl Acad Sci U S A 115:8430–8435.

Manbachi A, Cobbold RSC (2011) Development and application of piezoelectric materials for ultrasound generation and detection. Ultrasound 19:187–196.

Marder E (2011) Variability, compensation, and modulation in neurons and circuits. Proc Natl Acad Sci U S A 108:15542–15548.

Marder E, Bucher D (2007) Understanding Circuit Dynamics Using the Stomatogastric Nervous System of Lobsters and Crabs. Annu Rev Physiol 69:291–316.

McClellan AD, Kovalenko MO, Benes JA, Schulz DJ (2008) Spinal cord injury induces changes in electrophysiological properties and ion channel expression of reticulospinal neurons in larval lamprey. J Neurosci 28:650–659.

Mehić E, Xu JM, Caler CJ, Coulson NK, Moritz CT, Mourad PD (2014) Increased anatomical specificity of neuromodulation via modulated focused ultrasound.

PLoS One 9.

Melinek R, Muller KJ (1996) Action potential initiation site depends on neuronal excitation. J Neurosci 16:2585–2591.

Mendez J, Keys A, Anderson T, Grande F (1960) Density of fat and bone mineral of mammalian body. Metabolism 9:472–477.

Menz MD, Oralkan Ö, Khuri-Yakub PT, Baccus SA (2013) Precise neural stimulation in the retina using focused ultrasound. J Neurosci 33:4550–4560.

Menz MD, Ye P, Firouzi K, Nikoozadeh A, Pauly KB, Khuri-Yakub P, Baccus SA (2019) Radiation Force as a Physical Mechanism for Ultrasonic Neurostimulation of the Ex Vivo Retina. J Neurosci 39:6251–6264.

Mesce KA, Bigelow AW, Puhl JG (2018) Reorganization of proprioceptive inputs facilitates locomotor recovery after injury to the CNS. Neurosci Meet Plan from Soc Neurosci Program No.

Mesce KA, Esch T, Kristan WB (2008) Cellular substrates of action selection: A cluster of higher-order descending neurons shapes body posture and locomotion. J Comp Physiol A Neuroethol Sensory, Neural, Behav Physiol 194:469–481.

Mesce KA, Newhoff M (2020) The Neural Control of Movement. In: The Neural Control of Movement, 1st ed. (Whelan PJ, Sharples SA, eds). Acedemic Press.

Mesce KA, Pierce-Shimomura JT (2010) Shared strategies for behavioral switching: Understanding how locomotor patterns are turned on and off. Front Behav Neurosci 4.

Mesiwala AH, Farrell L, Wenzel HJ, Silbergeld DL, Crum LA, Winn HR, Mourad HR (2002) High-intensity focused ultrasound selectively disrupts the blood-brain barrier in vivo. Ultrasound Med Biol 28:389–400.

Mihran RT, Barnes FS, Wachtel H (1990) Temporally-specific modification of myelinated axon excitability in vitro following a single ultrasound pulse. Ultrasound Med Biol 16:297–309.

Mihran RT, Lineaweaver SK, Barnes FS, Wachtel H (1996) Effects of pulsed acoustic and mechanical stimuli on the excitability of isolated neuronal and cardiac cells. Appl Occup Environ Hyg 11:271–274.

Milburn T, Saint DA, Chung SH (1995) The temperature dependence of conductance of the sodium channel: Implications for mechanisms of ion permeation. Recept Channels 3:201–211.

Miller EW, Lin JY, Frady EP, Steinbach PA, Kristan WB, Tsien RY (2012) Optically monitoring voltage in neurons by photoinduced electron transfer through molecular wires. Proc Natl Acad Sci U S A 109:2114–2119.

Min BK, Bystritsky A, Jung KI, Fischer K, Zhang Y, Maeng LS, In Park S, Chung

YA, Jolesz FA, Yoo SS (2011) Focused ultrasound-mediated suppression of chemically-induced acute epileptic EEG activity. BMC Neurosci 12.

Minassian K, Hofstoetter US, Dzeladini F, Guertin PA, Ijspeert A (2017) The Human Central Pattern Generator for Locomotion: Does It Exist and Contribute to Walking? Neuroscientist 23:649–663.

Miocinovic S, Somayajula S, Chitnis S, Vitek JL (2013) History, applications, and mechanisms of deep brain stimulation. JAMA Neurol 70:163–171.

Mohammadjavadi M, Ye PP, Xia A, Brown J, Popelka G, Pauly KB (2019) Elimination of peripheral auditory pathway activation does not affect motor responses from ultrasound neuromodulation. Brain Stimul 12:901–910 Available at: https://doi.org/10.1016/j.brs.2019.03.005.

Money TGA, Rodgers CI, McGregor SMK, Robertson RM (2009) Loss of potassium homeostasis underlies hyperthermic conduction failure in control and preconditioned locusts. J Neurophysiol 102:285–293.

Moroz LL, Kocot KM, Citarella MR, Dosung S, Tigran P, Povolotskaya IS, Grigorenko AP, Dailey C, Berezikov E, Buckley KM, Ptytsyn A, Reshetov D (2014) The Ctenophore Genome and the Evolutionary Origins of Neural Systems. Nature 510:109–114.

Morris CE, Juranka PF (2007) Nav channel mechanosensitivity: Activation and inactivation accelerate reversibly with stretch. Biophys J 93:822–833 Available at: http://dx.doi.org/10.1529/biophysj.106.101246.

Muir GD, Steeves JD (1995) Phasic cutaneous input facilitates locomotor recovery after incomplete spinal injury in the chick. J Neurophysiol 74:358–368.

Muller KJ, McGlade-McCulloh E, Mason A (1987) Tinkering with successful synapse regeneration in the leech: adding insult to injury. J Exp Biol 132:207–221.

Muller KJ, Nicholls JG, Stent GS (1982) Neurobiology of the leech. Cold Spring Harb Lab.

Mullins OJ, Hackett JT, Buchanan JT, Friesen WO (2011) Neuronal control of swimming behavior: Comparison of vertebrate and invertebrate model systems. Prog Neurobiol 93:244–269.

Mulloney B, Smarandache-Wellmann C (2012) Neurobiology of the crustacean swimmeret system. Prog Neurobiol 96:242–267.

Muratore R, LaManna J, Szulman E, Kalisz A, Lamprecht M, Simon M, Yu Z, Xu N, Morrison B (2009) Bioeffective ultrasound at very low doses: Reversible manipulation of neuronal cell morphology and function in vitro. In: AIP Conference Proceedings, pp 25–29.

Murchison D, Chrachri A, Mulloney B (1993) A separate local pattern-generating

circuit controls the movements of each swimmeret in crayfish. J Neurophysiol 70:2620–2631.

Nagarah JM, Stowasser A, Parker RL, Asari H, Wagenaar DA (2015) Optically transparent multi-suction electrode arrays. Front Neurosci 9.

Narayanan KL, Irmady K, Subramaniam S, Unsicker K, von Bohlen und Halbach O (2008) Evidence that TRPC1 is involved in hippocampal glutamate-induced cell death. Neurosci Lett 446:117–122.

Naughton JR, Connolly T, Varela JA, Lundberg J, Burns MJ, Chiles TC, Christianson JP, Naughton MJ (2016) Shielded coaxial optrode arrays for neurophysiology. Front Neurosci 10.

Neuling T, Wagner S, Wolters CH, Zaehle T, Herrmann CS (2012) Finite-element model predicts current density distribution for clinical applications of tDCS and tACS. Front Psychiatry 3:1–10.

Newhoff M, Smith C, Ebbini ES, Mesce KA (2018) Low intensity ultrasound reversibly inhibits single neuron firing in a tractable invertebrate model. 2018 Neurosci Meet Planner San Diego, CA Soc Neurosci 2018 Program No:Online.

Newman PG, Rozycki GS (1998) The history of ultrasound. Surg Clin North Am.

Nicholls JG, Baylor DA (1968) Specific modalities and receptive fields of sensory neurons in CNS of the leech. J Neurophysiol 31:740–756.

Nicholls JG, Purves D (1970) Monosynaptic chemical and electrical connexions between sensory and motor cells in the central nervous system of the leech. J Physiol 209:647–667.

Northcutt AJ, Fischer EK, Puhl JG, Mesce KA, Schulz DJ (2018) An annotated CNS transcriptome of the medicinal leech, Hirudo verbana: De novo sequencing to characterize genes associated with nervous system activity.

O'Gara BA, Friesen WO (1995) Termination of leech swimming activity by a previously identified swim trigger neuron. J Comp Physiol A 177:627–636.

Orlovsky G, Deliagina TG, Grillner S (2012) Neuronal Control of LocomotionFrom Mollusc to Man.

Otto Friesen W, Pearce RA (1993) Mechanisms of intersegmental coordination in leech locomotion. Semin Neurosci 5:41–47.

Parker D (2017) The lesioned spinal cord is a "new" spinal cord: Evidence from functional changes after spinal injury in lamprey. Front Neural Circuits 11.

Pasquinelli C, Hanson LG, Siebner HR, Lee HJ, Thielscher A (2019) Safety of transcranial focused ultrasound stimulation: A systematic review of the state of knowledge from both human and animal studies. Brain Stimul 12:1367–1380.

Pavlov VA, Wang H, Czura CJ, Friedman SG, Tracey KJ (2003) The Cholinergic Anti-inflammatory Pathway: A Missing Link in Neuroimmunomodulation. Mol Med 9:125–134.

Peterson EJ, Tyler DJ (2014) Motor neuron activation in peripheral nerves using infrared neural stimulation. J Neural Eng 11.

Pietra A Della, Mikhailov N, Giniatullin R (2020) The emerging role of mechanosensitive piezo channels in migraine pain. Int J Mol Sci 21.

Pietrobon D, Moskowitz MA (2014) Chaos and commotion in the wake of cortical spreading depression and spreading depolarizations. Nat Rev Neurosci 15:379–393.

Pikov V, Arakaki X, Harrington M, Fraser SE, Siegel PH (2010) Modulation of neuronal activity and plasma membrane properties with low-power millimeter waves in organotypic cortical slices. J Neural Eng 7.

Pikov V, Siegel PH (2011) Millimeter wave-induced changes in membrane properties of leech Retzius neurons. Photonic Ther Diagnostics 7883:788356.

Pipkin JE, Bushong EA, Ellisman MH, Kristan WB (2016) Patterns and distribution of presynaptic and postsynaptic elements within serial electron microscopic reconstructions of neuronal arbors from the medicinal leech Hirudo verbana. J Comp Neurol 524:3677–3695.

Pipkin JE, Bushong EA, Ellisman MH, Kristan WB (2018) Verifying, challenging, and discovering new synapses among fully em-reconstructed neurons in the leech ganglion. Front Neuroanat 12.

Plaksin M, Shapira E, Kimmel E, Shoham S (2018) Thermal Transients Excite Neurons through Universal Intramembrane Mechanoelectrical Effects. Phys Rev X 8:11043 Available at: https://doi.org/10.1103/PhysRevX.8.011043.

Plaksin M, Shoham S, Kimmel E (2014) Intramembrane cavitation as a predictive bio-piezoelectric mechanism for ultrasonic brain stimulation. Phys Rev X 4.

Poliak S, Peles E (2003) The local differentiation of myelinated axons at nodes of ranvier. Nat Rev Neurosci 4:968–980.

Poon M, Friesen WO, Stent GS (1978) Neuronal control of swimming in the medicinal leech. V. Connexions between the oscillartoy interneurones and the motor neurones. J Exp Biol 75:45–63.

Portfors C V., Perkel DJ (2014) The role of ultrasonic vocalizations in mouse communication. Curr Opin Neurobiol.

Pozo K, Goda Y (2010) Unraveling mechanisms of homeostatic synaptic plasticity. Neuron 66:337–351.

Prieto ML, Firouzi K, Khuri-Yakub BT, Madison D V., Maduke M (2020) Spike-frequency dependent inhibition and potentiation of neural activity by

ultrasound. bioRxiv.

Prieto ML, Firouzi K, Khuri-Yakub BT, Maduke M (2018) Activation of Piezo1 but Not NaV1.2 Channels by Ultrasound at 43 MHz. Ultrasound Med Biol 44:1217–1232.

Prinz AA, Bucher D, Marder E (2004) Similar network activity from disparate circuit parameters. Nat Neurosci 7:1345–1352.

Puhl JG, Bigelow AW, Rue MCP, Mesce KA (2018) Functional recovery of a locomotor network after injury: plasticity beyond the central nervous system. eNeuro 5:1–16.

Puhl JG, Masino MA, Mesce KA (2012) Necessary, sufficient and permissive: A single locomotor command neuron important for intersegmental coordination. J Neurosci 32:17646–17657.

Puhl JG, Mesce KA (2008) Dopamine activates the motor pattern for crawling in the medicinal leech. J Neurosci 28:4192–4200.

Puhl JG, Mesce KA (2010) Keeping it together: Mechanisms of intersegmental coordination for a flexible locomotor behavior. J Neurosci 30:2373–2383.

Qiu Z, Guo J, Kala S, Zhu J, Xian Q, Qiu W, Li G, Zhu T, Meng L, Zhang R, Chan HC, Zheng H, Sun L (2019) The Mechanosensitive Ion Channel Piezo1 Significantly Mediates In Vitro Ultrasonic Stimulation of Neurons. iScience 21:448–457.

R. W. Wood and A. L. Loomis (1927) XXXVIII. The physical and biological effects of high-frequency sound-waves of great intensity. London, Edinburgh, Dublin Philos Mag J Sci 4:417–436.

Raghavan P (2018) Emerging Therapies for Spastic Movement Disorders. Phys Med Rehabil Clin N Am 29:633–644.

Retzius G (1892) Zur Kenntniss des centralen Nervensystems der Würmer (Samson, Wallin, eds).

Rhee AY, Li G, Wells J, Kao JPY (2008) Photostimulation of sensory neurons of the rat vagus nerve. Opt Interact with Tissue Cells XIX 6854:68540E.

Riccio A, Medhurst AD, Mattei C, Kelsell RE, Calver AR, Randall AD, Benham CD, Pangalos MN (2002) mRNA distribution analysis of human TRPC family in CNS and peripheral tissues. Mol Brain Res 109:95–104.

Richter CP, Matic AI, Wells JD, Jansen ED, Walsh JT (2011) Neural stimulation with optical radiation. Laser Photonics Rev 5:68–80.

Rinaldi PC, Jones JP, Reines F, Price LRR (1991) Modification by focused ultrasound pulses of electrically evoked responses from an in vitro hippocampal preparation. Brain Res 558:36–42.

Robertson RM, Money TGA (2012) Temperature and neuronal circuit function:

Compensation, tuning and tolerance. Curr Opin Neurobiol 22:724–734 Available at: http://dx.doi.org/10.1016/j.conb.2012.01.008.

Robertson RM, Pearson KG (1983) Interneurons in the flight system of the locust: Distribution, connections, and resetting properties. J Comp Neurol 215:33–50.

Robertson RM, Pearson KG (1985) Neural circuits in the flight system of the locust. J Neurophysiol 53:110–128.

Rodgers CI, Armstrong GAB, Shoemaker KL, LaBrie JD, Moyes CD, Robertson RM (2007) Stress preconditioning of spreading depression in the locust CNS. PLoS One 2.

Romanenko S, Siegel PH, Wagenaar DA, Pikov V (2014a) Effects of millimeter wave irradiation and equivalent thermal heating on the activity of individual neurons in the leech ganglion. J Neurophysiol 112:2423–2431.

Romanenko S, Siegel PH, Wagenaar DA, Pikov V (2014b) Effects of millimeter wave irradiation and equivalent thermal heating on the activity of individual neurons in the leech ganglion. J Neurophysiol 112:2423–2431.

Ross WN, Arechiga H, Nicholls JG (1987) Optical recording of calcium and voltage transients following impulses in cell bodies and processes of identified leech neurons in culture. J Neurosci 7:3877–3887.

Rossignol S, Chau C, Brustein E, Bélanger M, Barbeau H, Drew T (1996) Locomotor capacities after complete and partial lesions of the spinal cord. In: Acta Neurobiologiae Experimentalis, pp 449–463.

Rossignol S, Frigon A (2011) Recovery of Locomotion After Spinal Cord Injury: Some Facts and Mechanisms. Annu Rev Neurosci 34:413–440.

Rotstein HG, Schneider E, Szczupak L (2017) Feedback signal from motoneurons influences a rhythmic pattern generator. J Neurosci 37:9149–9159.

Saffari N, Wright CJ, Rothwell J (2017) Ultrasound neuro-stimulation effects of peripheral axons in-vitro. J Acoust Soc Am 142:2668–2668.

Sakurai A, Katz PS (2009) Functional recovery after lesion of a central pattern generator. J Neurosci 29:13115–13125.

Sato T, Shapiro MG, Tsao DY (2018) Ultrasonic Neuromodulation Causes Widespread Cortical Activation via an Indirect Auditory Mechanism. Neuron 98:1031-1041.e5.

Sawyer RT (1981) Leech biology and behavior. In: Neurobiology of the Leech, pp 7–26.

Schätzthauer R (1998) Neuron-silicon junction with voltage-gated ionic currents. Eur J Neurosci 10:1956–1962.

Schneider ER, Anderson EO, Gracheva EO, Bagriantsev SN (2014) Temperature Sensitivity of Two-Pore (K2P) Potassium Channels. Elsevier. Available at: http://dx.doi.org/10.1016/B978-0-12-800181-3.00005-1.

Shapiro MG, Homma K, Villarreal S, Richter CP, Bezanilla F (2012) Infrared light excites cells by changing their electrical capacitance. Nat Commun 3.

Sharma HS, Hoopes PJ (2003) Hyperthermia induced pathophysiology of the central nervous system. Int J Hyperth 19:325–354.

Sharples SA, Koblinger K, Humphreys JM, Whelan PJ (2014) Dopamine: A parallel pathway for the modulation of spinal locomotor networks. Front Neural Circuits 8.

Shealy CN, Henneman E (1962) Reversible Effects of Ultrasound on Spinal Reflexes. Arch Neurol 6:374–386.

Shimamura M, Kogure I (1983) Discharge patterns of reticulospinal neurons corresponding with quadrupedal leg movements in thalamic cats. Brain Res 260:27–34.

Sminia P, Zee J Van Der, Wondergem J, Haveman J (1994) Effect of hyperthermia on the central nervous system: A review. Int J Hyperth 10:1–30.

Smith RR, Shum-Siu A, Baltzley R, Bunger M, Baldini A, Burke DA, Magnuson DSK (2006) Effects of swimming on functional recovery after incomplete spinal cord injury in rats. J Neurotrauma 23:908–919.

Somjen GG (2001) Mechanisms of spreading depression and hypoxic spreading depression-like depolarization. Physiol Rev 81:1065–1096.

Song J, Ampatzis K, Björnfors ER, El Manira A (2016) Motor neurons control locomotor circuit function retrogradely via gap junctions. Nature 529:399–402.

Soofi W, Goeritz ML, Kispersky TJ, Prinz AA, Marder E, Stein W (2014) Phase maintenance in a rhythmic motor pattern during temperature changes in vivo. J Neurophysiol 111:2603–2613.

Spear M (2016) Medicinal leech therapy: Friend or foe. Plast Surg Nurs 36:121–125.

Spong KE, David Andrew R, Meldrum Robertson R (2016) Mechanisms of spreading depolarization in vertebrate and insect central nervous systems. J Neurophysiol 116:1117–1127.

Spruston N, Johnston D (2008) Out of control in the dendrites. Nat Neurosci 11:733–734.

St. John Smith E (2018) Advances in understanding nociception and neuropathic pain. J Neurol 265:231–238.

Stent GS, Kristan WB, Friesen WO, Ort CA, Poon M, Calabrese RL (1978) Neuronal generation of the leech swimming movement. Science (80-) 200:1348–1357.

Stern-Tomlinson W, Nusbaum MP, Perez LE, Kristan WB (1986) A kinematic study of crawling behavior in the leech, Hirudo medicinalis. J Comp Physiol A 158:593–603.

Stewart RR, Nicholls JG, Adams WB (1989) Na+, K+ and Ca2+ currents in identified leech neurones in culture. J Exp Biol 141:1–20.

Stuart AE (1970) Physiological and morphological properties of motoneurones in the central nervous system of the leech. J Physiol 209:627–646.

Takagi SF, Higashino S, Shibuya T, Osawa N (1960) The Actions of Ultrasound on the Myelinated Nerve, the Spinal Cord and the Brain. Jpn J Physiol 10:183–193.

Tang LS, Goeritz ML, Caplan JS, Taylor AL, Fisek M, Marder E (2010) Precise temperature compensation of phase in a rhythmic motor pattern. PLoS Biol 8:21–22.

Tomina Y, Wagenaar D (2018) Dual-sided Voltage-sensitive Dye Imaging of Leech Ganglia. BIO-PROTOCOL 8.

Tomina Y, Wagenaar DA (2017) A double-sided microscope to realize whole-ganglion imaging of membrane potential in the medicinal leech. Elife 6.

Tsirulnikov EM, Vartanyan IA, Gersuni G V., Rosenblyum AS, Pudov VI, Gavrilov LR (1988) Use of amplitude-modulated focused ultrasound for diagnosis of hearing disorders. Ultrasound Med Biol 14:277–285.

Tsui PH, Wang SH, Huang CC (2005) In vitro effects of ultrasound with different energies on the conduction properties of neural tissue. Ultrasonics 43:560–565.

Tufail Y, Matyushov A, Baldwin N, Tauchmann ML, Georges J, Yoshihiro A, Tillery SIH, Tyler WJ (2010) Transcranial Pulsed Ultrasound Stimulates Intact Brain Circuits. Neuron 66:681–694 Available at: http://dx.doi.org/10.1016/j.neuron.2010.05.008.

Turrigiano G (2012) Homeostatic synaptic plasticity: Local and global mechanisms for stabilizing neuronal function. Cold Spring Harb Perspect Biol 4.

Turrigiano G, Abbott LF, Marder E (1994) Activity-dependent changes in the intrinsic properties of cultured neurons. Science (80-) 264:974–977.

Turrigiano GG (1999) Homeostatic plasticity in neuronal networks: The more things change, the more they stay the same. Trends Neurosci 22:221–227.

Tyler WJ, Lani SW, Hwang GM (2018) Ultrasonic modulation of neural circuit activity. Curr Opin Neurobiol 50:222–231.

Tyler WJ, Tufail Y, Finsterwald M, Tauchmann ML, Olson EJ, Majestic C (2008) Remote excitation of neuronal circuits using low-intensity, low-frequency ultrasound. PLoS One 3.

Ueda M, Bureš J, Fischer J (1977) Spreading depression elicited by thermal effects of ultrasonic irradiation of cerebral cortex in rats. J Neurobiol 8:381–393.

Velling VA, Shklyaruk SP (1988) Modulation of the functional state of the brain with the aid of focused ultrasonic action. Neurosci Behav Physiol 18:369–375.

Vion-Bailly J, N'Djin WA, Mestas JL, Chapelon JY (2017) Feasibility and main mechanisms underlying in vivo ultrasound neurostimulation of the ventral nerve cord's giant axons of lumbricus terrestris. In: IEEE International Ultrasonics Symposium, IUS.

Volkers L, Mechioukhi Y, Coste B (2014) Piezo channels: from structure to function. Pflugers Arch Eur J Physiol 467:95–99.

Wagenaar DA (2015) A classic model animal in the 21st century: Recent lessons from the leech nervous system. J Exp Biol 218:3353–3359.

Wahab RA, Choi M, Liu Y, Krauthamer V, Zderic V, Myers MR (2012) Mechanical bioeffects of pulsed high intensity focused ultrasound on a simple neural model. Med Phys 39:4274–4283.

Walters ET, Carew TJ, Kandel ER (1979) Classical conditioning in Aplysia californica. Proc Natl Acad Sci U S A.

Walz W (2000) Role of astrocytes in the clearance of excess extracellular potassium. Neurochem Int 36:291–300.

Wang H, Wang B, Normoyle KP, Jackson K, Spitler K, Sharrock M, Miller CM, Best C, Llano D, Du R (2014) Brain temperature and its fundamental properties: A review for clinical neuroscientists. Front Neurosci 8.

Wattiez N, Constans C, Deffieux T, Daye PM, Tanter M, Aubry JF, Pouget P (2017) Transcranial ultrasonic stimulation modulates single-neuron discharge in macaques performing an antisaccade task. Brain Stimul 10:1024–1031.

Waxman SG, Murdoch Ritchie J (1985) Organization of ion channels in the myelinated nerve fiber. Science (80-) 228:1502–1507.

Wells J, Kao C, Konrad P, Milner T, Kim J, Mahadevan-Jansen A, Jansen ED (2007a) Biophysical mechanisms of transient optical stimulation of peripheral nerve. Biophys J 93:2567–2580 Available at: http://dx.doi.org/10.1529/biophysj.107.104786.

Wells JD, Thomsen S, Whitaker P, Jansen ED, Kao CC, Konrad PE, Mahadevan-Jansen A (2007b) Optically mediated nerve stimulation:

Identification of injury thresholds. Lasers Surg Med 39:513–526.

West AE, Chen WG, Dalva MB, Dolmetsch RE, Kornhauser JM, Shaywitz AJ, Takasu MA, Tao X, Greenberg ME (2001) Calcium regulation of neuronal gene expression. Proc Natl Acad Sci U S A 98:11024–11031.

Whelan PJ (1996) Control of locomotion in the decerebrate cat. Prog Neurobiol 49:481–515.

Whitaker IS, Rao J, Izadi D, Butler PE (2004) Historical article: Hirudo medicinalis: Ancient origins of, and trends in the use of medicinal leeches throughout history. Br J Oral Maxillofac Surg 42:133–137.

Wiederhold ML (1978) Auditory responses in cats produced by pulsed ultrasound. J Acoust Soc Am 63:1199–1205.

Willard AL (1981) Effects of serotonin on the generation of the motor program for swimming by the medicinal leech. J Neurosci 1:936–944.

Wirz M, Zemon DH, Rupp R, Scheel A, Colombo G, Dietz V, Hornby TG (2005) Effectiveness of automated locomotor training in patients with chronic incomplete spinal cord injury: A multicenter trial. Arch Phys Med Rehabil 86:672–680.

Wright CJ (2016) Investigation of Ultrasonic Neuro-stimulation Effects in Peripheral Axons. InTech Open:162 Available at: http://discovery.ucl.ac.uk/1505972/1/Thesis - Final Submission.pdf.

Wright CJ, Haqshenas SR, Rothwell J, Saffari N (2017) Unmyelinated Peripheral Nerves Can Be Stimulated in Vitro Using Pulsed Ultrasound. Ultrasound Med Biol 43:2269–2283.

Wright CJ, Rothwell J, Saffari N (2015) Ultrasonic stimulation of peripheral nervous tissue: An investigation into mechanisms. In: Journal of Physics: Conference Series.

Wu J, Fisher RS (2000) Hyperthermic spreading depressions in the immature rat hippocampal slice. J Neurophysiol 84:1355–1360.

Wu J, Nyborg WL (2008) Ultrasound, cavitation bubbles and their interaction with cells. Adv Drug Deliv Rev 60:1103–1116.

Wulff VJ, Fry WJ, Tucker D, Fry FJ, Melton C (1951) Effects of Ultrasonic Vibrations on Nerve Tissues. Proc Soc Exp Biol Med 76:361–366.

Xavier J, Gauthier S, Cohen D, Zahoui M, Chetouani M, Villa F, Berthoz A, Anzalone S (2018) Interpersonal synchronization, motor coordination, and control are impaired during a dynamic imitation task in children with autism spectrum disorder. Front Psychol 9.

Xia Q, Nyberg T (2019) Inhibition of cortical neural networks using infrared laser. J Biophotonics 12:1–12.

Xu B, Zhu M, Zhang W, Zhen X, Pei Z, Xue Q, Zhi C, Shi P (2016) Ultrathin MXene-Micropattern-Based Field-Effect Transistor for Probing Neural Activity. Adv Mater 28:3333–3339.

Yang PF, Phipps MA, Newton AT, Chaplin V, Gore JC, Caskey CF, Chen LM (2018) Neuromodulation of sensory networks in monkey brain by focused ultrasound with MRI guidance and detection. Sci Rep.

Yao J, Liu B, Qin F (2009) Rapid temperature jump by infrared diode laser irradiation for patch-clamp studies. Biophys J 96:3611–3619 Available at: http://dx.doi.org/10.1016/j.bpj.2009.02.016.

Ye J, Tang S, Meng L, Li X, Wen X, Chen S, Niu L, Li X, Qiu W, Hu H, Jiang M, Shang S, Shu Q, Zheng H, Duan S, Li Y (2018) Ultrasonic Control of Neural Activity through Activation of the Mechanosensitive Channel MscL. Nano Lett 18:4148–4155.

Ye PP, Brown JR, Pauly KB (2016) Frequency dependence of ultrasound neurostimulation in the mouse brain. Ultrasound Med Biol.

Yoo S, Mittelstein DR, Hurt R, Lacroix J, Shapiro MG (2020) Focused ultrasound excites neurons via mechanosensitive calcium accumulation and ion channel amplification. bioRxiv:1–15 Available at: https://www.biorxiv.org/content/10.1101/2020.05.19.101196v1.

Yoo SH, Croce P, Margolin RW, Lee SD, Lee W (2017) Pulsed focused ultrasound changes nerve conduction of earthworm giant axonal fibers. Neuroreport 28:229–233.

Yoo SS, Bystritsky A, Lee JH, Zhang Y, Fischer K, Min BK, McDannold NJ, Pascual-Leone A, Jolesz FA (2011a) Focused ultrasound modulates region-specific brain activity. Neuroimage 56:1267–1275.

Yoo SS, Kim H, Min BK, Franck E, Park S (2011b) Transcranial focused ultrasound to the thalamus alters anesthesia time in rats. Neuroreport 22:783–787.

Yoo SS, Yoon K, Croce P, Cammalleri A, Margolin RW, Lee W (2018) Focused ultrasound brain stimulation to anesthetized rats induces long-term changes in somatosensory evoked potentials. Int J Imaging Syst Technol 28:106–112 Available at: file:///C:/Users/Carla Carolina/Desktop/Artigos para acrescentar na qualificação/The impact of birth weight on cardiovascular disease risk in the.pdf.

Younan Y, Deffieux T, Larrat B, Fink M, Tanter M, Aubry JF (2013) Influence of the pressure field distribution in transcranial ultrasonic neurostimulation. Med Phys 40.

Yu X, Friesen WO (2004) Entrainment of leech swimming activity by the ventral stretch receptor. J Comp Physiol A Neuroethol Sensory, Neural, Behav Physiol 190:939–949.

Yu X, Nguyen B, Friesen WO (1999) Sensory feedback can coordinate the swimming activity of the leech. J Neurosci 19:4634–4643.

Yu Y, Hill AP, McCormick DA (2012) Warm body temperature facilitates energy efficient cortical action potentials. PLoS Comput Biol 8.

Zelenin P V., Orlovsky GN, Deliagina TG (2007) Sensory-motor transformation by individual command neurons. J Neurosci 27:1024–1032.

Zhao K, Tan X, Young H, Richter C-P (2016a) Biomedical Optics in Otorhinolaryngology: Head and Neck Surgery. In: Biomedical Optics in Otorhinolaryngology (Wong BJ, Ilgner J, eds). Springer.

Zhao L, Feng Y, Hu H, Shi A, Zhang L, Wan M (2016b) Low-Intensity Pulsed Ultrasound Enhances Nerve Growth Factor-Induced Neurite Outgrowth through Mechanotransduction-Mediated ERK1/2–CREB–Trx-1 Signaling. Ultrasound Med Biol 42:2914–2925.

Zhao L, Feng Y, Shi A, Zhang L, Guo S, Wan M (2017) Neuroprotective Effect of Low-Intensity Pulsed Ultrasound Against MPP+-Induced Neurotoxicity in PC12 Cells: Involvement of K2P Channels and Stretch-Activated Ion Channels. Ultrasound Med Biol 43:1986–1999.

Zhou W, Wang J, Wang K, Huang B, Niu L, Li F, Cai F, Chen Y, Liu X, Zhang X, Cheng H, Kang L, Meng L, Zheng H (2017) Ultrasound neuro-modulation chip: Activation of sensory neurons in: Caenorhabditis elegans by surface acoustic waves. Lab Chip 17:1725–1731.

Zhu S, Cocks FH, Preminger GM, Zhong P (2002) The role of stress waves and cavitation in stone comminution in shock wave lithotripsy. Ultrasound Med Biol 28:661–671.

Zou J, Meng L, Lin Z, Qiao Y, Tie C, Wang Y, Huang X, Yuan T, Chi Y, Meng W, Niu L, Guo Y, Zheng H (2020) Ultrasound Neuromodulation Inhibits Seizures in Acute Epileptic Monkeys. iScience 23:101066 Available at: https://doi.org/10.1016/j.isci.2020.101066.